To the Graduate Council:

We are submitting herewith a dissertation written by Huston Edward Howell, Jr. entitled "Studies of the Analytical Utility of Low-Temperature Photoacoustic Spectroscopy." We have examined the final copy of this dissertation for form and content and recommend that it be accepted in partial fulfillment of the requirements for the degree of Doctor of Philosophy, with a major in Chemistry.

Gleb Mamantov, Co-Chairman

Earl L. Wehry, Co-Chairman

We have read this dissertation
and recommend its acceptance:

William H. Fletcher

M J Sepaniak

R. W. Shaw

Dr. G Christian

Accepted for the Council:

L Evans Rock
Vice Chancellor
Graduate Studies and Research

Thesis
Ed
H8

STUDIES OF THE ANALYTICAL UTILITY OF LOW-TEMPERATURE PHOTOACOUSTIC SPECTROSCOPY

A Dissertation

Presented for the

Doctor of Philosophy

Degree

The University of Tennessee, Knoxville

Huston Edward Howell, Jr.

June 1983

1181805

DEDICATION

I dedicate this work to my loving wife, Susan, who has been a tremendous source of moral and emotional support during these years of graduate school; to my parents who encouraged me to seek a good education and worked hard to help me obtain it; and to the memory of my father-in-law, Jerre T. Appleton, for his generous moral and financial support.

ACKNOWLEDGEMENTS

I would like to thank Dr. Robert W. Shaw of the Oak Ridge National Laboratory for all the assistance that he gave me throughout the course of this work. I would also like to express my sincere appreciation to Prof. Gleb Mamantov and Prof. Earl L. Wehry for their patience and wise guidance. I am grateful to Drs. H. H. Ross, W. S. Lyon, and W. D. Shults for allowing me to use the research facilities at the Oak Ridge National Laboratory. I would like to acknowledge the assistance of Dr. Arlene A. Garrison for helping me to learn the technique of matrix isolation.

Personal financial support from the University of Tennessee Chemistry Department in the form of a Graduate Teaching Assistantship and from the Oak Ridge Associated Universities in the form of a Graduate Research Fellowship is gratefully acknowledged.

Finally, thanks to Mr. George McGhee for typing this manuscript.

THE RESEARCH WAS PERFORMED UNDER APPOINTMENT TO THE LABORATORY GRADUATE PARTICIPATION PROGRAM ADMINISTERED BY OAK RIDGE ASSOCIATED UNIVERSITIES FOR THE U.S. DEPARTMENT OF ENERGY.

ABSTRACT

The present study investigated the analytical utility of laser-excited, low-temperature photoacoustic (PA) spectroscopy, particularly for the detection of weakly fluorescing and non-fluorescing polycyclic aromatic compounds (PACs) isolated in low-temperature (5-20 K) vapor deposited matrices. Photoacoustic spectroscopy of other low-temperature samples was also studied.

In order to accomplish this objective, piezoelectric (PE) transducers were evaluated as low-temperature PA detectors. Two PE materials were studied, X-cut crystalline quartz and lead-zirconate-titanate (PZT). PZT was found to exhibit ~10 times higher sensitivity. PA spectra of $Nd(OH)_3$ powder at 6-8 K were taken to demonstrate the ability to acquire piezoelectrically-detected PA spectra at low-temperatures.

Laser-excited PA spectra were recorded for a number of matrix-isolated PACs. The detection limits were 500 ng for quinoline and 50 ng for pyrene. Both of these mass detection limits corresponded to a limiting detectable thermal energy liberated of ~175 nJ. Singlet-triplet intersystem crossing (i.e., $S_1 \sim\!\!\!\!\!\!\rightarrow T_1$) was determined to be the primary source of the liberated thermal energy which generates the PA signal. The S_1-T_1 energy gap is ~30-40 % of the total S_n-S_o energy gap (i.e., the absorbed photon energy) for most PACs. Attempts to significantly enhance the PA signal by using a heavy-atom matrix (Xe) to increase the $S_1 \sim\!\!\!\!\!\!\rightarrow T_1$ process were not successful.

The main limitation to the analytical utility of the technique was that most of the non- and weakly-fluorescing PACs studied did not

yield highly resolved spectra when matrix isolated. This fact adversely affected the ability to identify individual compounds in multi-component samples.

A detector was developed for obtaining PA spectra of samples in frozen solutions at 77 K. Laser-excited PA spectra of $Nd(OH)_3$ powder dispersed in low-temperature glasses (isopropanol and glycerine/H_2O) were obtained. However, attempts to obtain spectra of PACs in frozen n-alkane solutions were not successful because of the highly scattering nature of the samples.

TABLE OF CONTENTS

CHAPTER	PAGE
I. INTRODUCTION, BACKGROUND, AND THEORY	1
A. The Photoacoustic Effect and Photoacoustic Spectroscopy	1
B. Polycyclic Aromatic Compounds--An Environmental Problem	11
C. Analytical Chemistry of Polycyclic Aromatic Compounds	12
D. Purpose of the Present Work	25
II. EXPERIMENTAL DETAILS	26
A. Materials	26
B. Equipment	33
C. Procedure	59
III. RESULTS AND DISCUSSION	65
A. Low-Temperature Photoacousic Spectroscopy of Neodymium Hydroxide	65
B. Photoacoustic Spectroscopy of Matrix-Isolated Polycyclic Aromatic Compounds	73
C. Photoacoustic Spectroscopy of Polycyclic Aromatic Compounds and Neodymium Hydroxide in Frozen Solutions at 77K	144
IV. CONCLUSION	148
REFERENCES	151
VITA	158

LIST OF TABLES

TABLE		PAGE
II-1	POLYCYCLIC AROMATIC COMPOUNDS STUDIED	27
II-2	LASER DYES	31
II-3	LINEAR THERMAL CONTRACTION OF VARIOUS MATERIALS AT 20 K	49
III-1	PACS FOR WHICH MI-PA SPECTRA WERE RECORDED	100
III-2	PHYSICAL PROPERTIES OF VARIOUS MATERIALS	115
III-3	ACOUSTIC AMPLITUDE AND ACOUSTIC INTENSITY TRANSMITTANCE VALUES FOR VARIOUS MEDIA INTERFACES	116
III-4	COMPARISON OF FACTORS THAT AFFECT THE OBSERVED SENSITIVITIES OF PZT AND X-CUT QUARTZ DETECTORS	120
III-5	SINGLET-TRIPLET INTERSYSTEM CROSSING YIELDS FOR SOME PAHS IN RIGID MEDIA	124
III-6	THERMAL AND ELASTIC PROPERTIES OF SOME MATERIALS	134
III-7	RATIOS OF $\beta v_a/C_p$	135

LIST OF FIGURES

FIGURE PAGE

1. PA spectra of Ho_2O_3 powder at room temperature 9
2. Photophysical processes of a typical PAC 16
3. Diagram of the matrix gas-vacuum line 36
4. Diagram of the sublimation cell used for preparing MI samples 39
5. Diagram of the PA detector used for room-temperature solids . 42
6. Diagram of the low-temperature PA detector used to obtain spectra of $Nd(OH)_3$ powder at 6-8 K 43
7. Diagram of the modified MI-PA detector 46
8. Scale drawing of the final design of the MI-PA detector . . . 48
9. Diagram of the PA detector used for liquid nitrogen-temperature (77 K) samples 51
10. Diagram of the PA detector used for room-temperature liquids 53
11. Block diagram of the laser-excited PAS instrumentation 55
12. JFET preamplifier circuit 57
13. Oscilloscope pictures of pulsed-laser excited PA waveforms corresponding to Ho_2O_3 (room temperature) spectrum (Fig. 1, p. 9) 62
14. PA spectra of $Nd(OH)_3$ powder from 16,400-17,500 cm^{-1} 67
15. PA spectra of $Nd(OH)_3$ powder from 18,600-19,900 cm^{-1} 68
16. Room-temperature diffuse reflectance spectrum of $Nd(OH)_3$ powder from 16,500-20,000 cm^{-1} 69
17. Spectra of 3-bromoquinoline 75

FIGURE PAGE

18. Spectra of quinoline 76

19. Spectra of 3-methylisoquinoline 78

20. Spectra of 2,6-dimethylquinoline 80

21. MI-absorption spectrum of a mixture of dimethylquinoline (DMQ) isomers, 5 μg each in Ar at 10 K 82

22. MI-absorption spectrum of a mixture of methylquinoline (MQ) isomers and 3-methylisoquinoline (3-MIQ), 5 μg each in Ar at 10 K 83

23. Spectra of benzoquinoline (BQ) isomers 85

24. MI-absorption spectra of the individual benzoquinoline (BQ) isomers, 10 μg each in Ar at 10 K 86

25. Spectra of 5,6-benzoquinoline 88

26. MI-absorption spectra of (A) 10 μg of acridine and (B) 10 μg of phenazine in Ar at 10 K 90

27. Spectra of pyrene 92

28. (A) MI-PA spectrum and (B) MI-absorption spectrum of 30 μg of naphthalene (N) and 3 μg of 1-bromonaphthalene (BrN) in Ar at 5 K 93

29. MI-absorption spectra of (A) 5 μg of 2-nitrofluorene, (B) 10 μg of 1-nitronaphthalene, and (C) 5 μg of 6-nitroquinoline in Ar at 10 K 95

30. MI-absorption spectra of (A) 5 μg of 9-fluorenone, (B) 5 μg of anthraquinone, and (C) 20 μg of 1,4-naphthoquinone in Ar at 10 K 96

31. Spectra of dibenzothiophene 98

FIGURE PAGE

32. Spectra of dibenzofuran 99

33. (A) Output signal obtained from the 3 mm thick (7 mm diameter) PZT disc following pulsed laser excitation of the MI sample. (B) Power spectrum of the PA waveform shown in (A) 104

34. (A) Temporal profile of a UV (second harmonic) laser pulse, 310 nm. (B) Upper trace, power spectrum of the UV laser pulse shown in (A) 105

35. (A) Temporal profile of a visible (fundamental) laser pulse, 620 nm. (B) Upper trace, power spectrum of the visible laser pulse shown in (A) 107

36. (A) MI-PA spectrum and (B) MI-absorption spectrum of 20 μg naphthalene (N) and 20 μg of 1-bromonaphthalene (BrN) in Ar at 5 K 126

37. MI-PA spectrum of 20 μg of naphthalene (N) and 2 μg of 1-bromonaphthalene (BrN) in Xe at 5 K 129

38. (A) MI-PA spectrum and (B) MI-absorption spectrum of 5 μg of quinoline (Q) and 30 μg of 1-bromonaphthalene (BrN) in Ar at 5 K 132

39. PA spectrum of $Nd(OH)_3$ powder at 77 K from 17,000-17,500 cm^{-1} 146

CHAPTER I

INTRODUCTION, BACKGROUND, AND THEORY

A. The Photoacoustic Effect and Photoacoustic Spectroscopy

The photoacoustic (PA) effect, also referred to as the optoacoustic effect, occurs when optical energy is absorbed by a medium followed by a re-emission of all or part of the absorbed optical energy in the form of heat (i.e., non-radiative decay). Modulation of the optical energy causes a periodic heating effect that generates acoustic waves within the absorbing medium and its surroundings. This phenomenon is the basis of photoacoustic spectroscopy (PAS). Rosencwaig[1] and Pao[2] have recently reviewed the PA effect and PAS.

1. The Photoacoustic Effect

The discovery of the PA effect was first reported in 1880 by Alexander Graham Bell.[3] He observed that audible sound could be produced when certain solid materials were irradiated with amplitude modulated light. Bell further discovered, in a series of experiments performed in the following year, that the intensity of the audible PA signal was dependent upon how strongly the irradiated material absorbed the light. The intrinsic optical absorptive dependence of the PA effect was thus correctly deduced. Also in the same year, Mercadier[4] and Preece[5] proposed that the acoustic signal was produced when the light-absorbing material reemitted all or part of the incident radiation in the form of heat, some of which flowed to the surrounding gas layer. The periodic heating of the surrounding gas layer gives rise to

a pressure (or acoustic) wave which travels through the bulk of the gas volume. (In one sense, the PA signal is produced by a photo-thermal effect, but the name PA effect is still preferred by most scientists.) This account is in accord with the modern-day theory for the PA effect in the solid-gas case.

In addition to observing the PA effect for solids, Bell also discovered that, in a similar manner, the PA effect could also be obtained for liquids and gases. Tyndall[6] and Roentgen[7] also performed experiments dealing with the PA effect in gases. These authors and Bell concluded that the audible acoustic signal in gases was produced when the gas molecules absorbed a portion of the modulated incident radiation and subsequently reemitted some or all of the absorbed energy in the form of heat. Since the gas volume was held constant, the periodic heating of the gas resulted in a periodic pressure change, i.e., an acoustic signal. An explanation for the PA effect in liquids was not postulated by the nineteenth-century scientists, and only recently has a satisfactory theory been formulated. This theory is discussed below.

2. Photoacoustic Spectroscopy

After the initial reports of the PA effect in the 1880's, the area lay dormant until about half a century later. In 1938 after the advent of the microphone, Viengerov[8] used the PA effect to make quantitative measurements of CO_2 gas in N_2 gas at concentrations as low as ~0.2 volume %. In 1945 Viengerov[9] developed an infrared PA spectrometer. A Nernst glower and monochromator were used to obtain IR

absorption spectra of gases. This opened the way for the development of modern-day PAS.

Between 1950 and 1970, PAS was limited to the study of gaseous samples. In 1973, Rosencwaig[10] demonstrated that PAS can be a very powerful technique for the spectroscopic investigation of solids. The solid materials were placed in a closed cell containing a non-absorbing gas and a microphone. Chopped light from a monochromator was used to illuminate the sample and the resulting microphone signal was inputted to a lock-in amplifier. Thus, a new technique was developed for obtaining absorption spectra of opaque materials. During the following years, this type of gas-microphone cell was the standard arrangement used to obtain PA spectra of solids throughout the ultraviolet, visible, and infrared spectral regions.

3. Optically Generated Acoustic Waves in Condensed Media

Periodic heating of a condensed (i.e., solid or liquid) material gives rise to thermoelastic (or acoustic) waves which traverse the material at the speed of sound, and are generally non-dissipative except at very high frequencies (> 100 MHz).[1] In solids, two main types of waves can propagate over significant distances, longitudinal (or compressional) waves and shear (or transverse) waves. Longitudinal waves have a particle displacement colinear with the direction of propagation, whereas shear waves have a particle displacement normal to the direction of propagation. Liquids, on the other hand, will support only longitudinal waves; shear waves do not occur. Michaels[11] first demonstrated that elastic (acoustic) waves could be generated in condensed media via absorption of electromagnetic radiation. Light

pulses from an exploding wire source were used to irradiate one end of an aluminum rod. A piezoelectric transducer attached to the other end of the rod detected the acoustic signal generated by the light pulses. Soon thereafter, in an experiment similar to that of Michaels, White[12] demonstrated the use of a pulsed laser to generate acoustic waves in a solid sample. Subsequent detection was also accomplished with a piezoelectric transducer. These experiments represented the first cases in which the PA effect was observed directly in a solid medium rather than by employing a coupling gas and microphone detection. This direct detection of the acoustic waves in solid material was possible due to the existence of a solid-state acoustic detector, the piezoelectric transducer.

4. The Piezoelectric Effect

The piezoelectric (PE) effect was first discovered in 1880 by the brothers Pierre and Jacques Curie.[13] The term "piezoelectricity"[14] describes the generation of an electrical polarization in a substance induced by the application of a mechanical stress and, conversely, a change in the shape of a substance when an electric field is applied. An essential feature of the PE effect is the validity of a linear relationship between the the applied electric field and the subsequent mechanical stress or strain, and vice versa. Although piezoelectricity is a bulk property, the conversion of mechanical to electrical energy occurs primarily at the surfaces. The basis for this fact is related to the nature of the mechanical and PE properties of the material.

Substantial contributions to the PE process occur only at discontinuities in the material represented by the surfaces.

Many materials are piezoelectric.[14] The only requirement necessary for a material to exhibit the PE effect is the absence of a center of crystal symmetry. PE materials have been employed for many years as acoustic transmitters and receivers. Among the more commonly used PE materials are crystalline quartz, Rochelle salt ($KNaC_4H_4O_6 \cdot 4H_2O$), lithium niobate, barium titanate, and lead-zirconate-titanate (PZT). Crystalline quartz and PZT are widely used as PE receivers due to their favorable PE properties.

A popular shape in which the PE receivers (or transducers) are often used is the thin disc. Any thin disc material has a natural resonance frequency which is determined by the bulk properties of the material such as density and elasticity.[15] For PE transducers, the maximum efficiency for the conversion of mechanical stress to voltage, and vice versa, occurs at the resonance frequency. The frequency response of a PE device is often given in terms of the resonance frequency, f_o, and a Q factor. Q is a unitless term defined as $f_o/\Delta f$, where Δf represents the frequency bandwidth about f_o at which the response is $> e^{-1}$ of the f_o value. Although a PE device has a maximum response at its resonance frequency, it still has some amount of sensitivity far below resonance, all the way to DC. The sensitivity at frequencies much higher than resonance probably exists only for overtones of the resonance frequency. In a free crystal or disc, the Q value may be as high as 25,000 for crystalline quartz and

~500 for PZT. However, when mounted to a substrate, the Q values can fall to ca. 10-15 making these materials usable as wide-band receivers.

As mentioned previously, for a PE material there exists a linear relationship between applied stress and voltage. For a thin-disc PE material, the output voltage as a result of applied stress is[15,16]

$$V(t) = g_{xy} \ell \, p(t) \qquad (I\text{-}1)$$

where V(t) is the time-varying output voltage, g_{xy} is the appropriate PE sensitivity coefficient, ℓ is the disc thickness, and p(t) is the time varying pressure exerted on the disc.

5. Piezoelectric Detection in Photoacoustic Spectroscopy of Condensed Media

Hordvik and Schlossberg[17] first demonstrated the analytical use of a PE transducer for PA detection in a solid material. They and others[18-20] pointed out the fact that PE transduction in PAS of condensed media is generally more sensitive than the conventional gas-microphone method. The reason for this situation is the efficient acoustic coupling between a condensed sample and a PE transducer, ~90 % for solids and ~20 % for liquids. On the other hand, the acoustic coupling efficiency between a condensed sample and a surrounding gas is very poor, $\sim 10^{-3}$ %. The PA signal in the gas-microphone cell relies almost totally upon a transfer of heat from the condensed material to the gas.

Patel and Tam[18] have thoroughly reviewed pulsed laser PAS of condensed media using PE detection. In terms of sensitivity, they and

others[17,20,21] have demonstrated the measurement of optical absorbances as low as 10^{-6} using pulsed-laser excited PAS with PE detection. The basis for high sensitivity is the good acoustic coupling between the sample and PE transducer, a good frequency match between the pulsed laser and PE transducer, and the high pulse energy of the laser. These factors are important considerations for laser excited PAS with PE detection.[18]

An expression can be written to describe the acoustic pressure amplitude generated in a medium in a pulsed laser PA experiment:[18]

$$P_o = k \frac{\beta v_a}{C_p} E_o \ (1-10^{-A}) \qquad (I-2)$$

where P_o is the acoustic pressure amplitude, β is the thermal expansion coefficient of the medium, C_p is the heat capacity of the medium, v_a is the acoustic velocity in the medium, E_o is the laser pulse energy, A is the optical absorbance of the medium , and $1-10^{-A}$ is the fraction of E_o absorbed, E_a/E_o. The term A is equal to the conventional definition of absorbance, log E_o/E_o-E_a. For A < 0.05, P_o is proportional to A because $1-10^{-A} \approx 2.3$ A. The k term is used to account for the fractional amount of the generated acoustic wave that is detected, the fact that the value of the non-radiative quantum yield may be less than unity, and other variables which may be present but unknown.

Substituting Eq. (I-2) into Eq. (I-1) yields

$$V = k\, g_{xy}\, \ell\, \frac{\beta v_a}{C_p} E_o\, (1-10^{-A}) \qquad (I-3)$$

This equation is valid for the case in which the laser temporal pulse length (τ_p) is longer than both the non-radiative relaxation time (τ_{NR}) and the time required for an acoustic pulse to travel across the laser-illuminated region in the sample medium (τ_a), i.e., $\tau_p \gg \tau_{NR}$ and $\tau_p \gg \tau_a$. Furthermore, it is assumed that the laser pulse (τ_p) is longer than the response time of the PE transducer (τ_{PE}), i.e., $\tau_p \gg \tau_{PE}$.[18] The conditions in the present work ($\tau_{NR} < 10^{-8}$ s, $\tau_p \approx$ 1-2 μs, $\tau_a \approx$ 0.6 μs, and $\tau_{PE} \approx$ 0.8 μs) barely satisfy these criteria, but this equation is more applicable than other possibilities. Moreover, Patel and Tam[18] have verified this equation for experimental conditions almost identical to those in the present work.

In addition to high sensitivity, laser-excited PAS is also a high resolution spectroscopic technique.[22] Whereas conventional PAS in the UV-VIS region employs excitation by light from a Xe-arc lamp passed through a monochromator with a spectral bandwidth of 20-200 cm^{-1}, tunable dye-laser excitation in PAS provides a spectral bandwidth of *ca.* 1-3 cm^{-1}. By way of example, Figure 1 compares the PA spectra of Ho_2O_3 powder taken at room-temperature by excitation with a Xe-arc lamp/monochromator (left) having a 45 cm^{-1} spectral bandwidth with that obtained by laser excitation (right). The labeled arrows are used to identify equivalent lines in the two spectra. The dramatic enhancement

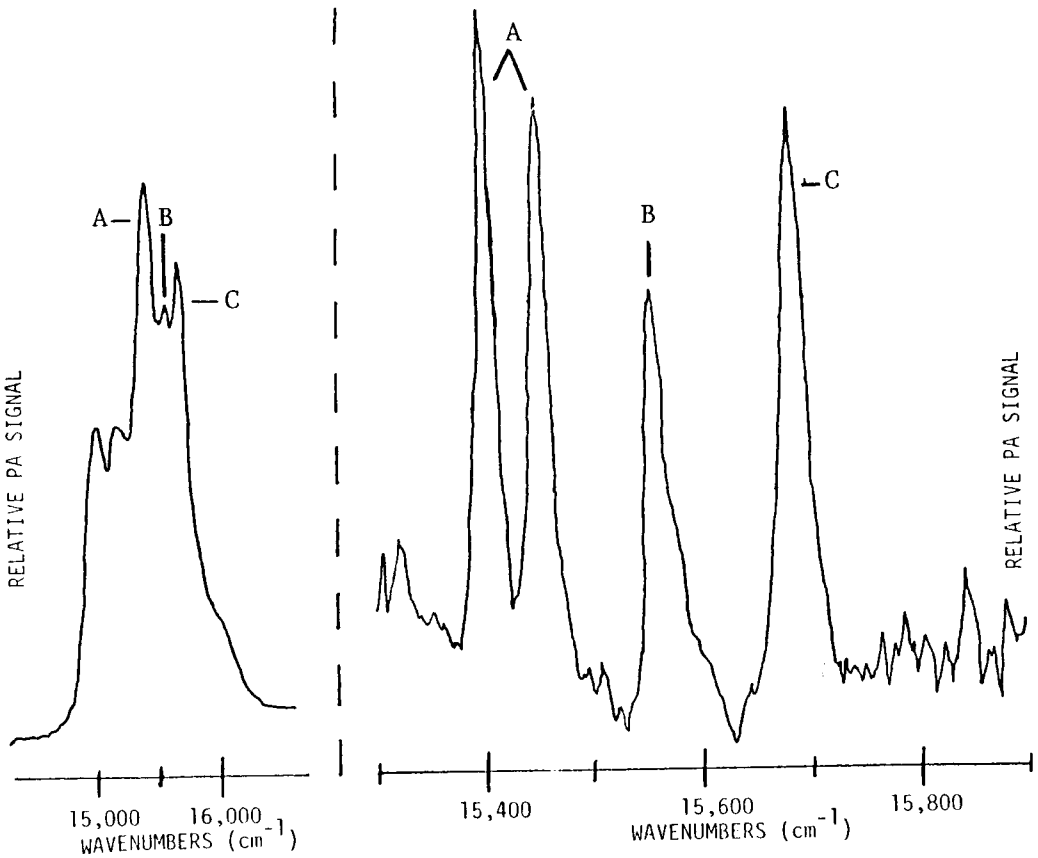


Figure 1. PA spectra of Ho_2O_3 powder at room temperature. Left; Xe-arc/momochromator excitation, 45 cm^{-1} resolution (Courtesy of R. W. Shaw, ORNL). Right; Laser excitation, 3 cm^{-1} resolution (present work). Labelled arrows indicate equivalent bands in each spectrum.

in resolution observed for the laser-excited spectrum is, of course, a direct consequence of the narrow spectral bandwidth of the laser light. Note that the line at ~15,400 cm^{-1} is resolved as a doublet in the laser-excited spectrum, whereas in the broadband excited spectrum it appears as a single line. Although laser excitation can provide very high spectral resolution, because of the experimental difficulty involved in scanning a tunable dye laser over large (> 30-50 nm) ranges, laser-excited PAS is best suited for applications requiring high resolution.

6. Low-Temperature Photoacoustic Spectroscopy

Spectra of low-temperature samples often exhibit enhanced resolution compared with the corresponding spectra of room-temperature samples. This fact is also applicable to PAS, especially when laser excitation is used so that the bandwidth of the excitation source is narrower than the spectral bandwidth(s) of the sample. Other workers have described low-temperature PA measurements. In these cases, detection of the PA signal was accomplished by superconducting bolometers[23-25] and gas microphones.[26-28] At the commencement of the present work, there were no reports of PE detection in low-temperature PAS. Nelson and Patel[29] have recorded PA spectra of the weak absorption features in the 550-750 nm range for liquid ethylene (108 K) and liquid methane (94 K). Recently, a PE transducer has been used in obtaining the laser-excited PA spectrum of Cs_2UCl_6 at 4.2 K.[30]

A class of compounds which seem to be good candidates for study by low-temperature PAS are the polycyclic aromatic compounds. Many of these compounds have very low photo-luminescence quantum

efficiencies,[31] thus indicating a high efficiency for non-radiative decay. This fact makes them well suited for PA detection.

B. Polycyclic Aromatic Compounds - An Environmental Problem

Polycyclic aromatic compounds (PACs) are widely found throughout the environment. Many are known or suspected carcinogens, or precursors to carcinogenic metabolites. PACs are formed from both natural and anthropogenic sources. Natural sources include biosynthesis by certain plants, algae, and bacteria, forest fires, and *in situ* synthesis from degraded biological materials such as fossil fuels (e.g., petroleum, coal, and shale oil). Anthropogenic sources are, however, the predominant contributors of PACs to the environment. This occurrence is primarily due to the incomplete combustion of organic materials,[33] mainly fossil fuels which constitute the large majority of the world's energy sources.[34]

As world energy needs increase, the amount of PACs released into the environment can be expected to increase also. The usage of coal conversion products which have an even higher PAC content than their petroleum counterparts is expected to increase dramatically in the future. Also, the anticipated production of petroleum substitutes from shale oil will provide another avenue of entry for PACs into the environment.[34]

The carcinogenic nature of PACs has been known for many years.[35] This area of study has received considerable attention in recent years because of an increased knowledge about the severity of the problem.[36-39] In terms of carcinogenic activity, more is known

about polycyclic aromatic hydrocarbons (PAHs) than any other type of PAC. However, recent studies have indicated a substantial carcinogenic potential associated with many PACs having $-NH_2$, -OH, -N=O, and -C=O functionalities, and PACs with heteroatoms, such as N, O, and S, substituted into the aromatic ring structure.[40] This latter group is referred to as "heterocyclic PACs" or "heterocycles." Although the presence of a heteroatom in PAC molecules sometimes decreases the carcinogenic activity, there are many instances in which the carcinogenic potency is maintained or even enhanced compared with the parent PAH.[41]

C. Analytical Chemistry of Polycyclic Aromatic Compounds

Because of the increased knowledge of the carcinogenic nature of PACs and the realization of increased dissemination of PACs into the environment, their determination in environmental media has become a high priority analytical problem. The types of environmental samples in which PACs are found vary from those containing only a few components to those containing literally hundreds of components. The complex nature of many environmental samples has mandated the development of sophisticated chemical and instrumental methodologies to provide an adequate means for PAC determinations.

Chromatographic and spectroscopic techniques, or combinations of both, are currently the predominant methods used for PAC determinations. These techniques allow PACs to be identified and quantitated at very low levels (sub-part per million) in complex samples.[33]

1. Chromatographic Methods for PAC Determinations

Chromatographic techniques utilize the physical properties (e.g., vapor pressure, solubility, dipole moment, etc.) of the individual molecules to separate the different molecular species from each other. The separation is monitored by a suitable detector which provides an instrumental response for each component separated.

Gas chromatography (GC) has been effectively used for both qualitative and quantitative determinations of PACs in a wide variety of sample types.[42] The high resolution capability of capillary GC used in conjunction with sensitive detectors allows the detection of dozens of PACs at sub-nanogram levels in a single sample. Highly sensitive GC detection methods include flame ionization, photoionization, electron capture (which is highly selective for compounds containing electronegative atoms), and nitrogen and sulfur selective detectors which respond preferentially to compounds containing these atoms.

High performance liquid chromatography (HPLC) during recent years has also been demonstrated to be a very effective tool for PAC determinations,[42] particularly for thermally labile compounds and those compounds having low vapor pressures at the maximum GC temperatures. Although the chromatographic efficiency in HPLC is not as high as in GC, HPLC is still a very useful method for PAC determinations. Recent advances in capillary HPLC offer the possibility of improved resolution and efficiency. The most common HPLC detectors are the ultraviolet (254 nm) spectrophotometric and fluorescence detectors.

With the chromatographic techniques molecular information is inferred by matching the retention time of an unknown compound with

that of an authentic sample of a known compound. Since any number of compounds could possibly have nearly identical physical properties, and, therefore, equivalent retention times, chromatography cannot in all cases provide unambiguous identification of unknowns. However, if proper safeguards are exercised, this problem can usually be avoided.

Detection in GC by mass spectrometry (MS), although not as sensitive as some other GC detectors, provides a wealth of information unmatched by most other techniques. In addition to the information inferred from the GC retention times, the molecular weight and fragmentation data provided by the MS makes GC/MS a very powerful instrumental method for dealing with complex PAC-containing samples.[42] Combined GC/MS has been used extensively for both qualitative and quantitative PAC determinations.[43-46] Even though GC/MS is a powerful technique, it alone is probably not capable of providing complete characterization of all PAC-containing samples; alternative analytical methods are needed, particularly for samples containing isomeric compounds because mass fragmentation patterns of isomers are often indistinguishable.[33,46]

In addition to the chromatographic methods discussed above, other related chromatographic techniques are often used to fractionate complex PAC-containing samples into less complex sub-groups.[47] This fractionation is usually performed on the basis of chemical class, molecular weight, or other physical properties. These methods include solvent extraction, distillation, preparative GC and HPLC, and conventional adsorption liquid chromatography.

2. Spectroscopic Methods for PAC Determination

Spectroscopic techniques comprise the second main category of methods used for PAC determinations.[48] For PACs the useful spectral ranges are the ultraviolet-visible (UV-VIS) region (200-700 nm) in which electronic transitions occur, and the infrared (IR) region (2-25 μm) in which vibrational transitions occur. The actual nature (i.e., shape, bandwidth, and intensity) of these electronic and vibrational transitions is dependent upon the individual molecules and their surroundings.

The various photophysical processes of PACs which are the basis for the various spectroscopic techniques have been discussed in many sources[31,49,50] and are depicted for a typical PAC in Figure 2.[31] Under normal temperature and pressure (~298 K and ~1 atm), and in the absence of any other external perturbation, almost all PAC molecules will be found in the lowest vibrational level of the electronic ground state, S_0. Absorption of electromagnetic radiation of the appropriate energy (or wavelength) will promote some of the molecules to the higher vibrational levels in S_0 and to the various vibrational levels in the excited electronic states, S_1, S_2, etc. The absorption of electromagnetic radiation occurs at discrete energies, which vary for different compounds, corresponding to the various energy levels of each particular molecule. This discrete absorption of energy gives rise to characteristic spectra which can be used to distinguish different compounds from each other.

In the UV-VIS region PACs can be determined at the 10^{-5}-10^{-6} M level in room-temperature liquid solutions by conventional absorption

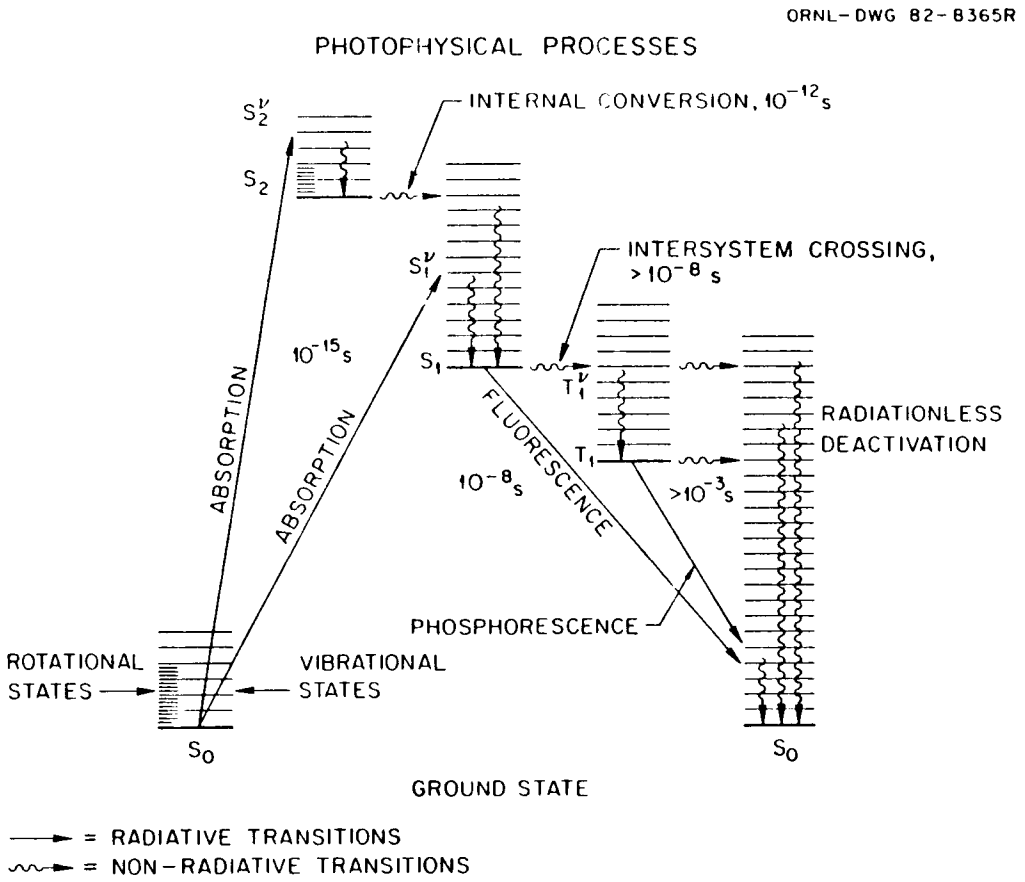


Figure 2. Photophysical processes of a typical PAC. N. J. Turro, "Modern Molecular Photochemistry", Benjamin/Cummings, Menlo Park, Calif., 1978.

measurements. However, due to the somewhat broad nature of the spectral bands, multi-component analysis is difficult. IR absorption spectra of PACs at room temperature, on the other hand, are generally much sharper than UV-VIS absorption spectra. Thus, IR absorption is better suited for multi-component samples at room temperature. Unfortunately, IR absorption measurements are less sensitive than UV-VIS absorption by a factor of ~100-1,000; typical IR detection limits for PACs are ~10^{-4}M.[51] The detection limits for both methods are determined by the smallest detectable difference in the amount of light transmitted by the sample. However, despite the higher spectral resolution for IR absorption than for UV-VIS absorption at room temperature, there is a finite limit to the number of components that can be resolved within a mixture. Adequate resolution for some mixtures, particularly of isomeric compounds, can only be achieved in low-temperature samples. Neither absorption method possesses the selectivity (or resolution) necessary to adequately characterize complex samples in room-temperature solution media.[52]

As noted previously, absorption of a UV-VIS photon of the appropriate energy will promote a molecule to any of the various vibrational levels in the excited electronic states (S_1, S_2, etc.). The molecule will then undergo rapid ($< 10^{-12}$ s) internal conversion to the lowest vibrational level of S_1 by the liberation of thermal energy. From this point the molecule may undergo further de-excitation by several paths: termination in S_o by re-emission of a photon by fluorescence ($S_1 \rightarrow S_o + h\nu$) or internal conversion by the liberation of thermal energy ($S_1 \sim\!\!\rightarrow S_o + kT$), or intersystem crossing by liberation of thermal

energy to an energy level in the triplet domain ($S_1 \rightarrow T_n \sim\!\!\!\rightarrow T_o$ + kT). For most PACs, internal conversion from S_1 to S_0 ($S_1 \sim\!\!\!\rightarrow S_0$ + kT) is a relatively slow process (~10^{-6} s) compared with fluorescence (10^{-8}-10^{-9} s) and intersystem crossing (10^{-8}-10^{-9} s), so that the latter two processes, fluorescence and intersystem crossing, are usually the predominant modes of de-excitation of S_1.[53]

As discussed above, fluorescence is one of the predominant photophysical processes for many PACs, in particular the PAHs and PAHs with -OH, $-NH_2$, and alkoxy substituents.[54] As in the case of absorption spectra, fluorescence spectra provide a molecular fingerprint and, thus, a means of identification for different compounds. Fluorescence spectrometry can be more sensitive than conventional UV-VIS absorption due to the fact that the fluorescence intensity is proportional to the absolute number of photons absorbed, rather than the relative amount of light transmitted by the sample as in absorption measurements. Hence, the fluorescence intensity increases as the light intensity of the excitation source is increased. This advantage allows fluorescence detection limits to be several orders of magnitude lower than those obtained by UV-VIS absorption. However, spectral resolution in room-temperature fluorescence is not significantly greater than that of room-temperature UV-VIS absorption; thus it is also rather limited for complex sample analyses.[52]

As an alternative to returning to S_0 from S_1 by fluorescence or internal conversion, a molecule may undergo intersystem crossing to the triplet domain. This is a predominant process for many PACs,[55] especially those containing N-, O-, and S- hetero-atoms, -C=O, -Br, and

-I substituents, and a few PAHs.[56] The presence of paramagnetic species and heavy atoms (e.g. Br, I, Xe, Pb, etc.) external to (but in the immediate surroundings of) an electronically excited PAC molecule is also known to enhance intersystem crossing for many PACs.[55]

Just as in the excited singlet states, a molecule initially arriving in a higher energy triplet state by intersystem crossing from the singlet domain undergoes rapid internal conversion by the liberation of heat to the lowest vibrational level in T_1 ($T_n \curvearrowright T_1 + kT$). At this point the molecules will usually return to the ground singlet state, S_0, by one of two paths: emission of a photon by phosphorescence ($T_1 \rightarrow S_0 + h\nu$) or intersystem crossing via liberation of thermal energy ($T_1 \curvearrowright S_0 + kT$). Because the lifetime of T_1 is $> 10^{-3}$ s, phosphorescence is usually not observed unless the molecule is "locked" into a rigid medium to prevent collisional deactivation. Otherwise the T_1 energy is liberated as thermal energy through collisional deactivation.

The de-excitation of excited states by photon emission, referred to as "radiative processes," gives rise to the phenomenon of photoluminescence (a collective term for fluorescence and phosphorescence). Although discussed above for PACs in particular, fluorescence and phosphorescence are not limited to PACs. Luminescence is observed for many other species.[57]

There are many PACs (as well as other molecules) which are weakly or non-luminescent, indicating that excited state de-excitation occurs predominantly via non-radiative (or radiationless) pathways. These non-photon emitting processes liberate the excited state energy as

thermal energy, or heat. Some classes of molecules for which excited-state decay is predominantly non-radiative include N- and S-heterocycles, aromatic carbonyl compounds, and halogenated (Br, I) and partially hydrogenated PACs. The thermal deactivation pathways form the basis of photoacoustic spectroscopy. Thus, photoacoustic spectroscopy serves as a complementary technique to molecular fluorescence and phosphorescence spectrometry.

3. Enhancement of Spectral Resolution and Selectivity

As noted above, the rather broad nature of UV-VIS absorption and fluorescence spectra makes PAC determinations difficult in complex samples at room temperature. Consequently, various techniques have been developed to improve the selectivity of the spectroscopic techniques or to enhance the spectral resolution of the sample, or both.[48] Those procedures falling into the first category include synchronous luminescence and derivative spectroscopy. The second category consists primarily of low-temperature sampling techniques.

In synchronous luminescence,[58] the excitation (or absorption) and emission wavelengths are simultaneously scanned at a fixed wavelength interval. Instead of a broad, multi-band spectrum as typically observed for PACs by conventional absorption or emission, the "synchronous" spectrum usually consists of a sharper single band in the region near the absorption-fluorescence origin. Acquisition of such a simplified spectrum generally improves the selectivity for unknown PACs in mixtures in liquid solution. Although this technique has a limited ability to deal with very complex samples, it has been shown to be a

very useful technique for the rapid screening of samples for certain specific components.

Derivative spectroscopy[59] involves the measurement of the first or higher derivative of the absorption or luminescence with respect to wavelength. The advantage of this method is that it is possible to resolve or enhance small peaks that are normally unresolved from larger peaks. Derivative spectroscopy has also been applied to synchronous luminescence for the determination for PACs.[60]

For spectroscopic analysis, perhaps the most commonly used method for dealing with complex samples relies upon enhancement of spectral resolution via low-temperature sampling techniques.[32,61] The two most important of these are frozen "Shpol'skii" solutions and matrix isolation.

When frozen in a suitable solvent at 77 K or below, many PACs exhibit much sharper absorption and luminescence spectra than are observed for room temperature liquid solutions. In particular, high resolution fluorescence spectra have been obtained for many PACs in frozen n-alkane solvents in which the molecular dimension of the PAC matches that of the n-alkane. This observation was originally made by Shpol'skii, et al.,[62] and has become known as the "Shpol'skii effect."

Experimentally, this technique is very simple because it only entails quench freezing the sample in a liquid N_2 or liquid He bath. However, Wehry, et al.[61] have pointed out some important disadvantages of this technique. First, different solvents are optimum for different solutes in terms of yielding the maximum spectral bandwidth

reduction. Second, spectral bandwidth reduction depends on experimental variables such as the freezing rate, final temperature of the sample, and sample concentration. Finally, background fluorescence from impurities is often a problem in organic solvents. But, despite these disadvantages, frozen solution fluorescence has proven to be a very simple and reliable method of PAC analysis. Kirkbright, et al. have made a thorough study of the analytical capability of this technique.[63-65]

Another low-temperature spectroscopic sampling technique which has been applied to PAC analyses is matrix isolation (MI). In MI, the analyte species (or guest) is mixed in the vapor phase with a large molar excess of the matrix (or host), and the resulting mixture is condensed onto a cryogenically-cooled surface to give a solid spectroscopic sample. The main purpose in MI is to reduce as much as possible guest-guest and host-guest interactions which may lead to undesirable spectroscopic properties such as band broadening, energy transfer, and quenching. Depending upon the type of spectroscopy performed and the nature of the guest, the host-guest molar ratio may range from 10^2 to 10^8.

MI was first introduced in 1954 by Pimentel, et al.[66] as a sampling method for trapping short-lived species. Since then, MI has been used in conjunction with many spectroscopic techniques such as IR, Raman, UV-visible absorption, fluorescence and phosphorescence, and mass spectrometry. Several monographs describing the experimental principles and spectroscopic applications of MI are available.[67-69]

The analytical applications and advantages of MI as a spectroscopic sampling technique for fluorescence and Fourier Transform Infrared (FTIR) spectroscopy have been reviewed by Wehry and Mamantov.[52] They compare the properties of a MI sample to an ideal spectroscopic sample which should provide the following spectral characteristics. First, the spectrum should be a simple, but unambiguous, fingerprint for each compound. Second, for qualitative and quantitative purposes, the appearance of the spectrum (i.e., wavelength maxima) and the quantitative constants (e.g., molar absorptivity and quantum yields) should be totally independent of the nature of the original sample. This requirement necessitates that the analyte always "see" the same environment. Finally, the optical properties of the sample must be compatible with the spectroscopic technique to be used. Although a MI sample is in reality not an ideal sample, it is remarkable how closely it comes to satisfying the above criteria for FTIR and fluorescence spectroscopy.

MI fluorescence and FTIR spectroscopy yield highly resolved spectra of many PAHs, showing a considerable enhancement in spectral resolution compared with spectra obtained by conventional room-temperature sampling techniques.[52] This fact is important for the identification of individual components of multi-component samples, and particularly for the identification of isomeric compounds. The detection limits for PACs are typically < 500 ng by MI-FTIR[52,70] and ca. 0.01 ng by MI-fluorescence.[52] These detection limits are, for both cases, determined by the relevant optical properties of the

analyte and its matrix, and the instrumental nature of the signal measurement for the respective techniques.

Several spectroscopic methods for PAC determinations have been developed which employ both low-temperature sampling techniques for improved spectral resolution and strategies for enhanced molecular selectivity. Narrow-band (i.e., laser) excitation into the origin of the S_1 absorption band of some PACs in low-temperature samples (such as those described above) gives rise to extremely narrow fluorescence emission spectra.[71] Whereas broadband excitation produces spectral bandwidths on the order of 50 cm^{-1}, narrow-band excitation produces spectral bandwidths from ~2-10 cm^{-1}. This occurence is referred to as "site selection," "fluorescence line narrowing," or "selective energy excitation."

4. Photoacoustic Spectroscopy of Polycyclic Aromatic Compounds

The PA detection limits and quantitative working curves for a number of PACs (mostly PAHs) in room-temperature liquid solutions have been reported.[72] Pulsed laser excitation and PE detection were employed. The pulsed laser excitation was performed at a fixed wavelength; consequently, no spectra were reported.

Recently (since the initiation of the present work), there has been one report of PAS of PACs in a low-temperature sample. Lai, et al.[73] have obtained a PA spectrum of 9,10-dimethylanthracene (10^{-4} M) in a frozen n-heptane solution at 77 K. The spectrum had a signal-to-noise ratio of ~2; however, it did seem to correspond to the fluorescence excitation spectrum of the same solution. PA spectra were not reported for any other compounds.

D. Purpose of the Present Work

The primary purpose of the present work was to explore the analytical utility of PAS for the determination of matrix-isolated PACs, particularly those which are weakly fluorescent or non-fluorescent. The fact that these compounds exhibit weak or no fluorescence indicates that non-radiative processes dominate their excited state photophysics, thus making them ideal candidates for PAS. Matrix-isolation sampling for PACs was employed to provide an enhancement of spectral resolution (for the sample) that is necessary for analysis of multi-component samples. The ability to obtain PA spectra for other low-temperature samples, such as rare-earth compounds and PACs in frozen solutions (77 K), was also investigated. PE transducers were evaluated for use as low-temperature PA detectors.

CHAPTER II

EXPERIMENTAL DETAILS

A. Materials

1. Gases and Cryogenic Fluids

Nitrogen (99.997 %), argon (99.997 %), and helium (99.99 %) gases, and liquid nitrogen were obtained locally at the Oak Ridge National Laboratory (ORNL). Xenon (99.9 %) gas was obtained in one liter glass flasks from the Linde Division of Union Carbide (New York, NY) and Air Products (Allentown, PA). Liquid helium was obtained in 30 liter storage Dewars from the Linde Division of Union Carbide (Knoxville, TN).

2. Rare Earth Compounds

Neodymium hydroxide ($Nd(OH)_3$, 99.9 %) was obtained from the Michigan Chemical Co. (St. Louis, Mich.). Holmium oxide (Ho_2O_3, 99.9 %) was obtained from R. W. Shaw, ORNL.

3. Polycyclic Aromatic Compounds

The polycyclic aromatic compounds (PACs) studied, including their sources and molecular structures, are presented in Table II-1. Unless otherwise noted, the manufacturers' specified purity was > 98 %.

4. Laser Dyes

The various laser dyes used in the present work are listed in Table II-2. Also shown in Table II-2 are the useful wavelength ranges for the dyes in the visible (fundamental) and UV (second harmonic)

TABLE II-1

POLYCYCLIC AROMATIC COMPOUNDS STUDIED

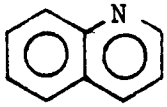
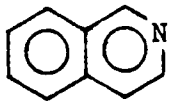
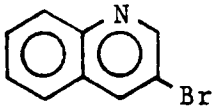
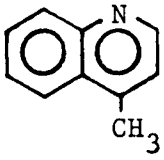
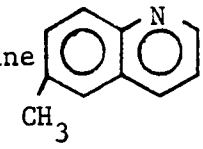
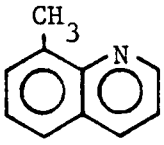
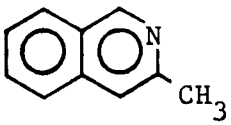
Compound	Structure	Source[a]	MI Deposition Temperature, °C
Quinoline		Aldrich	-25°
Isoquinoline		Aldrich	-25°
3-bromoquinoline		Aldrich	-10°
4-methylquinoline		Aldrich	-25°
6-methylquinoline		Aldrich	-15°
8-methylquinoline		Aldrich	-15°
3-methyl-isoquinoline		Aldrich	-15°

TABLE II-1 (Continued)

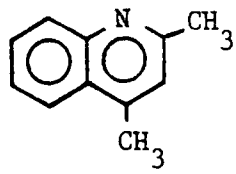
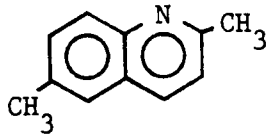
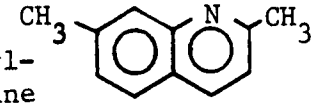
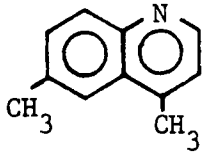
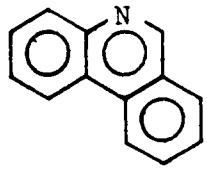
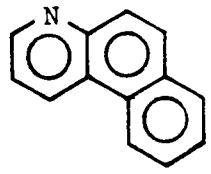
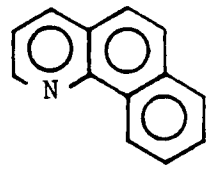
Compound	Structure	Source[a]	MI Deposition Temperature, °C
2,4-dimethyl-quinoline		Aldrich	-15°
2,6-dimethyl-quinoline		Aldrich	-5°
2,7-dimethyl-quinoline		Aldrich	-5°
4,6-dimethyl-quinoline		Aldrich	-5°
3,4-benzo-quinoline		Aldrich	+40°
5,6-benzo-quinoline		Aldrich	+40°
7,8-benzo-quinoline		Aldrich	+40°

TABLE II-1 (Continued)

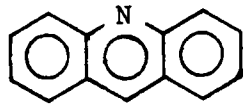
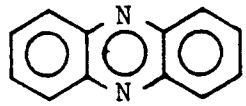
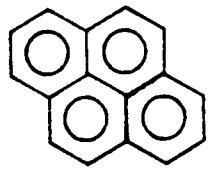
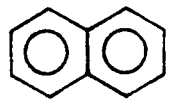
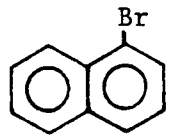
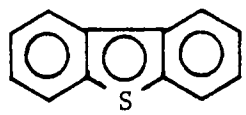
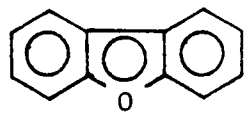
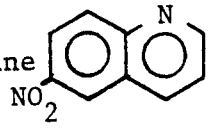
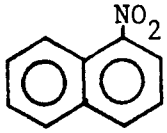
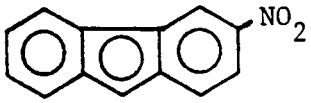
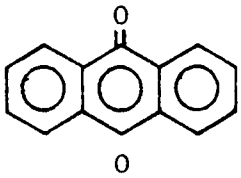
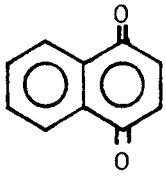
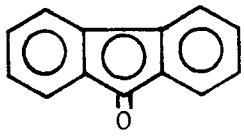
Compound	Structure	Source[a]	MI Deposition Temperature, °C
Acridine		Aldrich	+40°
Phenazine		Aldrich	+40°
Pyrene		Aldrich	+45°
Naphthalene		Fisher	-25°
1-bromo-naphthalene		Aldrich	-10°
Dibenzothiophene		MCB	+45°
Dibenzofuran		Aldrich	+35°

TABLE II-1 (Continued)

Compound	Structure	Source[a]	MI Deposition Temperature, °C
6-nitroquinoline		Eastman	0°
1-nitro-naphthalene		Eastman	0°
2-nitrofluorene		RFR	+40°
Anthraquinone		MCB	+50°
1,4-naphtho-quinone		Eastman	+30°
9-fluorenone		Eastman	+45°

[a]Aldrich Chemical Co., Milwaukee, WS; Fisher Scientific, Fair Lawn, NJ; (MCB) Matheson, Coleman, and Bell, Norwood, OH; Eastman Kodak Co., Rochester, NY; RFR Corp., Hope, RI.

TABLE II-2

LASER DYES

Dye	Source[a]	Wavelength Ranges, nm Visible	UV
Sulforhodamine 640	Exciton	692-648	345-326
Rhodamine 640	Exciton	685-640	340-322
Kiton Red 620 in Ammonyx-Lo/H_2O[b]	Exciton	660-625	328-315
Kiton Red 620 in MeOH/H_2O	Exciton	655-620	325-315
Rhodamine 6G in Ammonyx-Lo/H_2O[b]	Eastman	638-600	316-302
Rhodamine 6G in MeOH/H_2O[b]	Eastman	625-580	310-295
Rhodamine 575	Exciton	610-575	302-290
Coumarin 504	Exciton	550-505	not used
Coumarin 102	Eastman	520-470	not used

[a]Exciton Chemical Co., Inc., Dayton, OH; Eastman Kodak Co., Rochester, NY.

[b]Ammonyx-Lo is an organic surfactant.

regions, and their commercial sources. All laser dye solutions were made according to the laser manufacturer's recipe, except for Kiton Red 620 in methanol/H_2O and Sulforhodamine 640 (see Table II-2). It was found experimentally that the useful lasing range for Kiton Red 620 could be extended ~5-6 nm in the shorter wavelength direction by using a 1:1 v:v methanol/H_2O solvent instead of the solvent recommended by the manufacturer (Ammonyx-Lo/H_2O; Ammonyx-Lo is an organic surfactant). This small wavelength shift was useful for providing a higher laser pulse energy output in the UV region around 315 nm where both Rhodamine 6G in Ammonyx-Lo/H_2O and Kiton Red 620 in Ammonyx-Lo/H_2O have low pulse energies. The laser manufacturer, Chromatix, also had not specified the use of Sulforhodamine 640. Upon the suggestion of the dye vendor, Exciton Chemical Co., Suforhodamine 640 was used in the same solvent (1:1 v:v methanol/H_2O) and at the same molar concentration as Rhodamine 640.

5. Solvents

Reagent grade methanol, toluene, and glycerine were obtained from Fisher Scientific Co. (Fair Lawn, NJ). Reagent grade heptane, hexane, and acetone were obtained from Mallinkrodt, Inc. (Paris, KY), Ammonyx-Lo concentrate (no specified purity), used to prepare laser dye solutions, was obtained from Chromatix (Sunnyvale, CA) and Onyx Chemical Co. (Jersey City, NJ). All solvents, including laboratory distilled water, were used as obtained without further purification.

6. Miscellaneous

Super-Glue (Loctite Corp., Cleveland, OH) was used on several occasions for bonding the ceramic PZT (PE transducer) for

room-temperature PA measurements (Super-Glue was dissolved by acetone). "Versamid 140" - polyamide epoxy glue (General Mills Chemical, Inc., Minneapolis, Minn.) was used for bonding the ceramic PZTs for low-temperature PA measurements ("Versamid-140" was softened/dissolved with methylene chloride). Rubber cement (The Carter Ink, Co., Waltham, Mass.) was used to prepare room-temperature, solid-matrix samples for some PACs (The rubber cement was soluble in toluene). All low-temperature solder joints were made with indium/silver solder, 90:10 atomic-percent (Indium Corp. of America, Utica, NY, Alloy solder #3/Indalloy Flux No. 5-Mildly Activated Rosin).

B. Equipment

1. Cryostats

Three different cryostats were used for the low-temperature PAS and UV absorption measurements. The first one, which was used for the low-temperature PAS of $Nd(OH)_3$, was a variable temperature cryostat (Janis Research Co., Stoneham, Mass., Model DT). Temperature measurement and control were achieved by use of a temperature controller (Lake Shore Cryotronics, Westerville, OH, Model DTC-500). The cryostat had a ~3 liter liquid helium reservoir which was thermally insulated by vacuum and liquid nitrogen shields.

The $Nd(OH)_3$ sample and PA detector (described below) were aligned with the optical windows of the cryostat, positioned just above a heated orifice block maintained at 5 K by the temperature controller. A vaporized stream of liquid helium flowed through the heated orifice block cooling the sample and PA detector. The temperature of the $Nd(OH)_3$ sample and PA detector were held at 6-8 K for spectral

measurements by adjusting the flow of the cold helium gas with a needle valve, and by applying a partial vacuum to the sample chamber of the cryostat. A complete filling of the ~3 liter liquid helium reservoir provided 3-4 hours of operation at 6-8 K.

The second cryostat used was a closed-cycle refrigerator (CTI Cryogenics, Waltham, Mass., "Spectrim" model) which used helium gas supplied by a compressor (CTI Cryogenics, Model 21-SC). Stroupe[74] has given a detailed description of this cryostat. Basically, it was a dual expansion stage, closed-cycle refrigerator system which used helium gas as the refrigerant. The cryostat had a variable temperature cold finger with a sample window mount. The cryostat could lower the temperature of the window mount to ~10 K. Initially, it was hoped that this cryostat could be used for PAS work because of its ease of operation. However, mechanically induced vibrations of the PE transducer (i.e., acoustical noise) produced by the refrigerator drive motor were too severe (even at frequencies up to 500 kHz) for this cryostat to be used for MI-PAS measurements. This cryostat was useful for obtaining absorption spectra of MI samples.

The third cryostat used, primarily for MI-PAS measurements, was a flowing liquid helium cryostat (Air Products, Allentown, PA, Model LT-3-10 "Heli-Tran", cooling capacity 0.5 W at 4.2 K). Acoustical noise due to mechanical vibrations was not a significant problem with this cryostat; thus it could be satisfactorily used for PAS measurements. Gore[75] has thoroughly described the operation of this cryostat. Briefly, it consisted of a dual-jacketed liquid helium transfer line connected to a cold finger with a threaded mount for

attaching a sample window. The transfer line was thermally insulated by a vacuum jacket. Liquid helium was passed from a storage Dewar through the transfer line to the cold finger. Metering valves on the exit vents of the helium flow and a needle valve regulated the temperature of the cold finger. This cryostat was capable of cooling the sample window to 4.2 K; however, it was usually operated at 5-20 K. The sample window and PA detector used with this cryostat are described below. Six or seven MI deposits could be made per 30-liter Dewar of liquid helium.

Temperature measurement of the closed-cycle and flowing liquid helium cryostats was made by a digital temperature indicator/controller (Air Products, Model ADP-E) using a chromel vs. gold - 0.07 atomic-percent iron thermocouple. A cryogenic heater (Air Products, No. 250-294A) was used in combination with the temperature indicator/controller for the flowing liquid helium cryostat in order to hasten the warm-up time of the cold finger after spectral examination of a MI sample.

2. Vacuum Line

A vacuum line was constructed for storing and dispensing the matrix gases that were used for preparing MI samples. The general requirements for a matrix gas/vacuum line have been discussed by Meyer,[67] Hallam,[68] and Cradock and Hinchcliffe.[69] The one used in the present work was similar to the ones used by Garrison,[76] Stroupe,[74] and Gore,[75] and is diagrammed in Figure 3. It was constructed from 1/4" o.d. copper tubing joined to high vacuum bellows seal valves (Nupro Co., Willoughby, OH, Model B4H-K). A Bourdon-type vacuum gauge (Ametek, Inc., U.S. Gauge Division, No. 33002) was used to

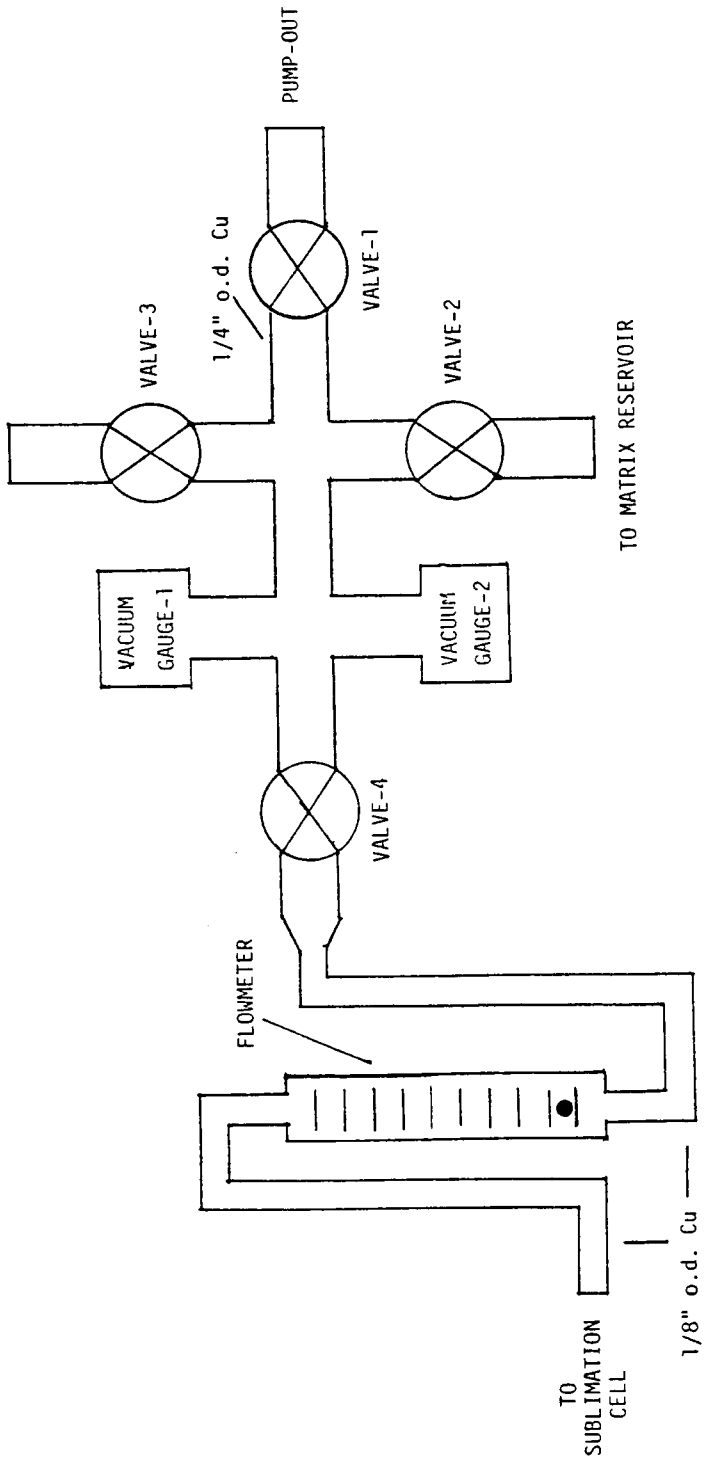


Figure 3. Diagram of the matrix gas-vacuum line.

measure the pressure (~40-700 torr) when the vacuum line was charged with matrix gas, and a vacuum thermocouple gauge (Hastings Instrument Co., Inc., Hampton, VA, Model DV-3M) was used to measure the low pressures (~10^{-2} torr) when the line was evacuated. All joints in the vacuum line were brazed with solid wire solder because adequate vacuum could not be maintained when standard compression fittings were used. When the vacuum line was evacuated to 10^{-2} torr and closed off from the vacuum pump (Welch Scientific Company, Skokie, IL, Model 1402), the leak rate was measured to be ~10^{-2} torr/day.

Matrix gases were stored in 1 liter glass bulbs sealed off with vacuum stopcocks (Kontes, Vineland, NJ, Model 826510-0004). The bulbs containing the various matrix gases could be easily connected to and disconnected from the vacuum line at Valve-2 (Fig. 3, p. 36) with high vacuum couplings (Cajon, Co., Macedonia, OH, Model B-UT-6). When exhausted, the matrix-gas bulbs were recharged (filled-evacuated three times) through Valve-3 (Fig. 3, p. 36).

A flow meter (Lab Crest Division of Fischer & Porter Co., Warminster, PA, Model 448-001) was connected between the vacuum line and the cryostat matrix-gas inlet in order to provide a means for a reproducible delivery rate of matrix gas during MI depositions. The flow meter was connected to the vacuum line and cryostat matrix-gas inlet by 1/8" o.d. copper tubing (with 1/4" o.d. brass tubing at the ends) in conjunction with vacuum couplings (Cajon, Co., Model B-UT-6). The flow meter was not used to measure (in absolute terms) the amount of matrix gas dispensed during MI depositions. This determination was

calculated by simple gas law relationships using partial pressure readings from the Bourdon-type vacuum gauge.

3. Sublimation Cells

The main type of sublimation cell used to vaporize PACs for MI depositions is shown in Figure 4. This type of cell was used in the previous MI work of Stroupe[74] and Gore.[75] A Kontes (Model 826510-0004) vacuum stopcock was modified to have a 1/4" o.d. inlet connection for the matrix gas, a well for the PAC sample, and a capillary tube to direct the vaporized PAC/matrix gas mixture toward the spectroscopic window. The capillary tube had an ~1 mm opening, and was sheathed with a 3/8" o.d. glass sleeve which protected it from breakage and allowed it to be inserted into the cryostat through a Cajon "Ultra-torr" adapter (No. B-6-UT-A-8BT) that was soldered to a copper window plate. This design allowed the cell to be moved back and forth while the cryostat was under vacuum. The capillary tube could be placed near (5-10 mm) the spectroscopic window during MI deposition and then pulled back out of the way when performing spectroscopic measurements.

A coolant bath was placed around the outside of the sample well to prevent the PAC sample from being pumped away during the cryostat cool-down period and to control the vapor pressure of the sample during MI deposition. This procedure is discussed in more detail below. The sample well and capillary tube were wrapped with nichrome heating wires when needed to vaporize samples that required above-ambient temperatures for MI deposition. The heating wire around the sample well was held in place with masking tape and wrapped with Laboratory

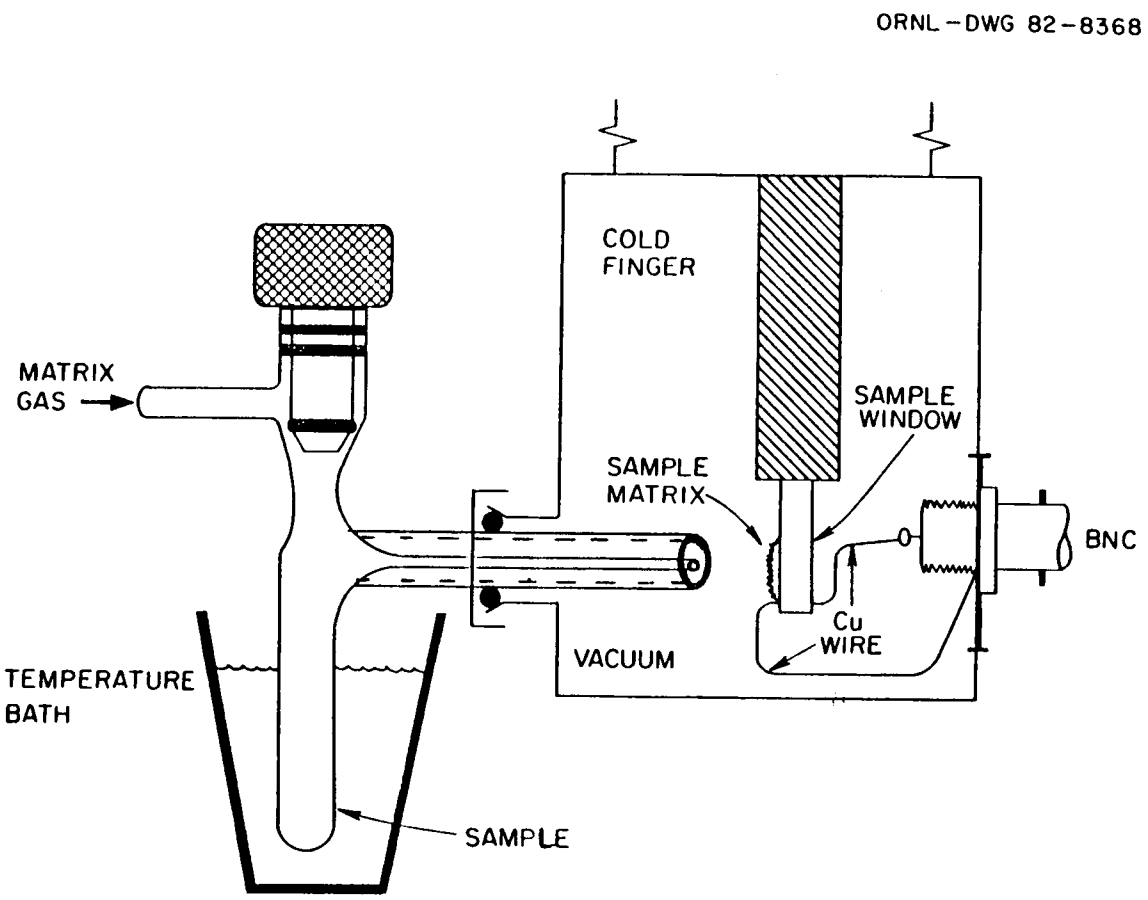


Figure 4. Diagram of the sublimation cell used for preparing MI samples.

Parafilm to prevent wetting by the temperature bath. Vacuum feedthroughs (Ceramaseal, New York, NY, No. 807A9297-1) were soldered into the copper window plate to provide electrical connection for the heating wire that surrounded the capillary tube.

4. PE Transducers

Two types of piezoelectric (PE) transducers were employed in the present work. One type was X-cut crystalline quartz (Valpey-Fisher Corp., Hopkinton, Mass.) obtained in 25 mm diameter discs with a thickness of 1.9 mm which corresponded to a natural resonance frequency for the thickness mode of 1.0 MHz. For use in MI-PAS experiments, the size of one piece was modified to 13 mm x 22 mm (no change in thickness) by the ORNL glass-shop. The reported PE sensitivity for the thickness mode, g_{11}, is 0.057 V m N^{-1} and the reported sensitivity for the shear mode, g_{14}, is 0.021 V m N^{-1}.[77] Both values vary $< \pm 10$ % over the temperature range of 5-300 K.[77,78] The relative dielectric constant, ε_{11}, is 4.6 and varies $< \pm 2$ % over the same temperature range.[79]

The other type of PE transducer used was a lead-zirconate-titanate (PZT) material (Edo Western Corp., Salt Lake City, Utah, type EC-65). The PZT was obtained as discs of three different thicknesses, 3.0, 1.6, and 0.89 mm, which corresponded to resonance frequencies for the thickness mode of 0.60, 1.1, and 2.0 MHz, respectively. The respective diameters of the discs were 7, 9, and 9 mm which corresponded to shear resonance frequencies of 285, 210, and 210 kHz. The PZT material had a specified thickness mode PE sensitivity, g_{33}, of 0.025 V m N^{-1} at 298 K and 0.033 V m N^{-1} at 10 K. The specified shear mode sensitivity, g_{31}, was 0.011 V m N^{-1} m at 298 K and 0.013 V m N^{-1} at 10

K.[16] The specified value of the dielectric constant, ε_{33}, was 1700 at 298 K and 310 at 10 K.[16] Each PZT disc had a thin silver film electrode on each face for efficient collection of the electrical charges.

5. PA Detectors

Several PA detector designs which used either X-cut quartz or PZT PE transducers were used in the present work. The one used for room-temperature PA measurements is shown in Figure 5. It consisted of two aluminum blocks clamped together with metal screws. The blocks were used to compress a PZT disc against one end of a 2-4 mm thick glass (or fused quartz) plate having the spectroscopic sample located at the other end of the plate. Upon laser excitation, the acoustic wave generated in the sample was transmitted through the glass plate to the PZT disc. A piece of thin brass foil was placed between the glass plate and the PZT disc in order to extract the PE signal from one face of the PZT disc. The other face of the PZT disc was in contact with the aluminum block which served to extract the PE signal from that face. A micro-dot connector was threaded into one of the aluminum blocks in order to connect a miniature coaxial cable (RG-174-U). A thin layer of Nonaq stopcock grease (Fisher Scientific Co.) was applied at each interface in order to maximize acoustical transmission at each interface.

The PA detector used to obtain low-temperature PA spectra of $Nd(OH)_3$ (taken in the Janis liquid helium cryostat) is shown in Figure 6. A two-piece clamp held together by nylon screws compressed a PZT disc against a fused quartz substrate upon which the $Nd(OH)_3$ sample was

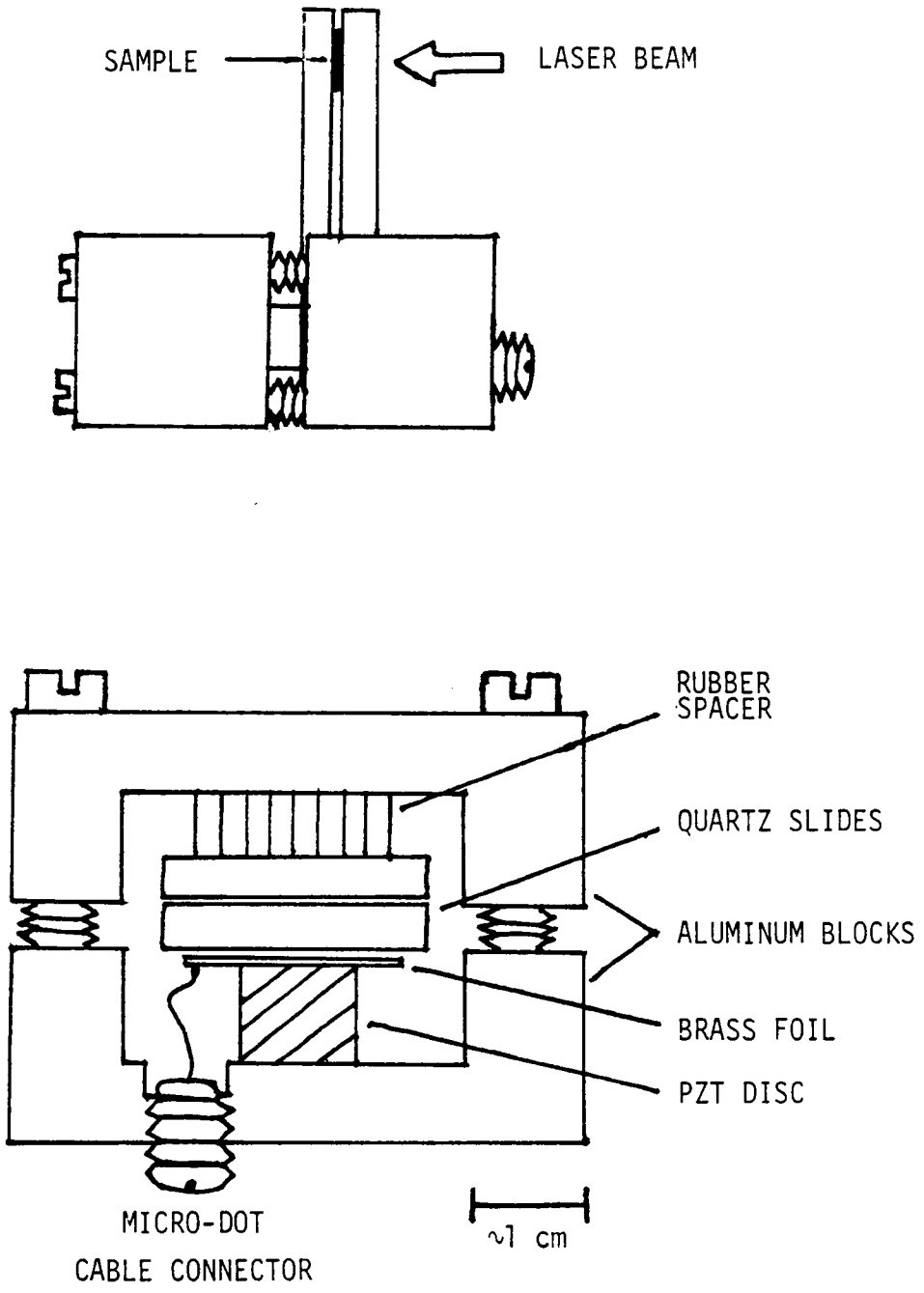


Figure 5. Diagram of the PA detector used for room-temperature solids.

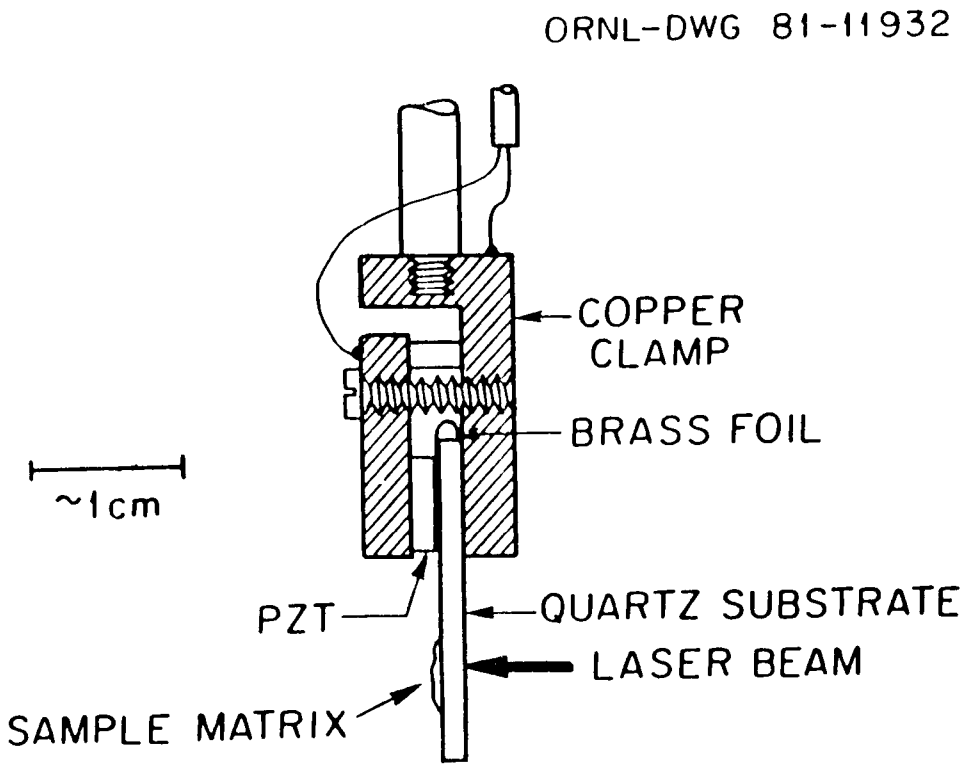


Figure 6. Diagram of the low-temperature PA detector used to obtain spectra of $Nd(OH)_3$ powder at 6-8 K.

located. A teflon block of the proper thickness was positioned opposite the PZT disc in order to prevent uneven compression of the PZT disc. A germanium resistance thermometer (not shown, Texas Instruments Co., Dallas, TX, type 106-model 341) was threaded into the top of the larger copper clamp half in order to monitor the temperature of the PA detector assembly. A thin brass foil was looped over the quartz substrate to electrically connect one face of the PZT disc to the larger copper clamp half. The smaller half of the copper clamp directly contacted the other PZT disc face. A miniature coaxial cable (RG-174/U) was used to connect the copper clamp halves (i.e. pick-up electrodes) to electrical feedthroughs at the top of the cryostat sample chamber. Nonaq stopcock grease filled with finely divided silver powder was used at all interfaces. Initially, it was thought that the addition of the silver powder to the grease was necessary to maintain electrical contact. However, it was later realized that a thin layer of grease alone was adequate. Therefore, in later experiments the silver powder was not used. Apparently, the thin film of grease had a sufficiently low electrical impedance to pass the high frequency (0.1-1.0 MHz) PE signals.

A similar design was initially used for PA measurements of matrix-isolated PACs. It was similar to the design used for the low-temperature $Nd(OH)_3$ samples, except for several modifications. The PZT disc was placed between the two nylon screws so that a teflon spacer block was not needed, a 1.6 mm thick sapphire sample window (12 x 22 mm) replaced the quartz sample window in order to provide higher thermal conductivity (10 vs. 0.0015 W cm^{-1} K^{-1}),[67] and the larger

half of the copper clamp was made to be threaded into the cold finger of the Air Products flowing liquid helium cryostat. Both copper clamp halves were made from oxygen-free copper and coated with a ~1 μm thick aluminum film to reduce the PA background signal produced by scattered UV laser light. The aluminum coating was prepared at ORNL by a plasma sputtering technique. Nonaq stopcock grease was used at all interfaces, and an indium gasket was placed between the sapphire sample window and the larger copper clamp half to ensure adequate thermal contact to the cryostat cold finger.

The PA detector used for MI-PAS was further modified in order to reduce the number of acoustical interfaces between the sample and PZT disc. This design is shown in Figure 7. The smaller clamp half was made from aluminum and evenly compressed a 3 mm thick PZT disc (7 mm diameter) at the disc perimeter. The area of the aluminum block covering the center of the PZT disc was open so that the center area of the disc (65 % of the total area) was not compressed. An aluminum film (prepared at ORNL by plasma sputtering) of ~1 μm thickness covered the area of the sapphire window surface contacted by the PZT disc. The aluminum film (contacted to a wire by a small spring) and the aluminum clamp half served as the pick-up electrodes for the PE signal. With this design, there was only one thick acoustic interface (made with Nonaq stopcock grease) between the PZT disc and the sapphire sample window, whereas in the earlier design, there were two.

A final design modification was made in which one face of a 3 mm thick PZT disc was glued directly to the aluminum film on the sapphire window with "Versamid-140"-polyamide epoxy (p. 33). This design is

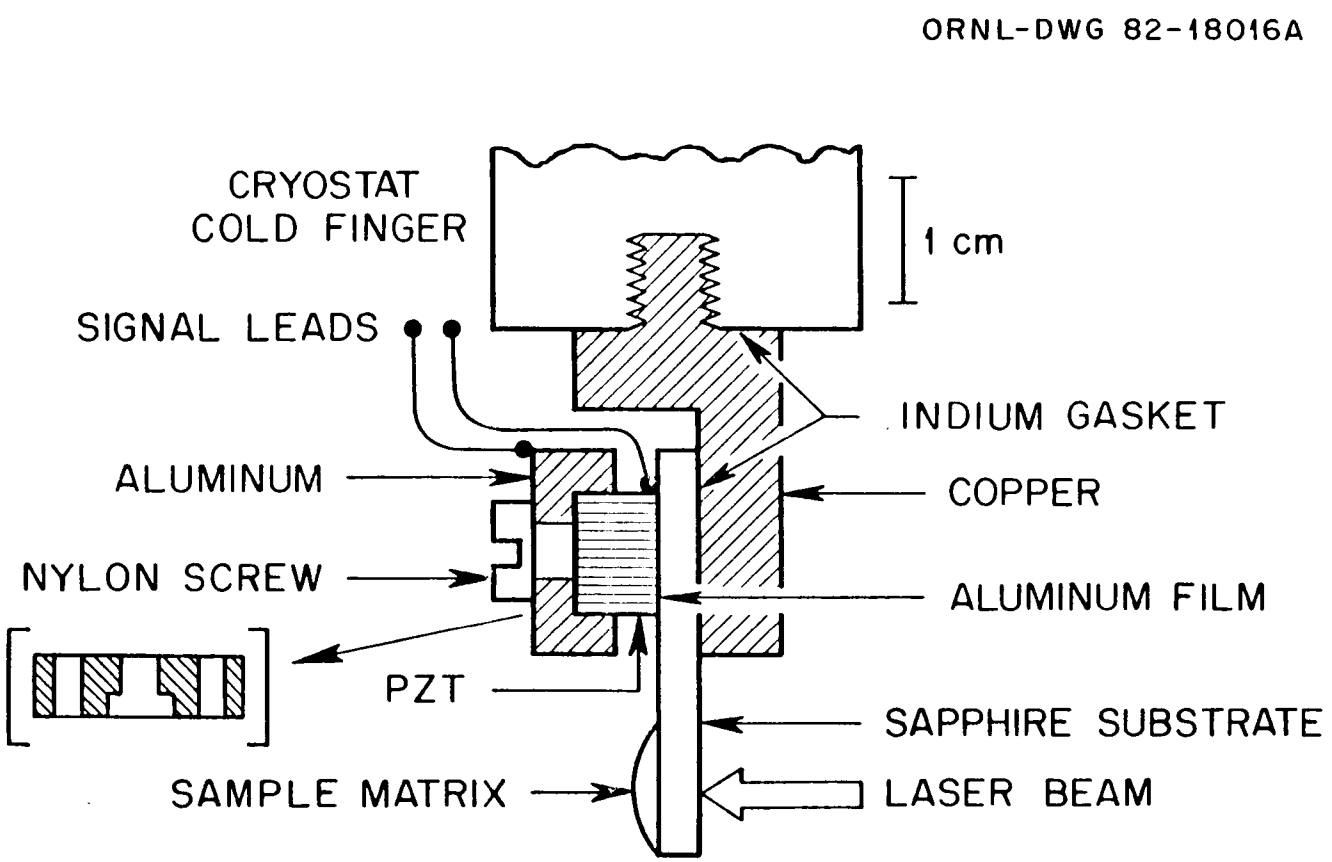


Figure 7. Diagram of the modified MI-PA detector.

shown in Figure 8. The PZT was glued to the sapphire in order to minimize the chance of acoustic bond failure of the PZT disc-sapphire sample window interface during temperature cycling of the PA detector assembly due to differential thermal contractions. Thermal contraction values for some of the materials used are shown in Table II-3. This design also allowed the disc to be unimpeded in the shear mode. The 1.6 mm thick sapphire sample window (22 x 12 mm) with the PZT disc rigidly bonded to it was compressed by an aluminum plate against the cooled copper (cold-finger) clamp without squeezing the PZT disc. An indium gasket was used for thermal contact between the sapphire and cold finger. A 1.2 mm thick copper tab having a 30 gauge wire soldered to it with indium:silver solder (90:10 atomic-percent, p. 33) was glued to the other PZT disc face. The PE signal was extracted from the aluminum plate which contacted the aluminum film on the sapphire and from the wire soldered to the copper tab.

An X-cut quartz slab (12 x 22 mm) was used as a PE transducer for MI-PAS by inserting it between the copper and aluminum clamp halves in place of the sapphire sample window (Fig. 7). Since X-cut quartz is piezoelectric, the PZT disc was not needed. Thus, the X-cut quartz substrate served the dual function of sample window and transducer with each of the clamp halves as pick-up electrodes. An indium gasket was placed between the X-cut quartz and the copper (cold-finger) clamp to ensure adequate thermal contact.

For all of the MI-PAS transducer assemblies described above, the PE signal was extracted from the cryostat by a vacuum BNC feedthrough (Kings Electronics Co., Inc., Tuckahoe, NY, No. KC-79-117) that was

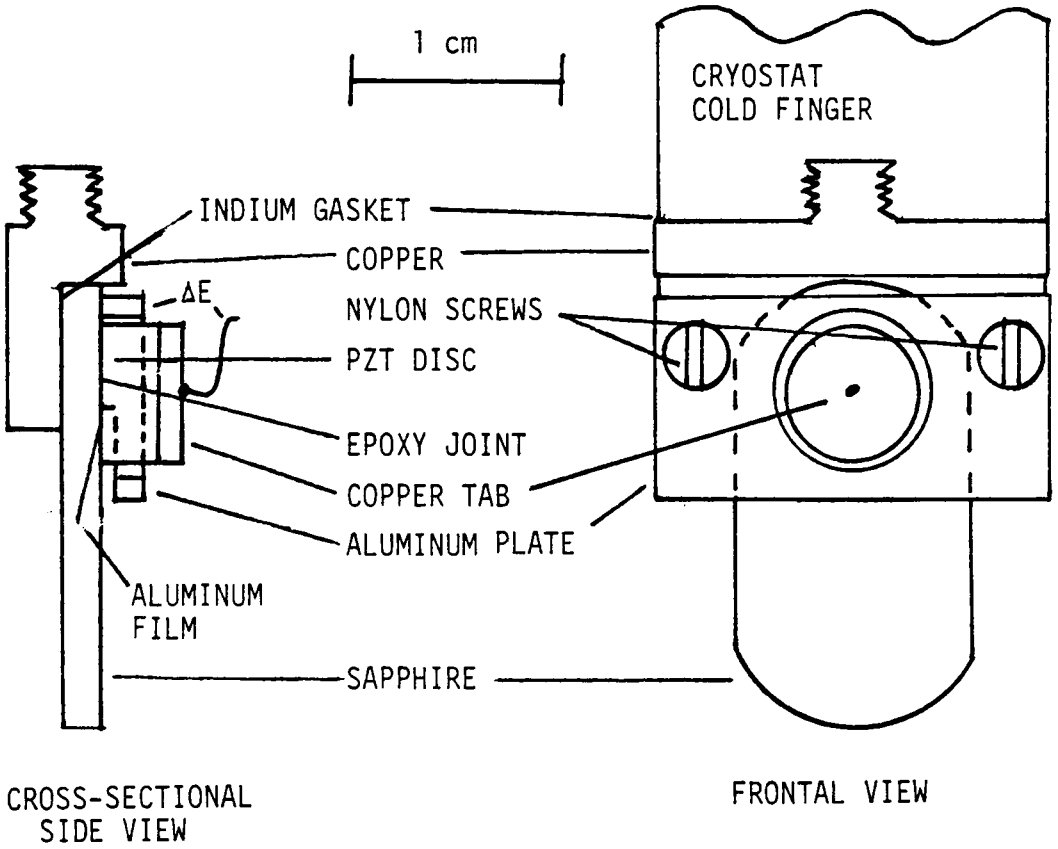


Figure 8. Scale drawing of the final design of the MI-PA detector.

TABLE II-3

LINEAR THERMAL CONTRACTION OF VARIOUS MATERIALS AT 20 K

Material	$(L_{293K}-L_{20K}/L_{293K})X10^{-4}$[a]
Aluminum	37
Copper	29
Indium	64
Fused Quartz	-7.4
Epoxy	93
Nylon	122
Sapphire	10[b]
PZT	<10[c]

[a]B. Meyer, "Low Temperature Spectroscopy", American Elsevier Pub. Co., New York, 1971.

[b]"Thermophysical Properties of Matter", Vol. 13, Plenum, New York, 1977.

[c]P. A. Walthers, Edo Western Corp., Salt Lake City, Utah, personal communication.

soldered into a brass plate which fit a cryostat window port. Small pin connectors were placed in the signal wires between the BNC feed-through and the PE transducer clamp halves for ease of removing the cryostat head.

A PA detector was also designed to be used for frozen samples in liquid nitrogen (77 K). This apparatus is shown in Figure 9. A piece of quartz tubing was sealed off at one end to contain the spectroscopic sample. The sample end of the tube was immersed in liquid nitrogen contained in a small spectroscopic Dewar made of quartz. A PZT disc was clamped to the other end of the quartz tubing, above the liquid nitrogen level. Two sizes of quartz tubing were used. One tube (Fig. 9) had a 4 mm o.d. and a 0.5 mm wall thickness. The tube was modified to have a square, 12 x 12 mm, section at the end so that the PZT disc could be attached to a flat surface. The other, a quartz capillary, had an 8 mm o.d. and a wall thickness of 3 mm. A 5 x 5 mm area at the top end of the tube was ground to a smooth, flat surface to provide a contact surface for a PZT disc. The PE signal was taken from the PZT disc clamp which contacted one face of the PZT disc and a thin piece of aluminum foil which was placed between the other disc face and the quartz tubing. Nonaq stopcock grease was used at all acoustic interfaces.

Two types of quartz liquid-nitrogen Dewars were used. The first Dewar (American Instrument Co., Urbana, IL, shown in Fig. 9), had an inside diameter of ~7 mm at the sample end. The second Dewar (constructed by the ORNL glass shop) had an inside diameter of ~25 mm; thus it could accommodate the 8 mm o.d. quartz tube and hold a larger

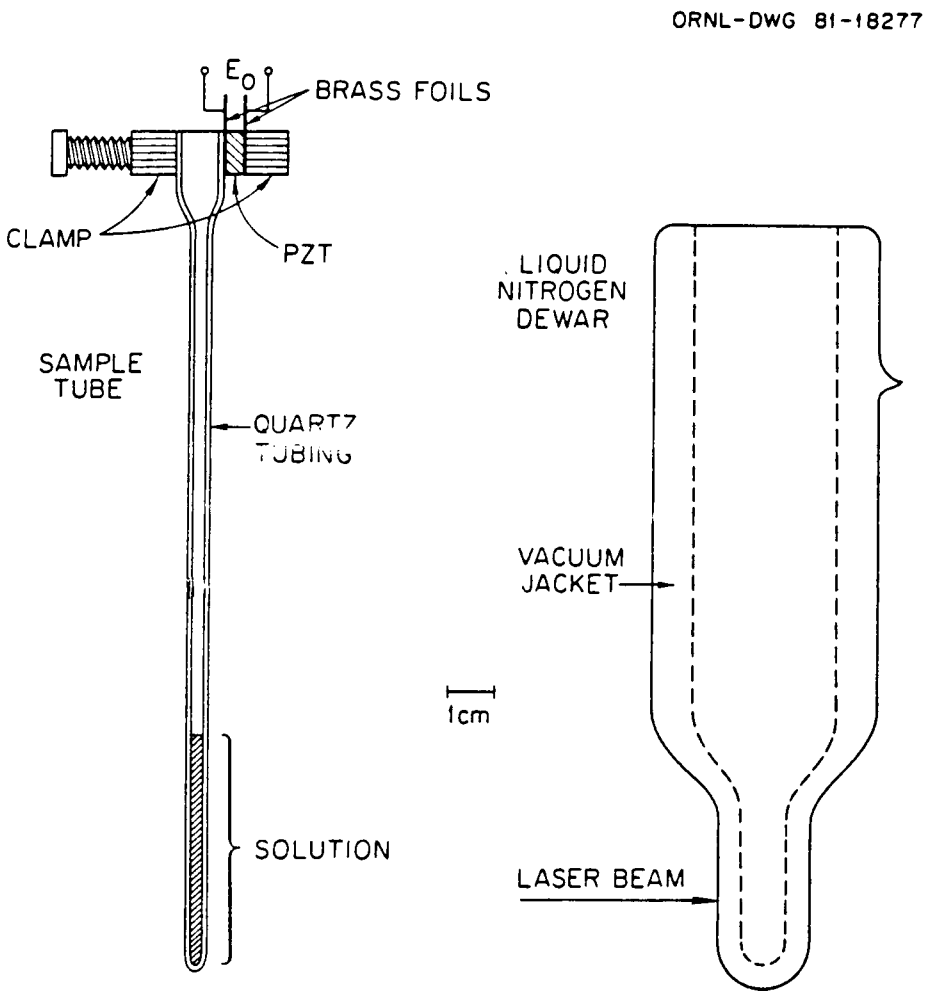


Figure 9. Diagram of the PA detector used for liquid nitrogen-temperature (77 K) samples.

charge of liquid nitrogen. In order to prevent frosting, the Dewars were placed inside a small housing that was purged with dry nitrogen gas.

PA measurements of room-temperature liquids were made using the detector cell assembly shown in Figure 10. A small pinch-type hose clamp was used to compress a PZT disc against the side of a 1 cm quartz cuvette. Thin strips of aluminum foil were placed on both sides of the PZT disc in order to extract the transducer signal. Nonaq stopcock grease was used at all acoustic interfaces.

6. Laser PAS Instrumentation

A flashlamp pumped dye laser (Chromatix, Sunnyvale, CA, Model CMX-4) was used as the excitation source for the PAS measurements. The laser provided light pulses having an ~1 μs temporal width at half-height and a nominal spectral bandwidth of 3 cm^{-1}. Typical pulse energies were 1-2 mJ in the fundamental (470-680 nm) and ca. 0.02-0.2 mJ in the UV (290-345 nm). Wavelength tuning was achieved by a birefringent tuning element mounted inside the laser cavity. Production of UV light (290-340 nm) was accomplished by intra-cavity second harmonic generation (SHG) using angle phase-matched ammonium dihydrogen phosphate crystals. Pulse to pulse energy stability was ~ ± 20 % in the fundamental and sometimes poorer in the UV. The laser was operated at a repetition rate of 5 or 10 Hz.

A Chromatix laser scanner was used for wavelength scanning in the fundamental and UV, simultaneously scanning the tuning element and SHG crystals. Unfortunately, because of the critical angle involved, the scanner unit could not scan the tuning element and SHG crystals with

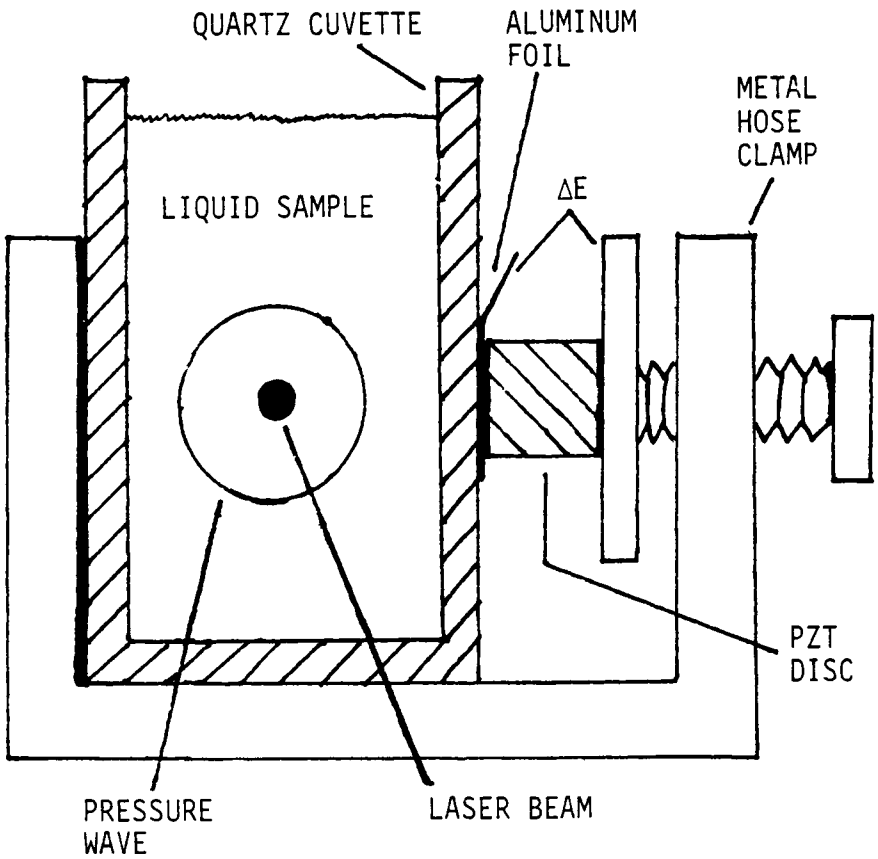


Figure 10. Diagram of the PA detector used for room-temperature liquids.

perfect synchronization. Therefore, when scanning in the UV, it was necessary to constantly observe the output energy level of the laser in order to make manual adjustments for maintaining the angle phase-matched condition. A digital-to-analog converter was used in conjunction with the laser scanner to drive the X-axis (wavelength axis) of an X-Y recorder (J. L. Moseley Co., Pasadena, CA, Model 2D-2A or Linseis Co., Princeton Junction, NJ, Model LY1800).

A schematic diagram of the pulsed laser-PAS instrumentation is shown in Figure 11. The optical beam emerging from the laser was passed through an iris when operating the laser in the fundamental in order to improve the spatial quality of the beam, or through a UV band-pass optical filter when operating the laser in the UV in order to remove the fundamental component of the beam. A quartz plate beam splitter was used to reflect ~5-10 % of the laser beam to a photodiode detector/preamplifier (Molectron Corp., Sunnyvale, CA, Model 141) for the purpose of providing PA spectra corrected for variations in the laser pulse energy. The preamplified photodiode signal was processed by a pulsed photometer (Molectron Corp., Model LP20) which averaged 30 pulses and provided a DC level output proportional to the averaged pulse energy. This output was fed to the denominator input channel of a ratiometer (EG&G Princeton Applied Research, Princeton, NJ, Model 118). A quartz lens was used to focus and position the laser beam upon the sample.

The signal generated by the PA detector following each laser pulse was inputted to a preamplifier, either a unity gain Junction Field Effect Transistor (JFET, 2N4416A, Texas Instruments) preamplifier

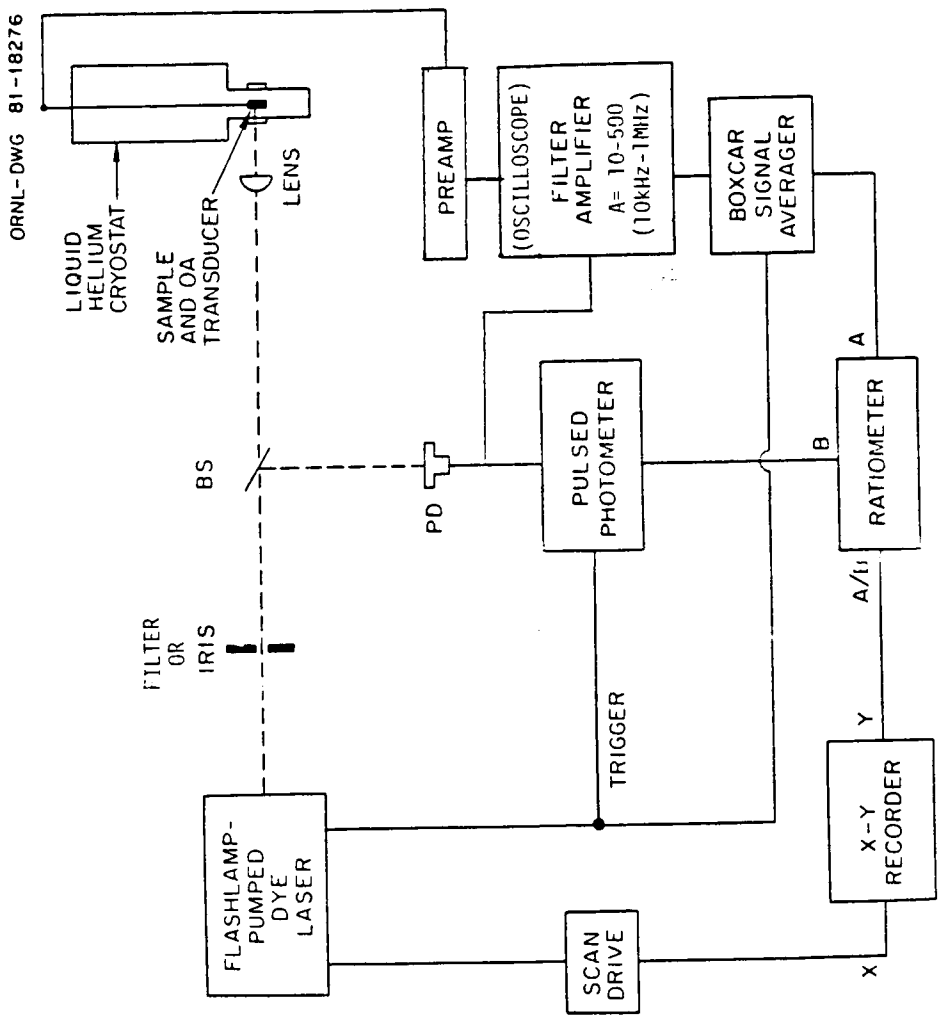


Figure 11. Block diagram of the laser-excited PAS instrumentation.

or a wideband preamplifier (EG&G Princeton Applied Research, Model 115) with a gain of 20 or 200. The unity gain JFET preamplifier, whose circuit is shown in Figure 12, was used when achieving maximum sensitivity was important. It was placed as close to the PE transducer as possible (~3-5 cm) in order to minimize attenuation in the signal due to capacitive cable loading. The wideband preamplifier was used when maximizing the sensitivity was not important (e.g., when recording the PA spectra of $Nd(OH)_3$).

After preamplification the PA signal was led to a filter amplifier (Tektronix, Inc., Beaverton, Ore., Model 7A22) plug-in in a storage oscilloscope (Tektronix, Inc., Model 7633). The filter amplifier was used in the band-pass mode with upper and lower corner frequencies of 1 MHz and 10 kHz, respectively, having a roll-off of -6 dB per frequency octave in both directions. The filter amplifier provided 10-500 amplification of the filtered signal. The amplified and filtered signal was then inputted to a boxcar averager (EG&G Princeton Applied Research, Model 162/164). A 0.5 μs gate at 10-100 μs delays was used. Twenty pulses were averaged to give 4 s or 2 s time constants for the laser repetition rate of 5 Hz or 10 Hz, respectively. The dc level output of the boxcar averager was connected to the numerator input channel of the ratiometer. The dc output of the ratiometer (i.e., PA signal ÷ laser pulse energy) was used for the Y-axis drive of the X-Y recorder.

When measuring very small (< 100 μV peak to peak) PA signals, an additional unity gain filter amplifier (Wavetek-Rockland Co., Rockleigh, NJ, Model 442) was placed between the output of the

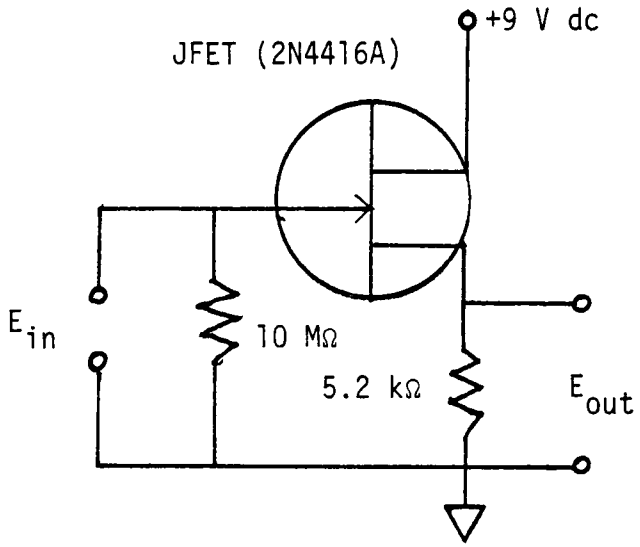


Figure 12. JFET preamplifier circuit.

Tektronix 7A22 filter amplifier and the input of the boxcar averager. The Wavetek-Rockland 442 filter amplifier was used in the band-pass mode (200-500 kHz) and had a roll-off of -24 dB per frequency octave in both directions.

Electronic trigger pulses, synchronous with the laser light pulses, were provided by the laser and used to trigger the filter amplifier-oscilloscope, boxcar averager, and laser photometer. Sometimes, a significant time jitter occurred between the electrical trigger pulses and the laser light pulses. When this problem occurred, ~5 % of the laser beam was deflected to a photodiode whose output was used to trigger the oscilloscope. A synchronous output gate from the oscilloscope was then used to trigger the boxcar averager and laser photometer.

7. Miscellaneous

Absorption spectra were obtained with either a Cary 14 or Cary 219 absorption spectrometer (Varian, Palo Alto, CA). A spectral band width of 0.1-0.2 nm was used unless otherwise indicated. All absorption spectra of room-temperature liquid solutions were obtained using a 1 cm path-length fused quartz cuvette. Diffuse reflectance spectra of rare-earth compounds were recorded on the Cary 14 spectrometer using a diffuse reflectance attachment developed locally. Power spectra of the laser pulse profiles and PZT response were measured with a Tektronix 7L5A spectrum analyzer. For power spectra of the laser pulses, a Molectron 141 photodiode/preamplifier was used in the fast response mode (0.025 μs rise-time).

C. Procedure

1. $Nd(OH)_3$ Sample Preparation

Samples of $Nd(OH)_3$ for both room-temperature and low-temperature PAS measurements were prepared by dispersing the powder (10 % by weight) in a 1:1 glycerine:H_2O mixture. The glycerine:H_2O mixture became a transparent glass when frozen, thereby reducing PA background signal caused by scattered excitation striking the PE transducer and transducer assembly. For the preparation of room-temperature samples, several drops of the $Nd(OH)_3$-glycerine:H_2O dispersion were placed between two glass microscope slides and clamped into the room-temperature PA detector assembly (Fig. 5, p. 42).

For the preparation of the low-temperature samples, one or two drops of the $Nd(OH)_3$-glycerine:H_2O dispersion were placed on the quartz window of the PA detector assembly (Fig. 6, p. 43). Then, while keeping the quartz window as horizontal as possible, the detector assembly was slowly lowered into liquid N_2 contained in a widemouth Dewar. After about 30 s, the entire PA detector assembly was immersed into the liquid N_2 until the violent boiling ceased. At this point, the assembly was quickly (1-2 s) transferred to the Janis liquid helium cryostat which was maintained at ~77 K. When the sample was transferred quickly, frosting was minimal. Once the PA detector assembly was correctly positioned in the cryostat, the temperature was lowered to 6-8 K for acquisition of PA spectra.

2. Preparing Matrix Isolated PAC Samples

The equipment used to prepare the MI samples has been described above. Solutions of the PACs dissolved in either hexane or acetone were introduced into the well of the sublimation cell (Fig. 4, p. 39) with a microliter syringe. A gentle stream of air was passed over the sample solution in order to evaporate most of the solvent. The sublimation cell was then fitted into the cryostat through the Cajon vacuum adapter and the matrix-line was connected to the matrix-gas inlet. A dry ice/methanol bath (-78°C) was placed around the sample well and evacuation of the cryostat was begun. The sublimation cell valve was opened in order to evacuate the matrix line up to Valve-4 (see Fig. 3, p. 36). When the pressure inside the cryostat reached ~10^{-1} torr, a second coolant bath, having a higher temperature than the first one, was placed around the sample well for 1-2 min. in order to remove the last traces of the solvent. This precaution was necessary because it was observed that not all of the solvent was removed at -78°C. The temperature of the second bath varied depending on the volatility of the PAC sample. In general, the temperature used for the second bath was ~20°C below the sublimation temperature used during the MI deposit (discussed below). After 1-2 min., the -78°C bath was replaced around the sample well. When the pressure inside the cryostat was lowered to ~5 x 10^{-2} torr, cooldown of the cryostat was begun.

Once the cryostat cooldown was achieved, Valve-4 (Fig. 3, p. 36) was opened to allow matrix gas to enter the cryostat and condense upon the spectroscopic window. The matrix gas was delivered at a rate of ~100 μmole/hr (corresponding to a flowmeter setting of 6-8). The

temperature of the sublimation cell was then raised to begin sublimation of the PAC sample. As the sample sublimed, its vapors were entrained in the matrix gas, swept through the sublimation cell, and codeposited with the matrix gas upon the spectroscopic window. The sample well was maintained at the sample deposition temperature (discussed below) for 15-30 min. Then, in order to assure that all of the sample was deposited, the sample well temperature was raised at three 10°C intervals, each for ~5-10 min., until the sample well was ~30°C above the sample deposition temperature.

For samples that required sub-ambient temperatures for sublimation, the sample cell temperature was maintained with cold baths of methanol cooled with dry ice, ice-H_2O, or cool H_2O. For samples requiring above-ambient sublimation temperatures, the nichrome heating wires were used. Some samples required sublimation temperatures near ambient. For these sample, the combination of both cold baths and nichrome wire heating was used.

Cradock and Hinchcliffe[69] recommend a sample vapor pressure of 10^{-2}-10^{-4} torr for MI depositions. Experimentally, it was found that a sample vapor pressure of 10^{-3}-10^{-4} torr was adequate to deposit ca. 1 µg of a compound (~0.008 µmole of quinoline) in ~15 min, thus allowing a matrix:sample ratio of ~10^4:1. Vapor pressure vs. temperature data for various PACs are available from several sources.[80,81] The sample deposition temperatures used for PACs in the present work are listed in Table II-1 (p. 27).

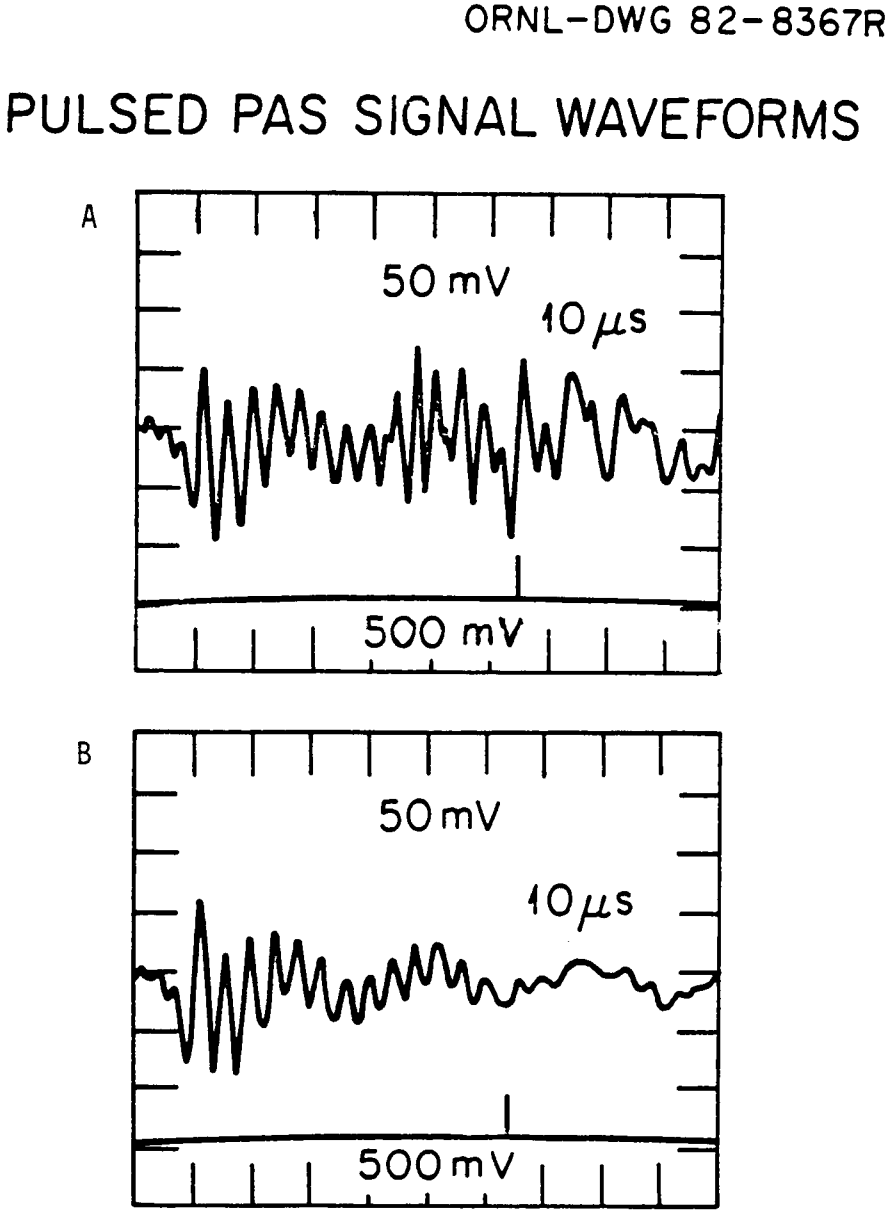


Figure 13. Oscilloscope pictures of pulsed-laser excited PA waveforms corresponding to Ho_2O_3 (room temperature) spectrum (Fig. 1, p. 9). (A) upper trace, on resonance at 15,400 cm^{-1}. (B) upper trace, off resonance at 15,390 cm^{-1}. Lower traces in (A) and (B) show the boxcar averager gate. Vertical divisions, mV. Horizontal divisions, μs.

3. Obtaining Pulsed-Laser PA Spectra

Typical PA signal waveforms produced by the PE transducers (the 0.89 mm thick PZT disc in this case) for each laser pulse striking the sample are shown in the top traces of Figures 13-A and 13-B. Presumably, the original pressure wave closely resembled the laser pulse waveform (~1 μs FWHM).[12] However, reflections and reverberations of the original pressure wave within the PE transducer assembly gave rise to complex, dampened bipolar oscillations. For the present work, the major frequencies observed were in the 100-500 kHz range. The waveform probably carries no analytically useful information. Fisher, et al.[82] have performed a frequency analysis of a similar pulsed PA signal waveform. As one might conclude from closer inspection of the PA signal waveforms in Figure 13, they found that the waveform was actually composed of a broad envelope of frequencies centered around the resonance frequency of their PE device.

The PA signals in Figures 13-A and 13-B were obtained while recording the spectrum of Ho_2O_3 powder shown in Figure 1 (p. 9). The upper trace in Figure 13-A was obtained when the laser was resonant with a spectral line (15,400 cm^{-1}) in the Ho_2O_3 spectrum, while the upper trace in Figure 13-B was obtained when the laser was non-resonant (15,390 cm^{-1}) with a Ho_2O_3 spectral line. The signals occurring in the 40-90 μs regions in both of the upper traces represent the PA signals coming from the Ho_2O_3 sample. The PA signals in the 10-30 μs regions of the upper traces were produced, presumably, from scattered excitation light striking either the PE transducer or a part of the transducer assembly located near the transducer. The temporal delay

between the two signals occurred because the transit time from the Ho_2O_3 sample to the PE transducer was relatively instantaneous for the scattered light compared with that of the PA pressure wave. Thus, the temporal delay of the PA signal originating from the sample was often useful for discrimination against PA background signals produced by scattered excitation light and electrical noise pick-up coming from the firing of the laser.

In order to process the PA signals, the gate of the boxcar integrator (shown in the lower traces of Figures 13-A and 13-B) was set to one of the predominant, early occurring peaks, usually 10-100 μs following the laser pulse. The actual time delay varied from sample to sample. The PA signal was processed as described above (pp. 52-58) to yield a PA spectrum.

4. Preparing Solid-Host PAC Samples at Room Temperature

Samples of several PACs in thin-film, room-temperature glue matrices were prepared in order to emulate the geometrical properties of PAC-containing low-temperature matrices. Rubber cement was mixed 1:1 (v:v) with toluene. An equal volume of the PAC sample solution (1 mg mL^{-1} in toluene) was then added to the glue solution. Several drops of the resulting mixture were pipetted onto one end of a quartz slide and the solvent was allowed to evaporate, yielding a thin film of glue impregnated with the PAC. The quartz slide was then mounted into the room-temperature PA detector (Fig. 5, p. 42) for PA measurements.

CHAPTER III

RESULTS AND DISCUSSION

A. Low-Temperature Photoacoustic Spectroscopy of Neodymium Hydroxide

The PA spectra of rare-earth compounds, primarily the lanthanide oxide powders, have been studied by numerous investigators.[22,83-89] Throughout the visible wavelength region (~400-700 nm), the absorption (or PA) spectra of most of these compounds are characterized by very weak and highly resolved spectral lines (even at room temperature). These spectral lines are due to formally forbidden transitions occurring within the 4f-electronic subshell. The unusually sharp spectra result due to the forbidden nature of the transitions[90] and because the f-electronic subshells lie beneath closed s^2p^6 shells which shield the f-subshells from strong interactions with their environments.[91] Because of the relatively high resolution and low absorptivities of the spectra of these compounds, they have become popular materials for demonstrations of resolution and sensitivity capabilities in PAS.

Initial experiments in the present work involved the acquisition of piezoelectrically detected pulsed dye-laser excited PA spectra of $Nd(OH)_3$ powder at room temperature and low temperature (6-8 K). PA spectra of $Nd(OH)_3$ powder at room temperature were obtained first in order to gain familiarity with the experimental instrumentation, and to become acquainted with the usage of PE transducers. After completing the room-temperature PA experiments, low-temperature PA experiments were begun.

For both room-temperature and low-temperature PAS experiments, the 1.6 mm thick PZT disc transducer was used. The PA detector assemblies, sample preparation procedures, and methods used to obtain the PA spectra have been discussed in Chapter II. The PZT-PE transducer functioned well at room temperature and low temperature, giving characteristic dampened, ringing signals similar to the ones shown in Figure 13 (p. 61). The wavelength ranges 16,400-17,600 cm^{-1}, 18,600-19,600 cm^{-1}, and 19,400-20,000 cm^{-1} were obtained using laser dyes Rhodamine 575, Coumarin 504, and Coumarin 102, respectively (see Table II-2, p 31).

The PA spectra of $Nd(OH)_3$ powder in the wavelength ranges 16,400-17,600 cm^{-1} and 18,600-20,000 cm^{-1} are presented in Figures 14 and 15, respectively. The steeply sloping baseline at the higher-energy ends of some of the spectra is an instrumental artifact involved in taking the ratio of the PA signal (numerator) with respect to the laser energy (denominator). When the laser energy is very low, small drifts in the DC offsets in the numerator and denominator cause the value of the ratio to be very large. In accordance with the spectral state assignments made by Caro and Derouet[92] for absorption spectra of single crystal $Nd(OH)_3$, the PA spectral lines in the 17,200-17,400 cm^{-1} region are assigned $^4I_{9/2} \rightarrow {}^4G_{5/2}$, $^2G_{7/2}$ and the lines in the 19,000-19,600 cm^{-1} region are assigned $^4I_{9/2} \rightarrow {}^4G_{7/2}$, $^4G_{9/2}$. The appearances of these PA spectra are also in good agreement with the room-temperature diffuse reflectance spectra recorded for $Nd(OH)_3$ powder which are shown in Figure 16.

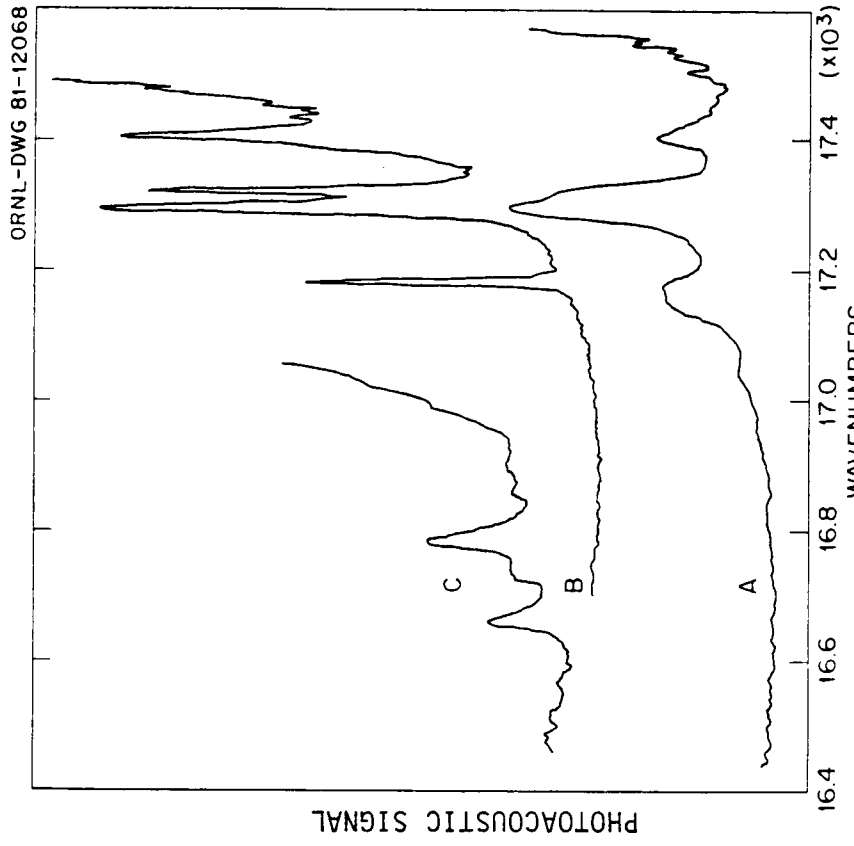


Figure 14. PA spectra of $Nd(OH)_3$ powder from 16,400-17,500 cm^{-1}. (A), room temperature. (B) and (C), 6-8 K.

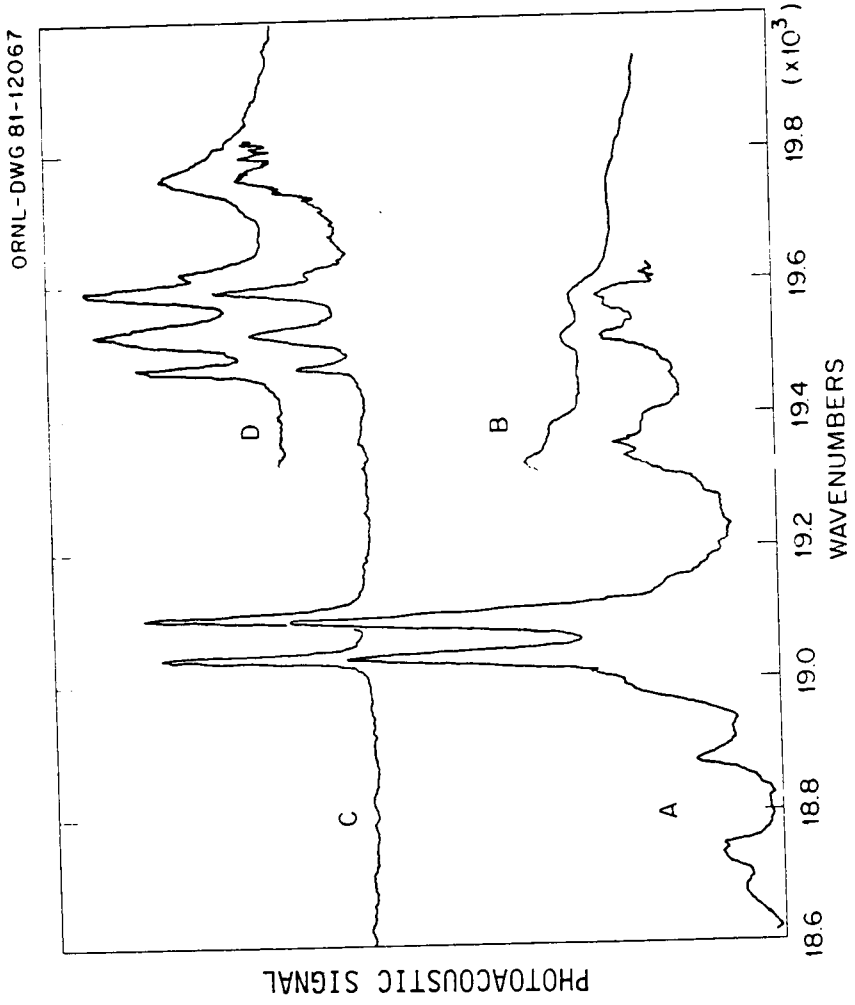


Figure 15. PA spectra of $Nd(OH)_3$ powder from 18,600-19,900 cm^{-1}. (A) and (B), room temperature. (C) and (D), 6-8 K.

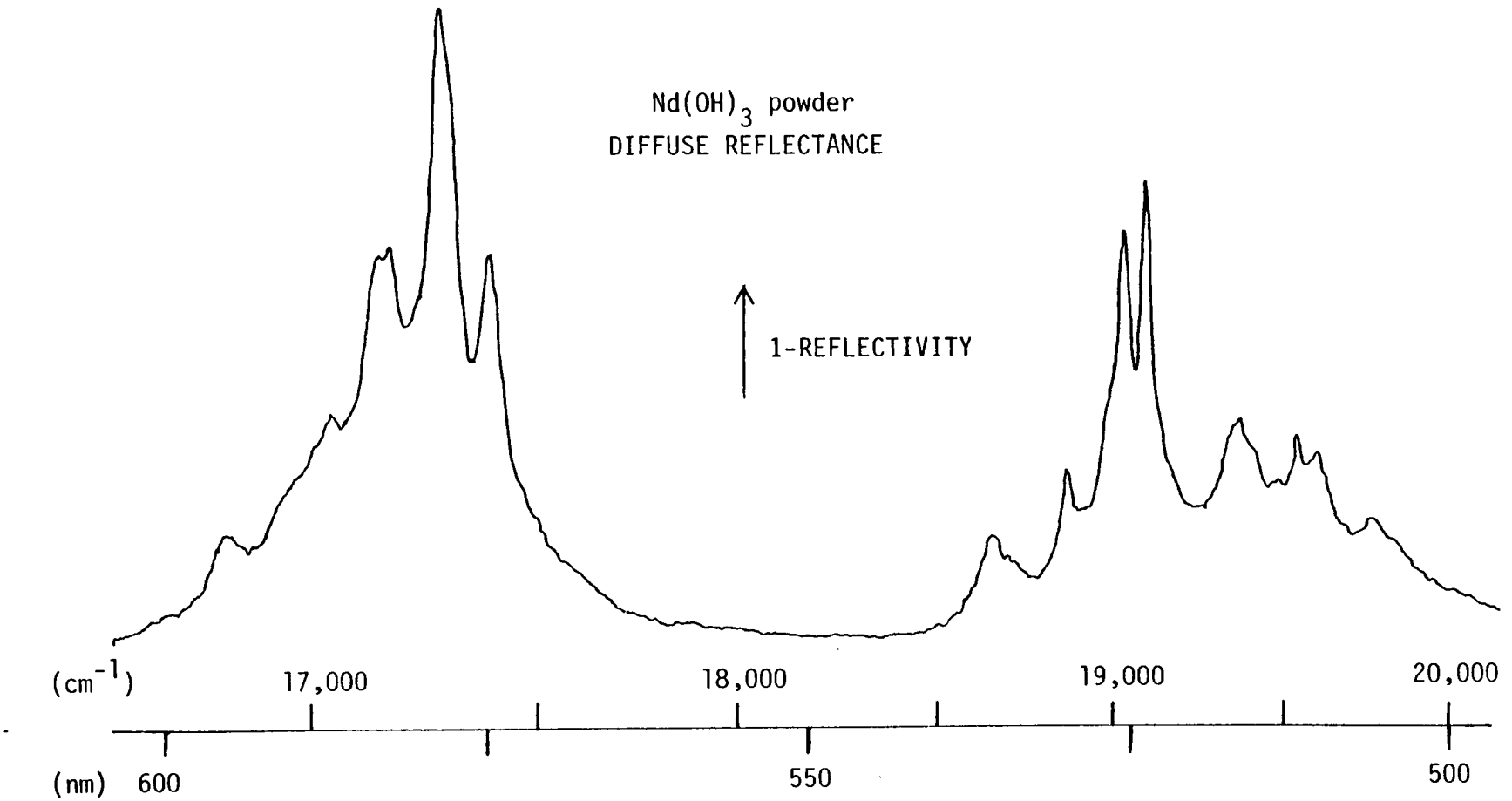


Figure 16. Room-temperature diffuse reflectance spectrum of $Nd(OH)_3$ powder from 16,500-20,000 cm^{-1}.

The PA spectra of the low-temperature $Nd(OH)_3$ sample (Figures 14(B) and 14(C), and 15(C) and 15(D), courtesy of R. W. Shaw, ORNL) show two major changes compared with the corresponding PA spectra of the room-temperature sample (Figures 14(A), and 15(A) and 15(B)). It is evident that the spectral lines become sharper and some disappear in the spectra of the low-temperature sample. The linewidths are 20-50 cm^{-1} at room temperature and decrease to 10-20 cm^{-1} at 6-8 K. According to simplified theory,[90] in the ideal case, rare-earth ions in perfect crystals at low temperature should have nearly infinitely small linewidths. This occurrence is predicted by theory because of the "forbidden" nature of the transitions. However, in reality, the observed linewidths are usually broadened compared with the linewidths predicted for the ideal case. Line broadening in crystalline rare-earth compounds can be attributed to two primary factors: imperfect lattice conditions (i.e., inhomogeneous broadening) and phonon contributions.[90]

The fact that "infinitely" narrow lines were not observed in the PA spectra of the low-temperature sample in the present work is most likely due to the first factor cited above, i.e., imperfect lattice conditions. Since the recorded PA spectra were of powdered (polycrystalline) $Nd(OH)_3$, it is probable that the Nd^{3+} ions did not reside in identical lattice environments. The sharpening of the spectra upon cooling the sample is probably due to a reduction in phonon interactions. Phonon interactions occur when optical transitions couple with the weak, natural vibrational modes (i.e., the phonon modes) of the

solid-state lattice. In general, the magnitude of this broadening decreases as the sample temperature decreases.[90]

In order to ensure that the $Nd(OH)_3$ sample was adequately cooled at 6-8 K for the elimination of significant phonon contributions to the spectral linewidths, Shaw[93] measured PA spectra of the $Nd(OH)_3$ powder at 1.5 K in which the entire sample and PA detector were immersed in liquid helium below the lambda point. No additional line narrowing was observed compared with that observed for the sample at 6-8 K. Therefore, it is concluded that the limiting factor in the linewidth reduction resulted from nonequivalent lattice environments of the Nd^{3+} ions.

Since some of the linewidths observed in the PA spectra of the low-temperature samples were ~10 cm^{-1}, it is also possible that some artificial broadening was added as a result of the finite spectral linewidth (~3 cm^{-1}) of the laser excitation source. The linewidths of the recorded PA spectra ($\Delta\bar{\nu}_{OBS}$) are, thus, a convolution of the real linewidths ($\Delta\bar{\nu}_S$) of the sample with the laser linewidth ($\Delta\bar{\nu}_L$). However, the amount of broadening imparted by the ~3 cm^{-1} laser linewidth was probably not severe enough to cause significant distortions of the real line widths of the sample. For a Gaussian line, the real linewidth is calculated by $\Delta\bar{\nu}_S = (\Delta\bar{\nu}^2_{OBS} - \Delta\bar{\nu}^2_L)^{1/2}$. For $\Delta\bar{\nu}_{OBS}$ = 10 cm^{-1} and $\Delta\bar{\nu}_L$ = 3 cm^{-1}, $\Delta\bar{\nu}_S$ = 9.5 cm^{-1}.

In addition to the narrowing of the spectral lines in the PA spectra of the low-temperature $Nd(OH)_3$ sample, it is also observed that some spectral lines disappear, viz. 18,700, 18,900, and 19,375 cm^{-1} in Figure 15, and 17,050 cm^{-1} in Figure 14. In the room-temperature samples, these lines originate from upper Stark components of the

ground state which are thermally populated according to Boltzmann's law. This law states that the relative distribution among states above the ground state resulting from thermal energy is equal to $\frac{g_n}{g_o} e^{-E_n/kT}$, where g is the state degeneracy (2J+1), E_n is the energy level above the the ground state, k is the Boltzmann constant, and T is the absolute temperature in K. When a rare earth ion is placed in a crystalline lattice, it experiences electrical interactions with other ions in its near vicinity that modify the energy locations of the free ion levels.[90] For Nd^{3+}, the degeneracy of the ground state energy level is removed to produce up to five energy levels. Shaw[93] has estimated a total ground state crystal field splitting of at least 370 cm^{-1} for $Nd(OH)_3$ by diffuse reflectance measurements in the Nd^{3+} nephelauxetic scale determination region, i.e., the $^2P_{1/2}$ state at 23,250 cm^{-1}. The thermal energy, kT, can be expressed in cm^{-1} by letting k = 0.695 cm^{-1} K^{-1}. Accordingly, for E_n = 370 cm^{-1} (the ground state splitting) and 298 K, kT = 206 cm^{-1} and $e^{-E_n/kT}$ = 0.17; whereas, at 6 K, kT = 4.2 cm^{-1} and $e^{-E_n/kT} = 5.5 \times 10^{-39}$. The net result is that in the low-temperature sample, the majority of the ground state population resides in the lowest Stark component; hence the spectral lines due to upper ground state components at room temperature vanish at low temperature.

The weak lines at 16,700-16,800 cm^{-1} in Figure 14(C) are believed to belong to Nd_2O_3 (sesquioxide), a minor impurity in the $Nd(OH)_3$. Some of the $Nd(OH)_3$ was converted to Nd_2O_3 by heating to 1,000°C. The resulting material had prominent PA spectral lines at these positions.

This work represented the first demonstration of the use of PE transducers for acquiring PA spectra of solids at cryogenic temperatures (< 77 K). The PZT disc-PE transducer was shown to function well for PA detection at 6-8 K (and as low as 1.5 K).[93] The success of these experiments led to subsequent investigations that focused on extending the application of piezoelectrically-detected, low-temperature PAS to matrix-isolated polycyclic aromatic compounds.

B. Photoacoustic Spectroscopy of Matrix-Isolated Polycyclic Aromatic Compounds

1. MI-PA Spectra of Selected PACs

Photoacoustic spectra were recorded for a number of matrix-isolated PACs using the X-cut quartz and PZT piezoelectric transducers. Since the primary purpose of the present work was to investigate the analytical utility of MI-PAS for the detection of weakly fluorescing and non-fluorescing PACs, a large portion of the experimentation focused upon studying such compounds (e.g., N-, O-, and S-heterocycles, and PACs having -C=O and $-NO_2$ functional groups). MI-absorption spectra were also obtained for some of these compounds to help identify which compounds exhibited absorption spectra with sufficiently high resolution to warrant studying them by laser-excited PAS. MI-absorption spectra were also taken in some cases and compared with the PA spectrum in order to relate the PA signal to absorptivity.

a. N-heterocycles. A number of N-heterocycles were among the first compounds studied. Many of these compounds are reported to have very low fluorescence quantum efficiencies,[55] which is usually

attributed to the fact that their lowest excited singlet states are $n-\pi^*$. For $n-\pi^*$ singlet states, the singlet-triplet intersystem crossing rate is usually large relative to that of $S_1 \rightarrow S_0$ fluorescence.

A survey of reference sources[94,95] containing room-temperature absorption spectra was conducted to identify which N-heterocycles had prominent absorption bands in the wavelength regions accessible with the laser. It was found that the quinoline family of N-heterocycles had prominent absorption bands at room temperature in the region of 310-325 nm with molar absorptivities of ~3,000 $\underline{M}^{-1}$ cm^{-1}. Thus, initial MI-PAS experiments involved studying the various isomers of the quinoline family of N-heterocycles.

Figure 17-A shows the PA spectrum of 3-bromoquinoline (4 μg) isolated in Ar at 10 K from 314 to 324 nm. This is the first PA spectrum obtained for a matrix-isolated PAC. The X-cut quartz slab was employed as both the transducer and sample window. For the purpose of comparison, the room-temperature solution absorption spectrum (10^{-4} $\underline{M}$ in heptane) is shown in Figure 17-B. The spectral bandwidth in the room-temperature spectrum is 505 cm^{-1}, whereas in the MI-PA spectrum, it is reduced to 145 cm^{-1}. Also, a 170 cm^{-1} blue shift in the peak maximum is observed for the MI-PA spectrum. This occurrence was observed for many of the samples in Ar and N_2 matrices. The molecules experience a weaker solvation in N_2 and Ar matrices than in organic solvents.

Figure 18-A compares the room-temperature solution absorption spectrum of quinoline (10^{-4} $\underline{M}$ in hexane) in the 305-316 nm region with MI-absorption and MI-PA spectra (Figures 18-B and 18-C) obtained for

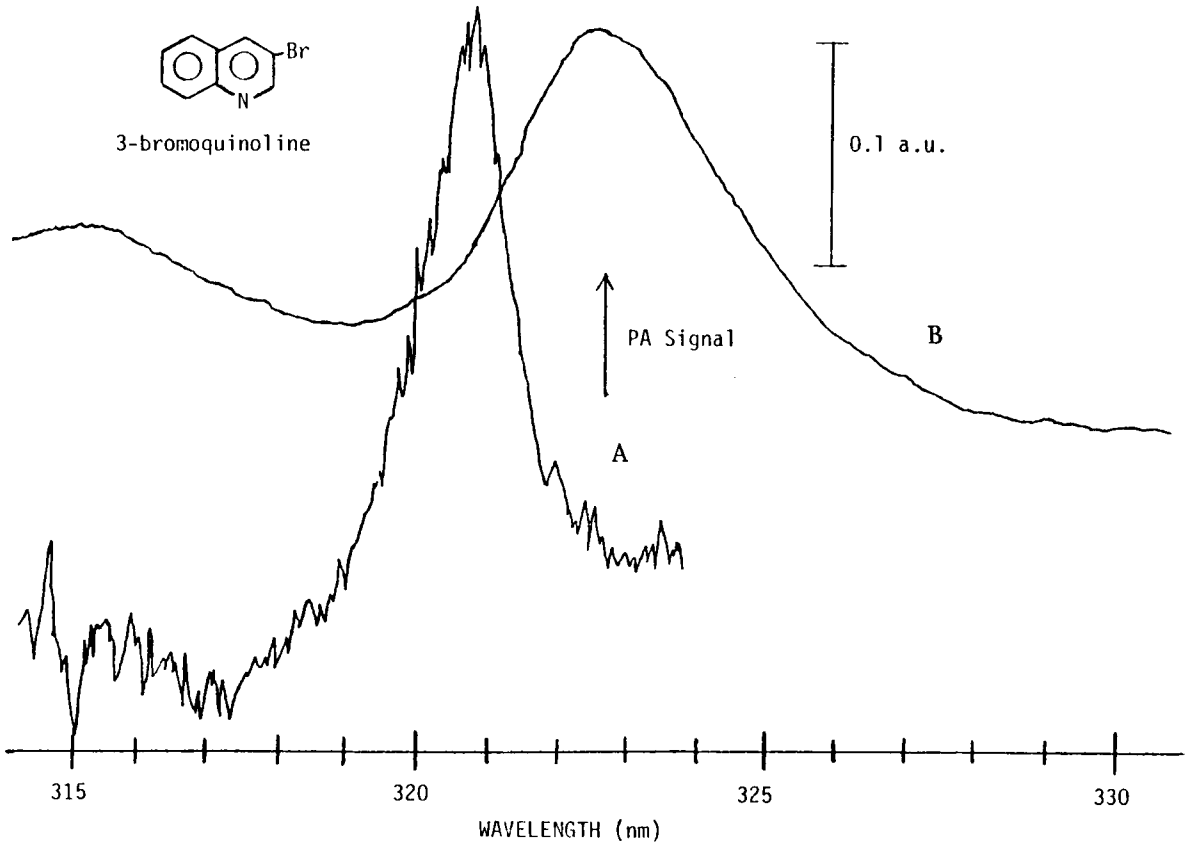


Figure 17. Spectra of 3-bromoquinoline. (A) MI-PA spectrum of 4 μg in Ar at 10 K. (B) Room-temperature solution absorption spectrum, 10^{-4} M in hexane.

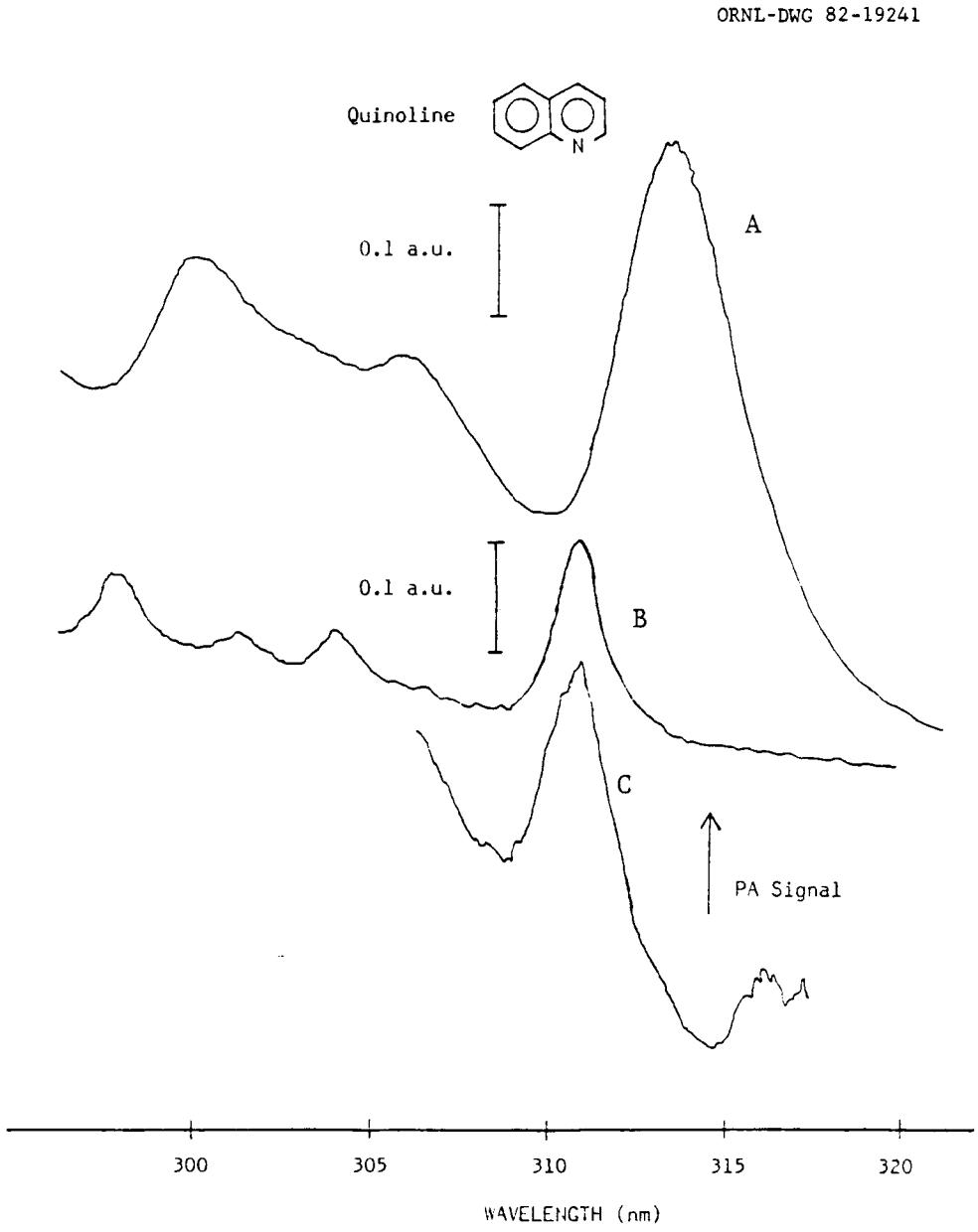


Figure 18. Spectra of quinoline. (A) Room-temperature solution absorption spectrum, 10^{-4} M in hexane. (B) MI-absorption and (C) MI-PA spectra for the same MI sample, 5 μg in N_2 at 10 K.

the same MI sample (5μg in N_2 at 10 K). The MI-PA spectrum was obtained using the 1.6 mm thick PZT disc compressed against the sapphire window. The MI-PA and MI-absorption spectra have identical bandwidths (185 cm^{-1}) and exhibit approximately a threefold resolution enhancement compared with the bandwidth of the room-temperature spectrum (510 cm^{-1}). The peak positions of the PA and absorption spectra of the MI sample are also equal, and are blue shifted by 405 cm^{-1} compared with the room-temperature spectrum. Although the peak position and bandwidths are approximately the same in the MI-absorption and MI-PA spectra, the baseline in the PA spectrum has a steep, upward slope in the blue direction, whereas the baseline in the MI-absorption spectrum has only a slight upward slope. The reason for the steep slope in the MI-PA spectrum is attributed to an instrumental artifact which results from DC offsets occurring in the normalization of the spectrum as described on p. 65. MI-PA spectra of quinoline were also obtained in Ar and Xe and exhibited comparable bandwidths (185 cm^{-1}); however, a blue shift in the peak maximum was not observed with the Xe. The steeply sloping baseline did not appear in these spectra.

The MI-PA spectrum of 3-methylisoquinoline (20 μg in Ar at 10 K) and room-temperature solution absorption spectrum (10^{-4} M in hexane) are shown in Figures 19-A and 19-B, respectively. The X-cut quartz slab was used as transducer and cold finger for obtaining the PA spectrum. The bandwidths in the MI-PA spectrum is 115 cm^{-1} which are significantly less than the 490 cm^{-1} bandwidths in the room-temperature spectrum. It appears that the relative peak heights in the MI-PA spectrum do not correspond to the ratio of peak heights in the

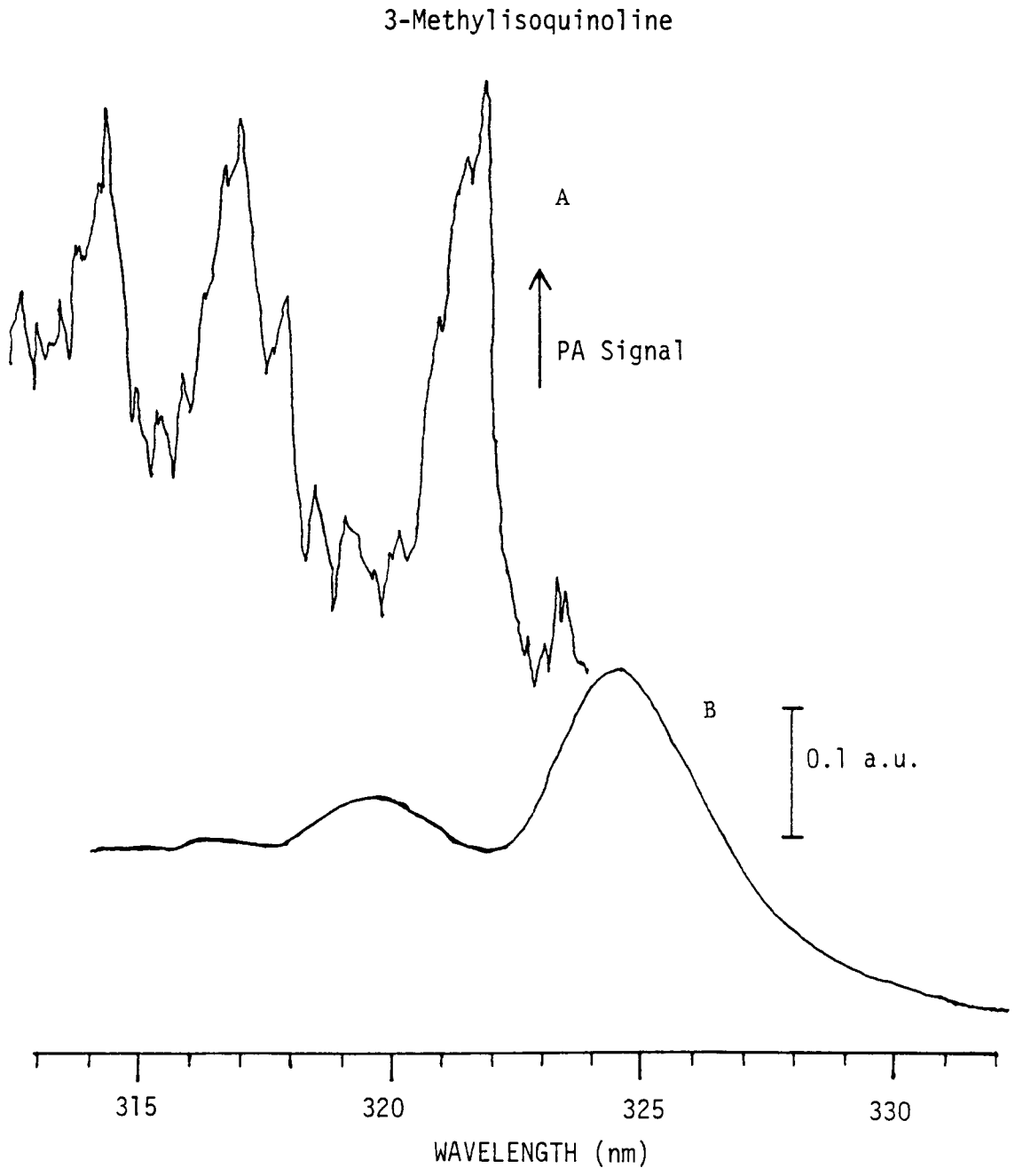


Figure 19. Spectra of 3-methylisoquinoline. (A) MI-PA spectrum of 20 μg in Ar at 10 K. (B) Room-temperature solution absorption spectrum, 10^{-4} M in hexane.

room-temperature solution absorption spectrum. Initially, this observation was puzzling, but after comparing this result with MI-absorption spectra of 3-methylisoquinoline obtained in subsequent experiments, the reason became obvious. From data obtained in other MI-absorption experiments and based upon the quantity of 3-methylisoquinoline in the MI sample, it is estimated that the peaks at 322 nm and 317 nm had absorbances of ~1.2 and ~0.55, respectively. In this case, the PA signal magnitude is no longer proportional to the absorbance, A. It is instead proportional to $1-10^{-A}$ which yields a peak height ratio of 1.3:1 for the A values of 1.2 and 0.55. This is close to the ratio observed in the MI-PA spectrum (1.4:1). This situation was not understood at the time this particular experiment was performed, and no absorption spectrum was recorded for the sample.

Figure 20-A shows the MI-PA spectrum of 2,6-dimethylquinoline (1 μg in Xe at 10 K) in the 315-327 nm region and compares it with the room-temperature solution (10^{-4} M in hexane) absorption spectrum in Figure 20-B. The MI-PA spectrum was obtained with the 1.6 mm thick PZT disc compressed against the sapphire window. Unlike the MI-PA spectra of 3-bromoquinoline, quinoline, and 3-methylquinoline (Figs. 17-19) which were obtained in either Ar or N_2 matrices, a significant blue shift in the peak maximum was not observed. The lack of a significant blue shift was found to be characteristic of spectra in Xe matrices. A two-fold bandwidth reduction is observed, 190 cm^{-1}, in the MI-PA spectrum compared with 385 cm^{-1} in the solution spectrum.

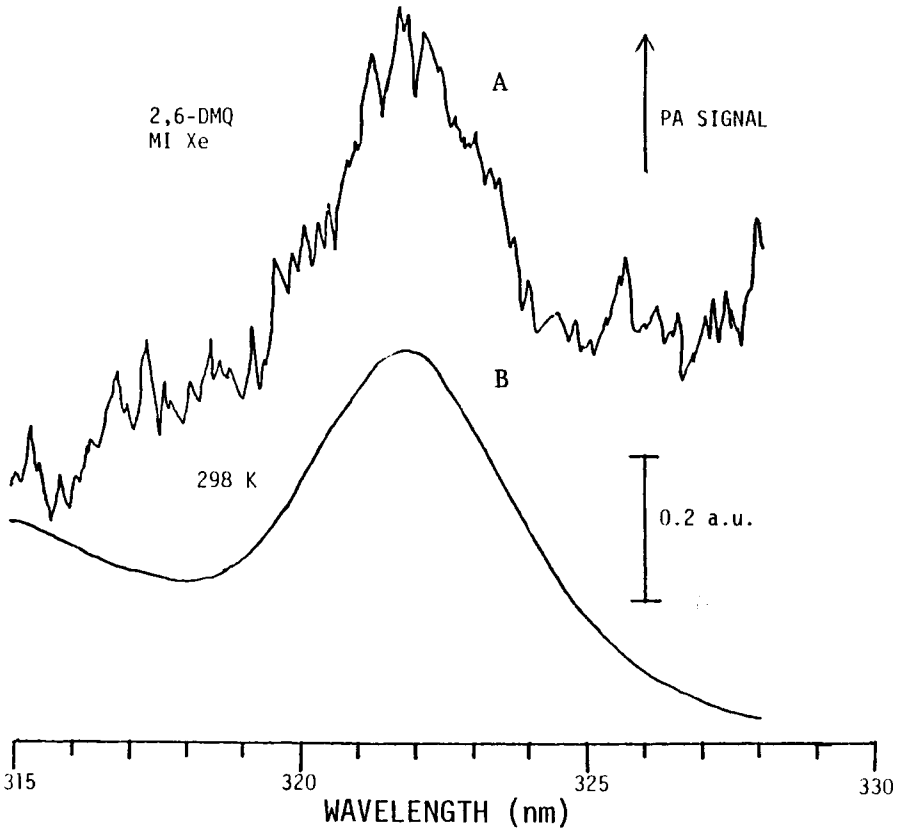


Figure 20. Spectra of 2,6-dimethylquinoline. (A) MI-PA spectrum of 1 μg in Xe at 10 K. (B) Room-temperature solution absorption spectrum, 10^{-4} M in hexane.

After obtaining MI-PA spectra for several individual members of the quinoline family of N-heterocycles, attempts were made to resolve mixtures of the various isomeric compounds of the quinoline family. MI-absorption spectra of several methylquinoline, methylisoquinoline, and dimethylquinoline isomers were taken in order to determine if these isomers could be resolved. The MI-absorption spectrum of four dimethylquinoline (DMQ) isomers in Ar is shown in Figure 21. As the spectrum shows, the isomers are not completely resolved in the MI sample. The 2,6-DMQ peak at 318 nm is partially resolved from those of the other isomers. The large band at 316 nm results from the overlap of bands due to 4,6-DMQ and 2,7-DMQ. The 2,4-DMQ peak at 314 nm can just be seen on the tailing edge of the large 4,6-DMQ/2,7-DMQ peak. The identification of the peaks of the isomers is based upon the values obtained for MI-absorption spectra of the individual compounds. Notice that the peak of 2,6-DMQ is at 318 nm in the Ar matrix (Fig. 21), whereas it was found at 322 nm in the Xe matrix (Fig. 20).

Figure 22 shows the MI-absorption spectrum of three isomeric methylquinolines (MQ) and 3-methylisoquinoline (3-MIQ), an isomer of the methylquinolines. As in the case of the dimethylquinolines, the spectra of these isomers are not completely resolved, except for that of 3-methylisoquinoline. The 3-MIQ peak at 322 nm is completely resolved from those of the rest of the isomers. The overlapping peaks at 316 nm, 315 nm, and 312 nm are assigned to 6-MQ, 8-MQ, and 4-MQ, respectively. The assignment of these peaks is made on the basis of the values obtained from the MI-absorption spectra of the individual compounds.

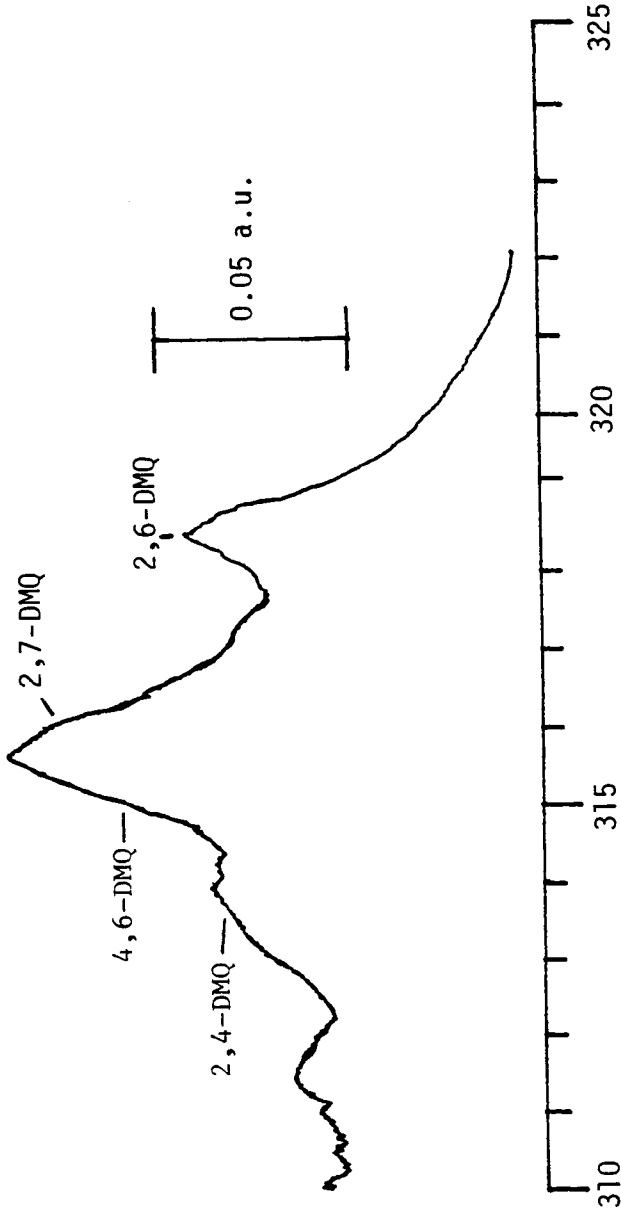


Figure 21. MI-absorption spectrum of a mixture of dimethylquinoline (DMQ) isomers, 5 µg each in Ar at 10 K.

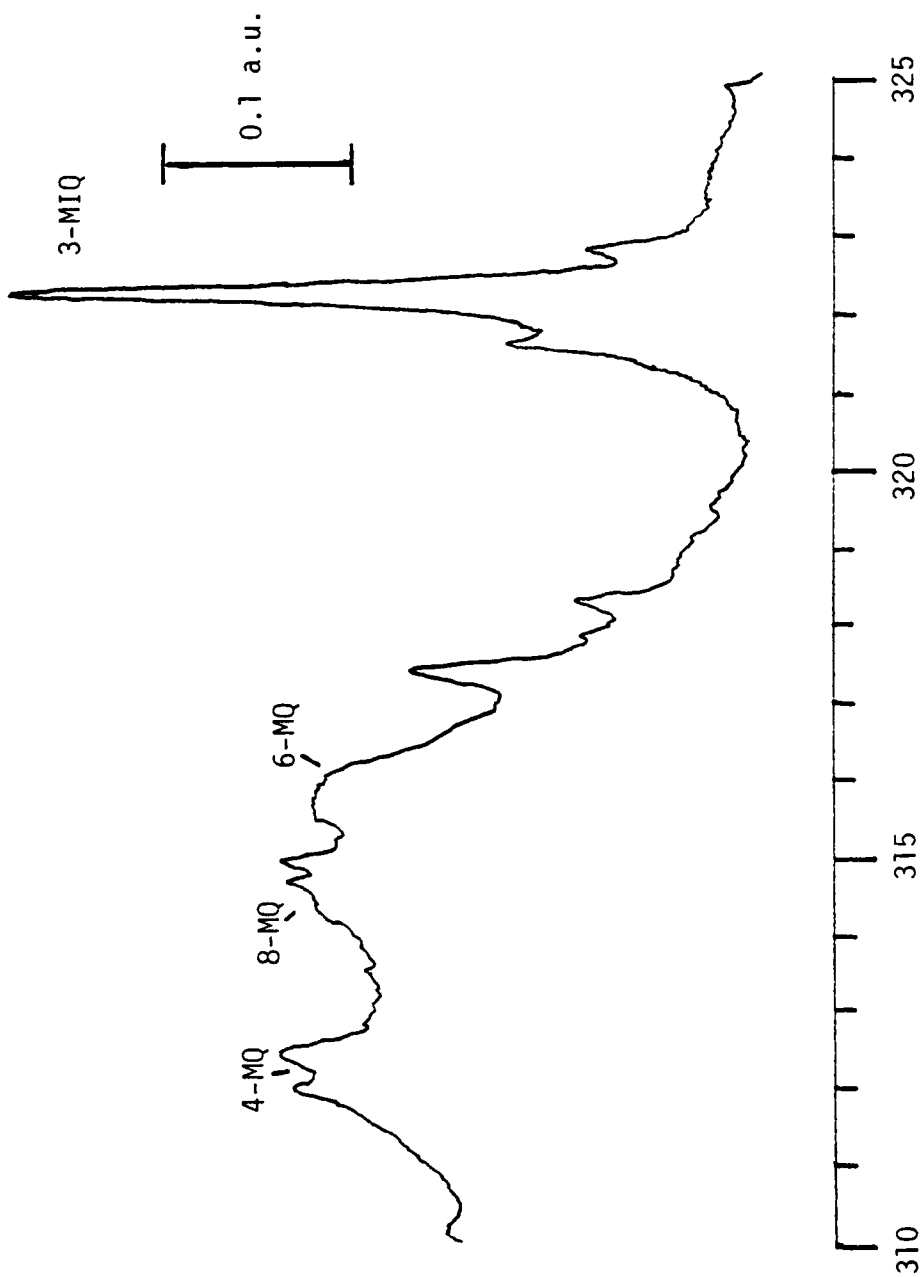


Figure 22. MI-absorption spectrum of a mixture of methylquinoline (MQ) isomers and 3-methylisoquinoline (3-MIQ), 5 µg each in Ar at 10 K.

It may have been possible to achieve better resolution of these two groups of isomers by using "Shpol'skii" (i.e., n-alkane) matrices. However, attempts to obtain MI-PA spectra using these types of matrices were unsuccessful due to the extremely large background produced by scattered light striking the transducer or parts of the transducer assembly. All n-alkane matrices are very "frosty", i.e., translucent, and scatter light much more effectively than Ar and N_2 matrices. The magnitude of the scattered light background signal produced by highly scattering matrices was much larger than the PA signal typically produced by the analytes in Ar and N_2 matrices. For the same reason, attempts to obtain MI-absorption spectra of n-alkane matrix samples were also unsuccessful. In a typical MI-absorption experiment, < 1% of the incident light was transmitted through an n-alkane matrix.

More useful results were obtained for the angular benzoquinoline (BQ) isomers, 7,8-BQ, 5,6-BQ, and 3,4-BQ. It was possible to resolve a mixture of these three isomers. The MI-PA spectrum of this isomeric mixture (2 μg of each compound in Ar at 5 K) in the 325-345 nm range is shown in Figure 23-A. The 3 mm thick PZT disc glued to the sapphire window was used to obtain the MI-PA spectrum. In the MI-PA spectrum, the peaks at 344 nm, 342 nm, and 341 nm belong to 7,8-BQ, 5,6-BQ, and 3,4-BQ, respectively. These isomers were identified from MI-absorption spectra of the individual compounds shown in Figure 24. For the purpose of comparison, the room-temperature solution (3×10^{-5} M each in hexane) absorption spectrum of the mixture is shown in Figure 23-B, and an overlay of the individual room-temperature solution (10^{-4} M each in hexane) absorption spectra is shown in Figure 23-C. The spectrum of

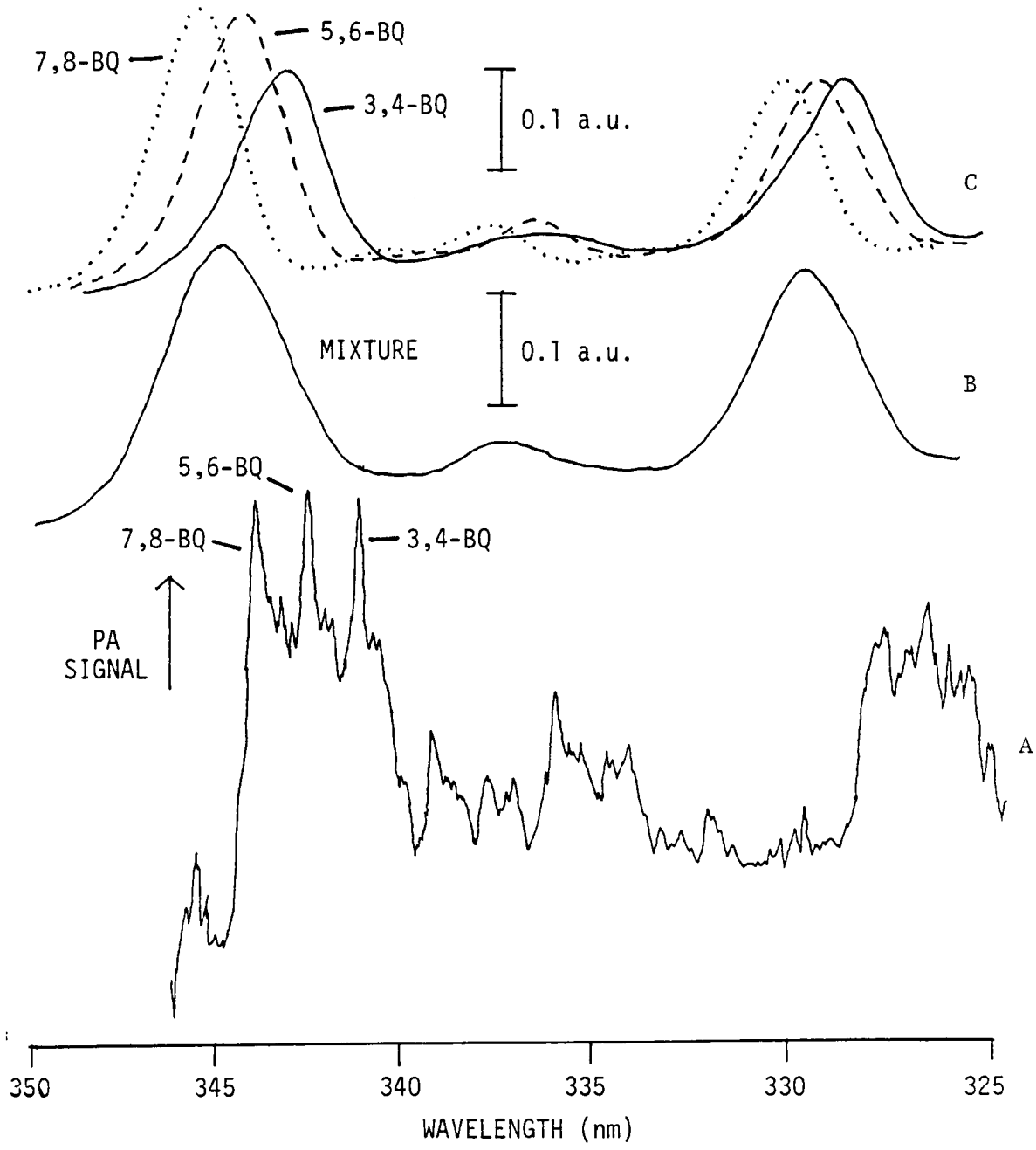


Figure 23. Spectra of benzoquinoline (BQ) isomers. (A) MI-PA spectrum of 2 μg each of 3,4-BQ, 5,6-BQ, 7,8-BQ in Ar at 5 K. (B) Room temperature solution absorption spectrum of the isomeric mixture, 3×10^{-5} M each in hexane. (C) Overlay of room-temperature solution absorption spectra of the individual isomers, 10^{-4} M each in hexane.

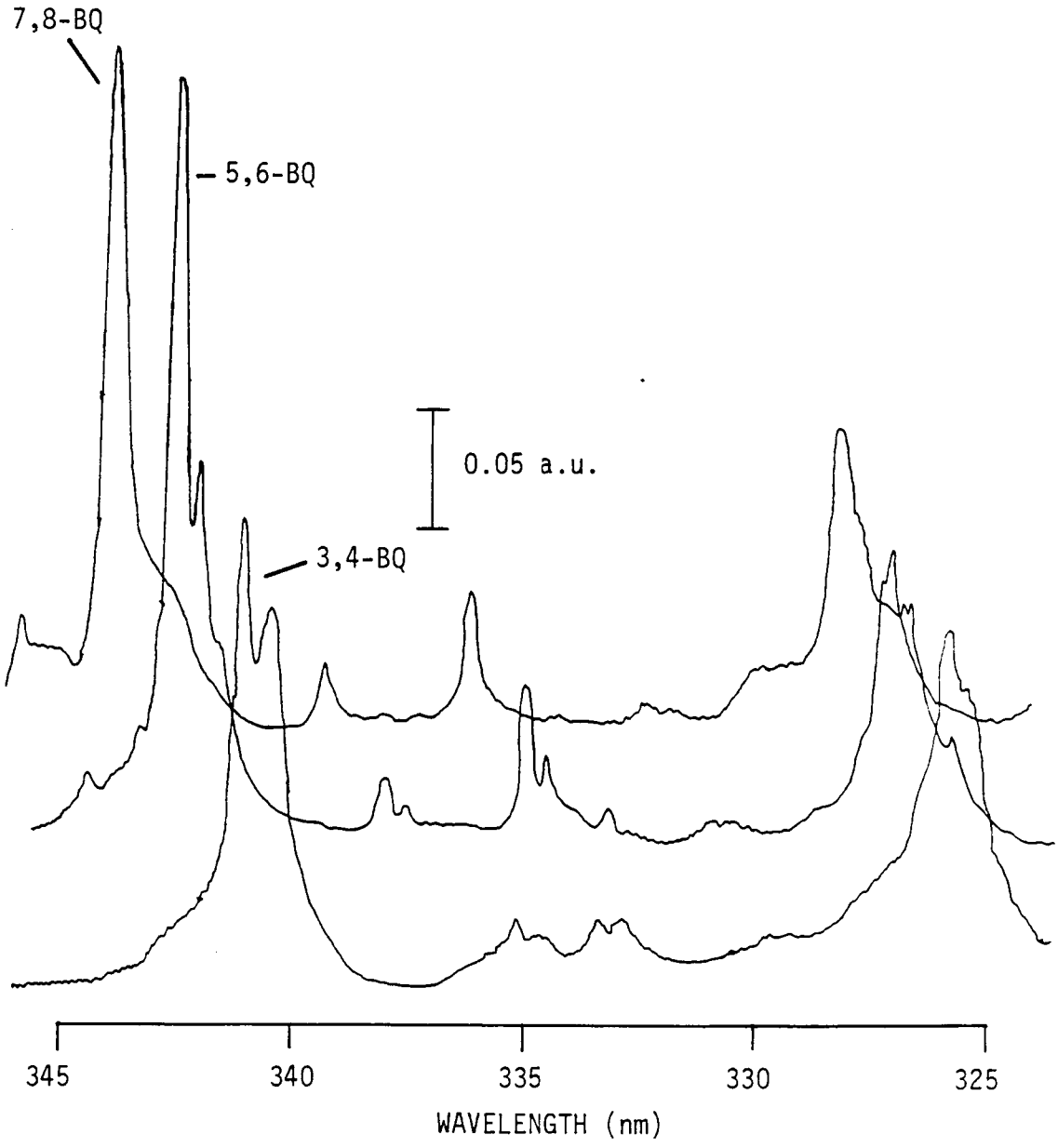


Figure 24. MI-absorption spectra of the individual benzoquinoline (BQ) isomers, 10 μg each in Ar at 10 K.

the room-temperature mixture is completely devoid of any resolution for the individual compounds, whereas in the MI-PA spectrum, the three isomers are identified. Furthermore, these particular isomers cannot be unambiguously identified by conventional mass spectrometry.[33] The benzoquinoline isomers exhibited the highest MI-PAS spectral resolution obtained for any of the N-heterocycles studied. The bandwidth of the spectrum of any one of the isomers was 120 cm^{-1} in the MI-PA spectrum compared with 330 cm^{-1} in the room-temperature solution spectrum. In the MI-PA spectrum of the three isomers (Fig. 23-A), there is a ~5 % overlap of the bands of 3,4-BQ and 7,8-BQ, and a ~25 % overlap between the band of 5,6-BQ and the bands of 3,4-BQ or 7,8-BQ. Thus, it is estimated that 3,4-BQ could be determined in the presence of 20 times as much 7,8-BQ and vice versa; 5,6-BQ could be determined in the presence of 4 times as much 3,4-BQ or 7,8-BQ. These estimates are for a 50 % accuracy.

Figure 25-A shows the MI-PA spectrum in the 320-335 nm range of 5,6-benzoquinoline (5 μg) in Xe at 18 K. The MI-PA spectrum was obtained with the 3 mm thick PZT disc compressed against the sapphire window. The room-temperature solution (10^{-4} M in hexane) absorption spectrum is shown in Figure 25-B for comparison. The MI-PA spectrum exhibits an ~20 % reduction in bandwidth compared with the room-temperature spectrum (260 cm^{-1} vs. 330 cm^{-1}). There is no appreciable blue shift in the maximum in the MI-PA spectrum (as compared with the solution spectrum), which is typical of other spectra in Xe matrices. The MI-PA spectrum in the 340-345 nm region, where the benzoquinolines are well resolved (Fig. 23-A), was not obtained for this sample

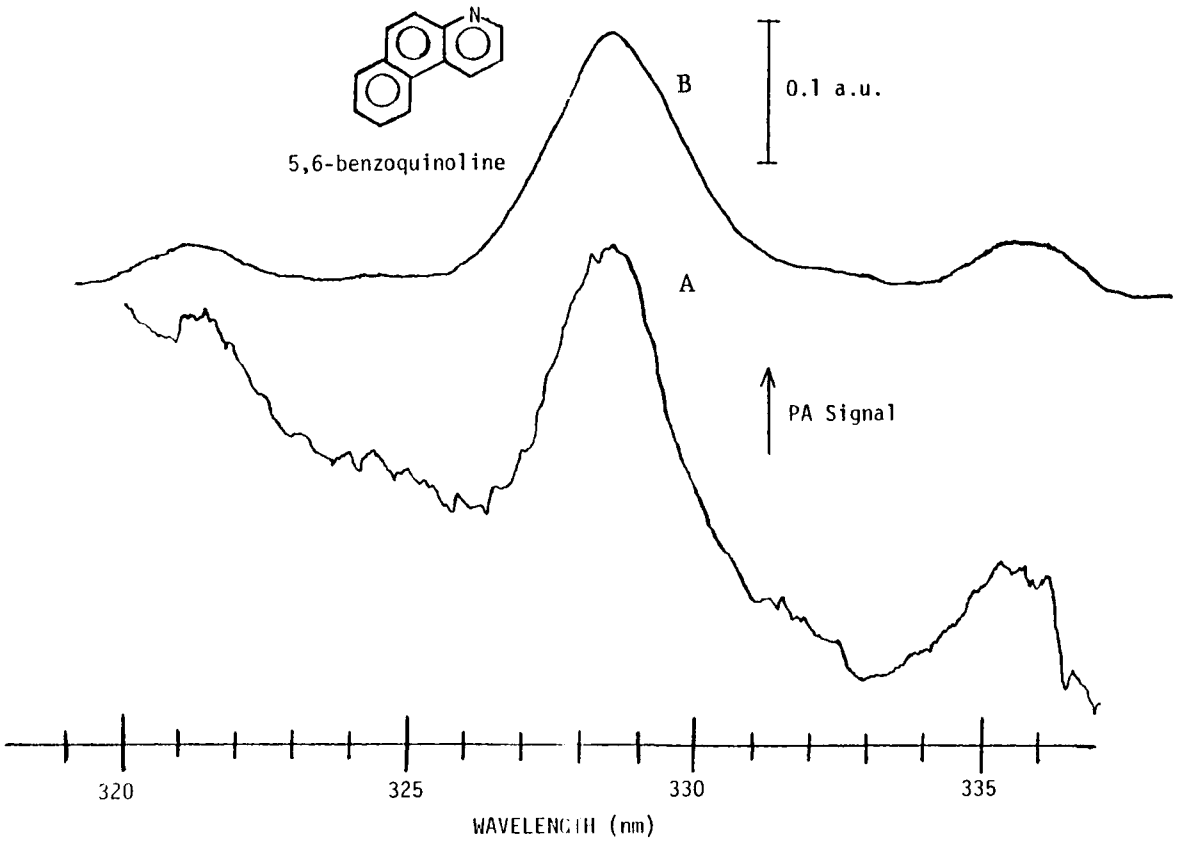


Figure 25. Spectra of 5,6-benzoquinoline. (A) MI-PA spectrum of 5 μg in Xe at 18 K. (B) Room-temperature solution absorption spectrum, 10^{-4} M in hexane.

because, at the time, the laser dye (Sulforhodamine 640, Table II-2, p. 31) required to cover the 340-345 nm wavelength range was not accessible.

Some other N-heterocycles were investigated to determine if they would yield well-resolved MI spectra. Figure 26 shows the MI-absorption spectra of acridine (10 μg) and phenazine (10 μg) in Ar at 10 K. The MI-absorption spectra of these two compounds have bandwidths of > 300 cm^{-1}. The bandwidths at 298 K are > 600 cm^{-1}. Acridine is an isomer of the benzoquinolines (which yielded well resolved MI spectra). The reason for the disparity in the behavior of these isomeric compounds is not known. Attempts to obtain "site-selected" fluorescence spectra of matrix-isolated acridine have also been unsuccessful.[96] On the other hand, "site-selection" fluorescence spectra have been obtained for other N-heterocycles in low-temperature Ar matrices.[97] However, there is no obvious procedure for achieving "line narrowing" in absorption or PA spectroscopy analogous to the "site selection" technique in fluorescence[61]; that is, the effect of inhomogeneous broadening observed in an absorption or PAS experiment for a given solute in a given matrix cannot be altered by the experimenter.

The results in the present work indicate that matrix isolation does not produce highly resolved absorption spectra for all N-heterocycles. This is consistent with the results obtained for broadband-excited MI fluorescence by Bilotta.[98] He found that many 3- and 4-ring N-heterocycles exhibited very broad MI-fluorescence spectra in a variety of matrices (e.g., Ar, N_2, n-alkanes, and SF_6). Thus, matrix

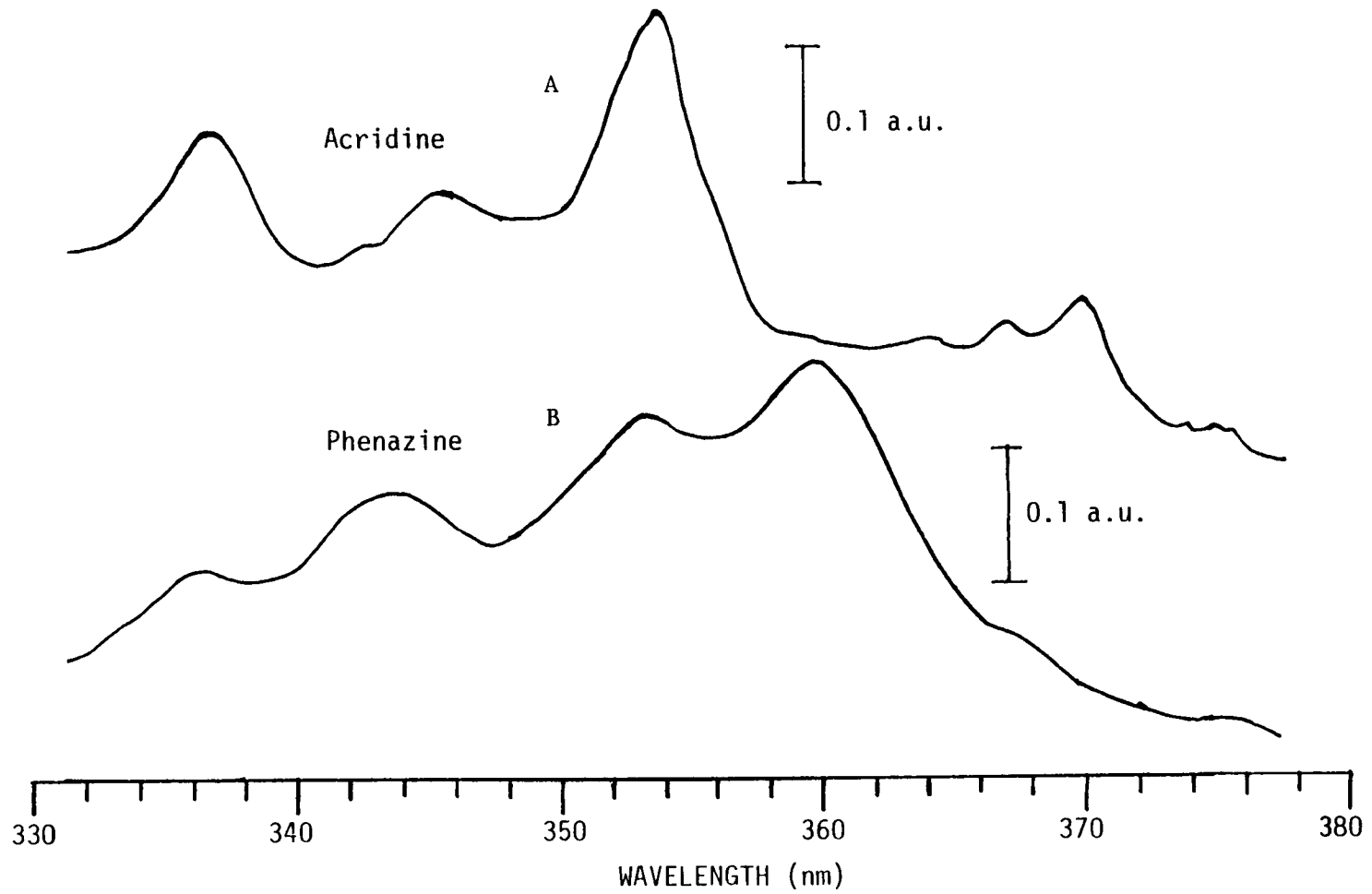


Figure 26. MI-absorption spectra of (A) 10 µg of acridine and (B) 10 µg of phenazine in Ar at 10 K.

isolation seems to be selectively advantageous for significantly enhancing the spectral resolution for the N-heterocycles.

b. PAHs. Although the present work was primarily concerned with the detection of weakly fluorescing and non-fluorescing PACs, MI-PA spectra were obtained for several PAHs in order to show the applicability of the technique to various types of molecules. The PAHs are, in general, strongly fluorescing compounds, but some have appreciable singlet-triplet (non-radiative) intersystem crossing efficiencies.[49] The MI-PA spectrum of pyrene (500 ng in Ar at 5 K) in the 325-335 nm region is shown in Figure 27-A. The room-temperature solution (10^{-5} M in hexane) absorption spectrum is shown in Figure 27-B. A two-fold improvement in the resolution (185 cm^{-1} vs. 350 cm^{-1}) and the characteristic blue shift of the peak maximum is observed in the MI-PA spectrum. The sloping baseline is due to an instrumental artifact involved in the normalization process (p. 66).

The MI-PA and MI-absorption spectra of naphthalene (30 μg) and 1-bromonaphthalene (3 μg) in the same Ar matrix at 5 K in the 305-315 nm region are shown in Figures 28-A and 28-B, respectively. The 3 mm thick PZT disc glued to the sapphire window was used to obtain the MI-PA spectrum. By comparing the MI-PA and MI-absorption spectra, it is observed that the relative peak heights for naphthalene and 1-bromonaphthalene are not equal in the two spectra. In the MI-absorption spectrum, the peak height ratio of naphthalene:1-bromonaphthalene is ~7:1, whereas in the MI-PA spectrum the ratio is ~2:1. The different ratios of peak heights are attributed to the different non-radiative quantum yields of the two compounds. The effect of

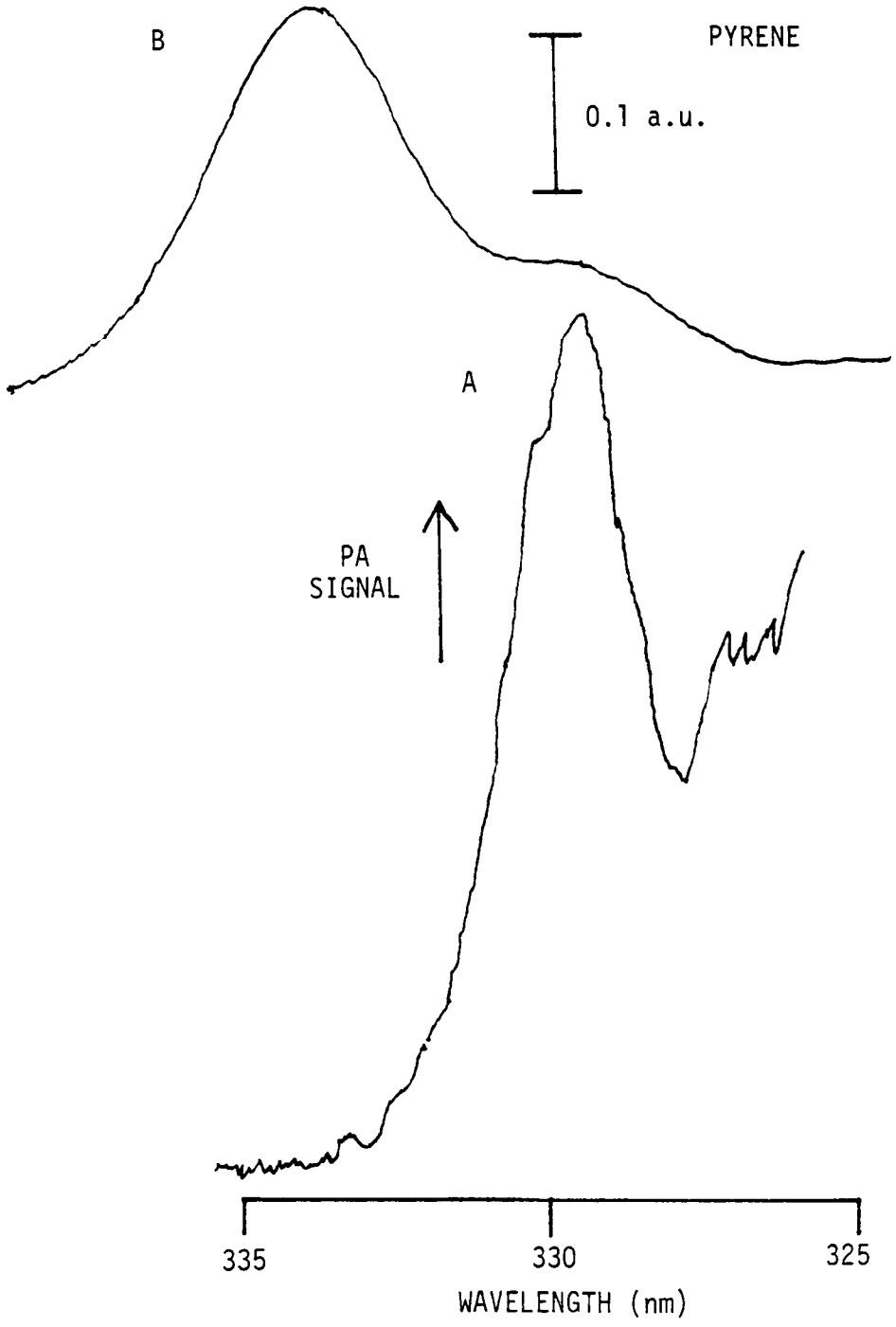


Figure 27. Spectra of pyrene. (A) MI-PA spectrum of 500 ng in Ar at 5 K. (B) Room-temperature solution absorption spectrum, 10^{-5} M in hexane.

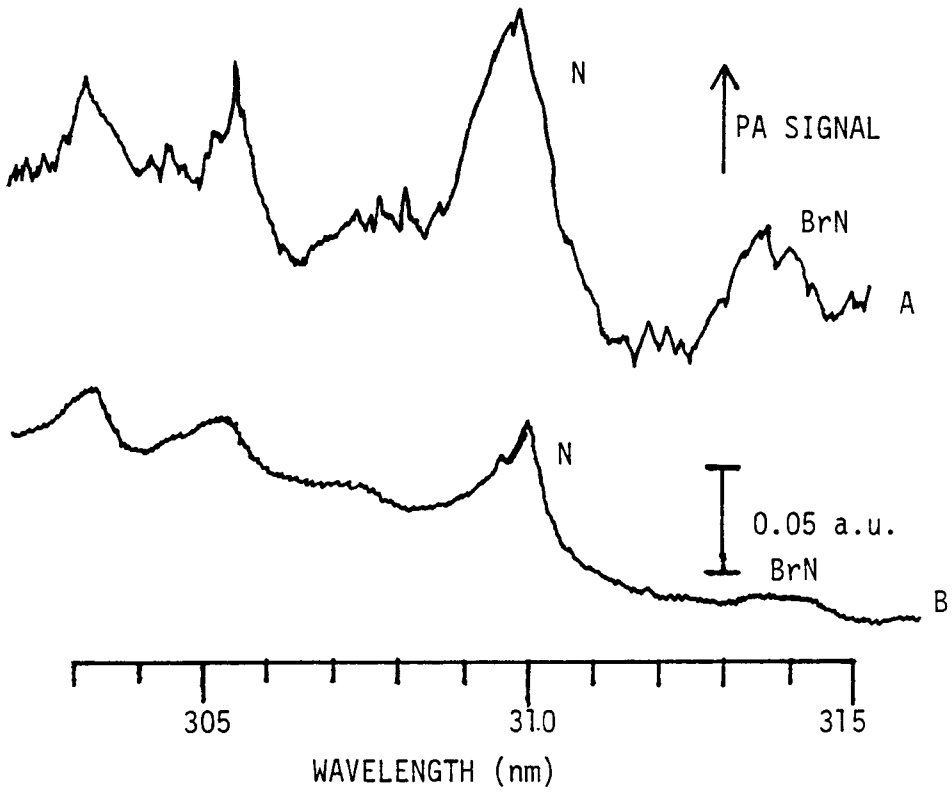


Figure 28. (A) MI-PA spectrum and (B) MI-absorption spectrum of 30 μg of naphthalene (N) and 3 μg of 1-bromonaphthalene (BrN) in Ar at 5 K.

non-radiative quantum yields upon the PA signal, for this case and other cases, is discussed in a subsequent section (p. 123).

c. Other Weakly Fluorescing PACs. Two other classes of non-fluorescing or weakly-fluorescing compounds were also characterized by MI-absorption to determine the resolution of their MI spectra. The MI-absorption spectra of 6-nitroquinoline (10 μg), 1-nitronaphthalene (10 μg), and 2-nitrofluorene (10 μg) in Ar at 10 K are shown in Figure 29. As the figure shows, these nitro-substituted PACs do not produce highly-resolved spectra. The bandwidths of the 2-nitrofluorene and 6-nitroquinoline peaks at 335 nm are 180-270 cm^{-1}, but there is sufficient overlap that these two compounds could not be completely resolved in a mixture. The relatively broadband spectra and high density of spectral bands made these compounds undesirable for study by laser excited PAS.

MI-absorption spectra of three carbonyl PACs, anthraquinone (10 μg), 1,4-naphthoquinone (10 μg), and 9-fluorenone (10 μg) in Ar at 10 K, are shown in Figure 30. As the figure shows, the resolution of the absorption spectra of these representative carbonyl PACs is poor. The three peaks in the 9-fluorenone spectrum between 300-330 nm have bandwidths of ~200 cm^{-1}, which are comparable to those of the quinoline (N-heterocyclic) compounds. The spectrum of 1,4-naphthoquinone is a broad continuum from ~290-350 nm with some fine structure superimposed upon it. Anthraquinone has a relatively sharp band (295 cm^{-1} bandwidth) on the shoulder of a much stronger band which peaks at ~250 nm (not shown). However, in general the carbonyl PACs, like the nitro PACs, did not yield sufficiently highly resolved MI spectra

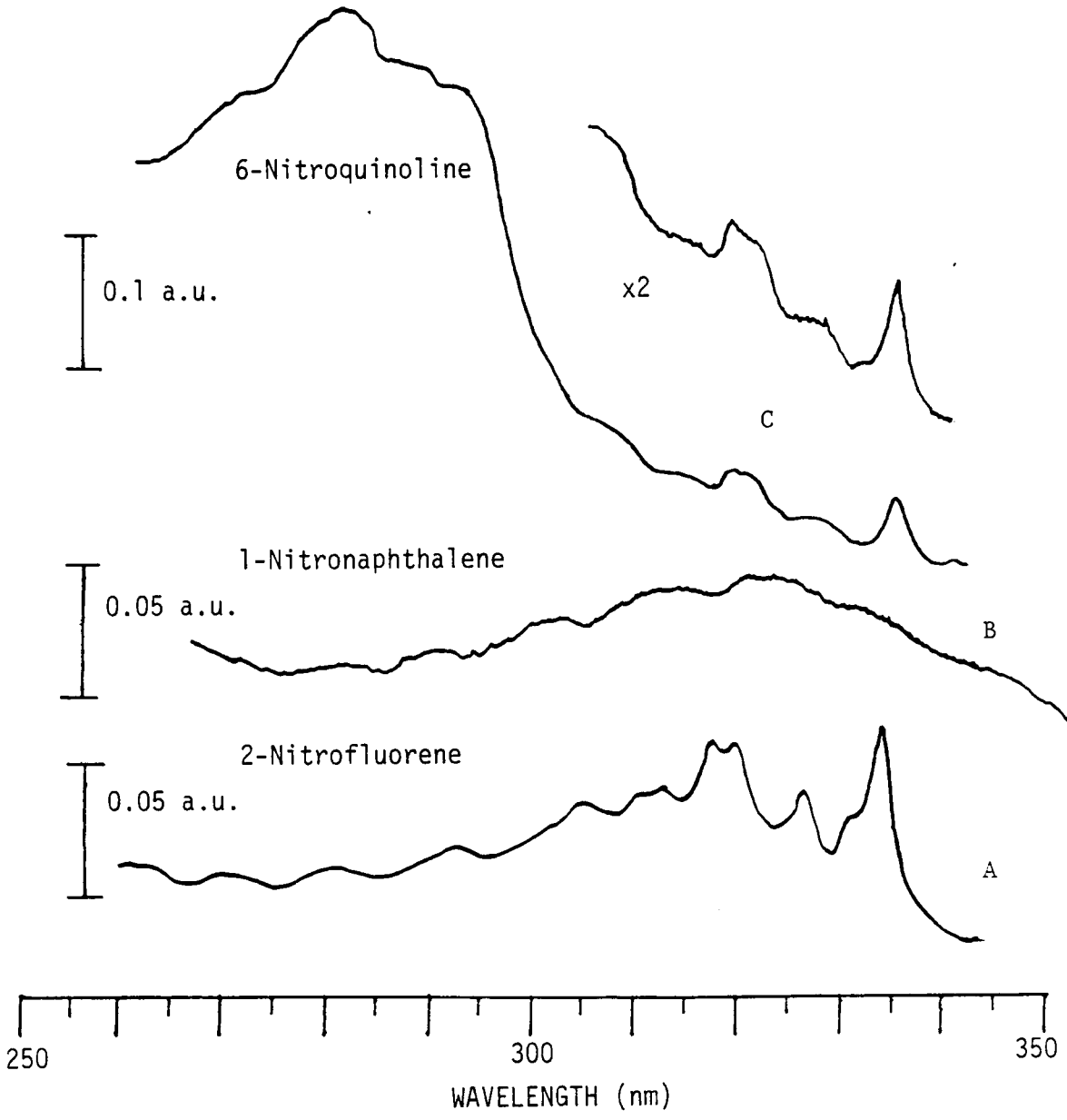


Figure 29. MI-absorption spectra of (A) 5 μg of 2-nitrofluorene, (B) 10 μg of 1-nitronaphthalene, and (C) 5 μg of 6-nitroquinoline in Ar at 10 K.

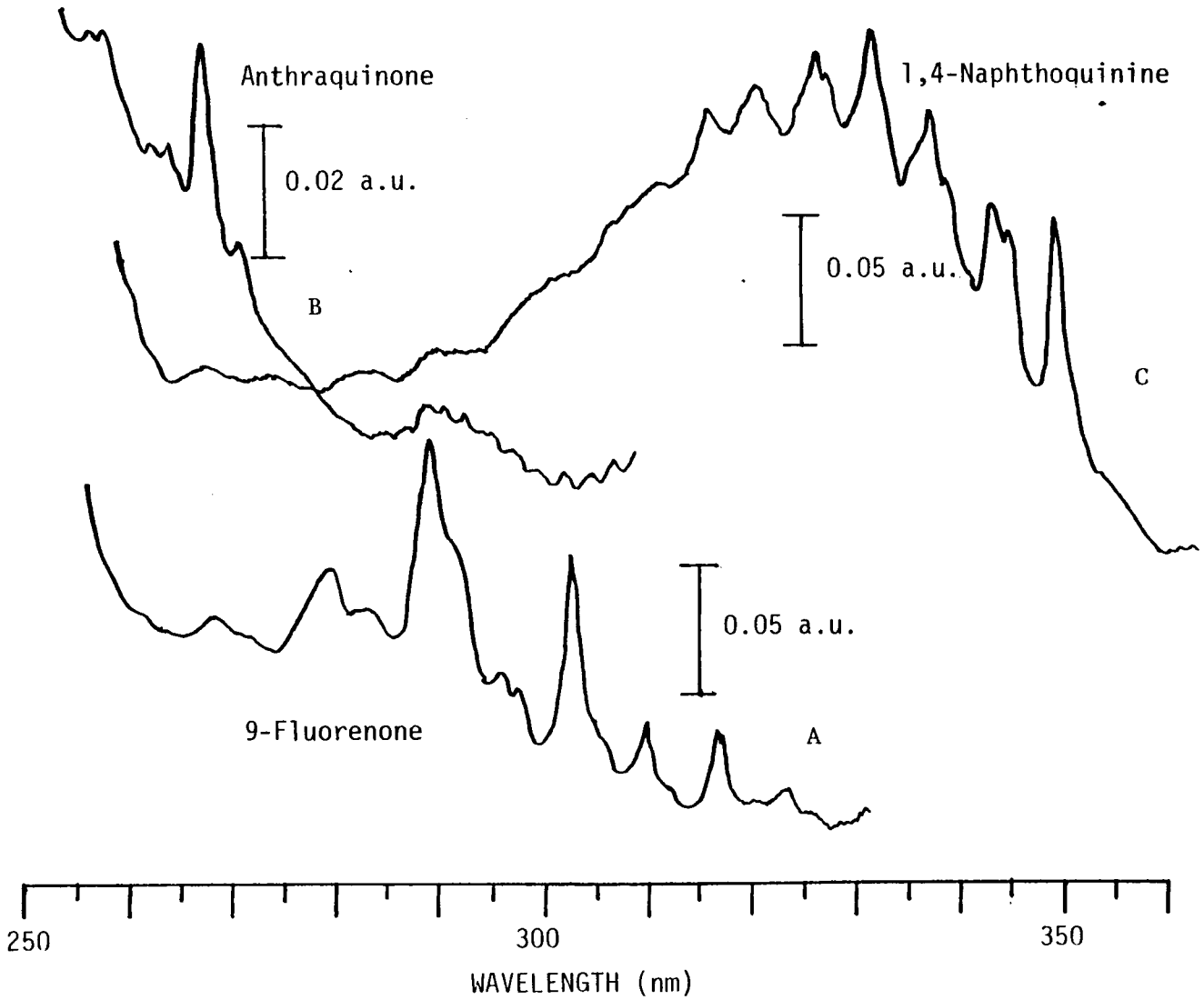


Figure 30. MI-absorption spectra of (A) 5 µg of 9-fluorenone, (B) 5 µg of anthraquinone, and (C) 20 µg of 1,4-naphthoquinone in Ar at 10 K.

to warrant studying them by laser excited PAS. Furthermore, the high density of bands in the spectra would be a severe complication in the analysis of multi-component samples.

Many sulfur and oxygen containing PACs (i.e., S- and O-heterocycles) are also reported to have low (< 0.1) fluorescence quantum efficiencies.[55] These classes of compounds were not studied in detail, but MI-PA spectra were obtained for one member of each class. Figure 31-A shows the MI-PA spectrum of dibenzothiophene (5 μg) in Ar at 5 K in the 315-325 nm range. The MI-PA spectrum corresponds well to the room-temperature solution (10^{-4} M in hexane) absorption spectrum shown in Figure 31-B. A 1.7-fold resolution enhancement is observed in the MI-PA spectrum (300 cm^{-1} vs. 520 cm^{-1}). Figure 32-A shows the MI-PA spectrum of dibenzofuran (5 μg) in Ar at 5 K in the 300-290 nm range. The room-temperature solution (10^{-4} M) in hexane) absorption spectrum is shown in Figure 32-B for comparison. The MI-PA spectrum exhibits a slight improvement in resolution. Both MI-PA spectra were obtained with the 3 mm thick PZT disc glued to the sapphire window. Fairly intense violet-blue phosphorescence with a ~5 s lifetime was visually observed for MI samples of both dibenzothiophene and dibenzofuran. No other O- and S-heterocycles were studied.

Table III-1 provides a recapitulation of the MI-PA spectra recorded for various PACs. MI band positions, bandwidths, and band reduction factors are also listed.

2. Factors Affecting the PA Signal and the Limit of Detection

In piezoelectrically-detected PAS of condensed media, the magnitude of the PA signal is dependent upon many factors. These

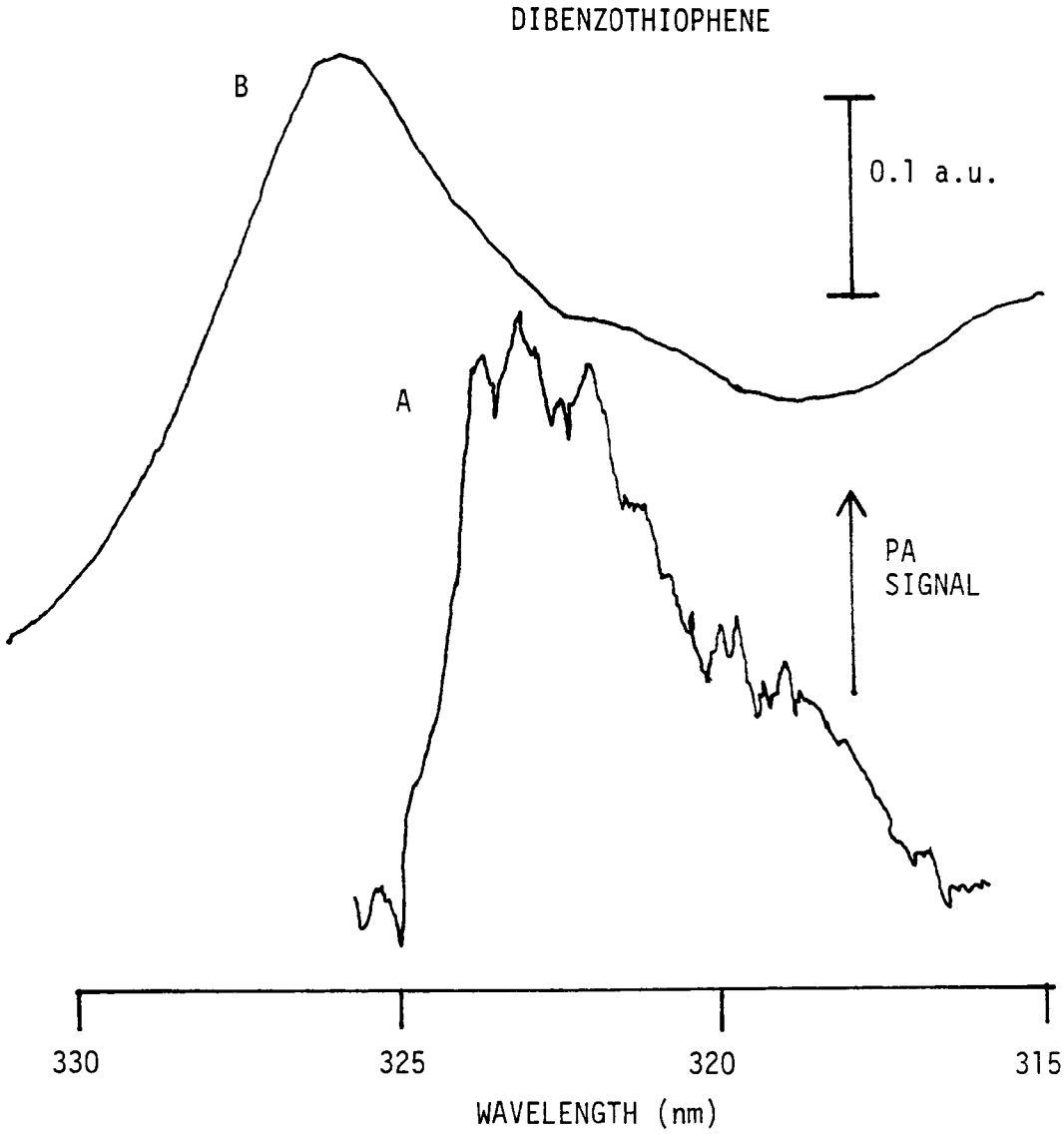


Figure 31. Spectra of dibenzothiophene. (A) MI-PA spectrum of 5 μg in Ar at 5 K. (B) Room-temperature solution absorption spectrum, 10^{-4} M in hexane.

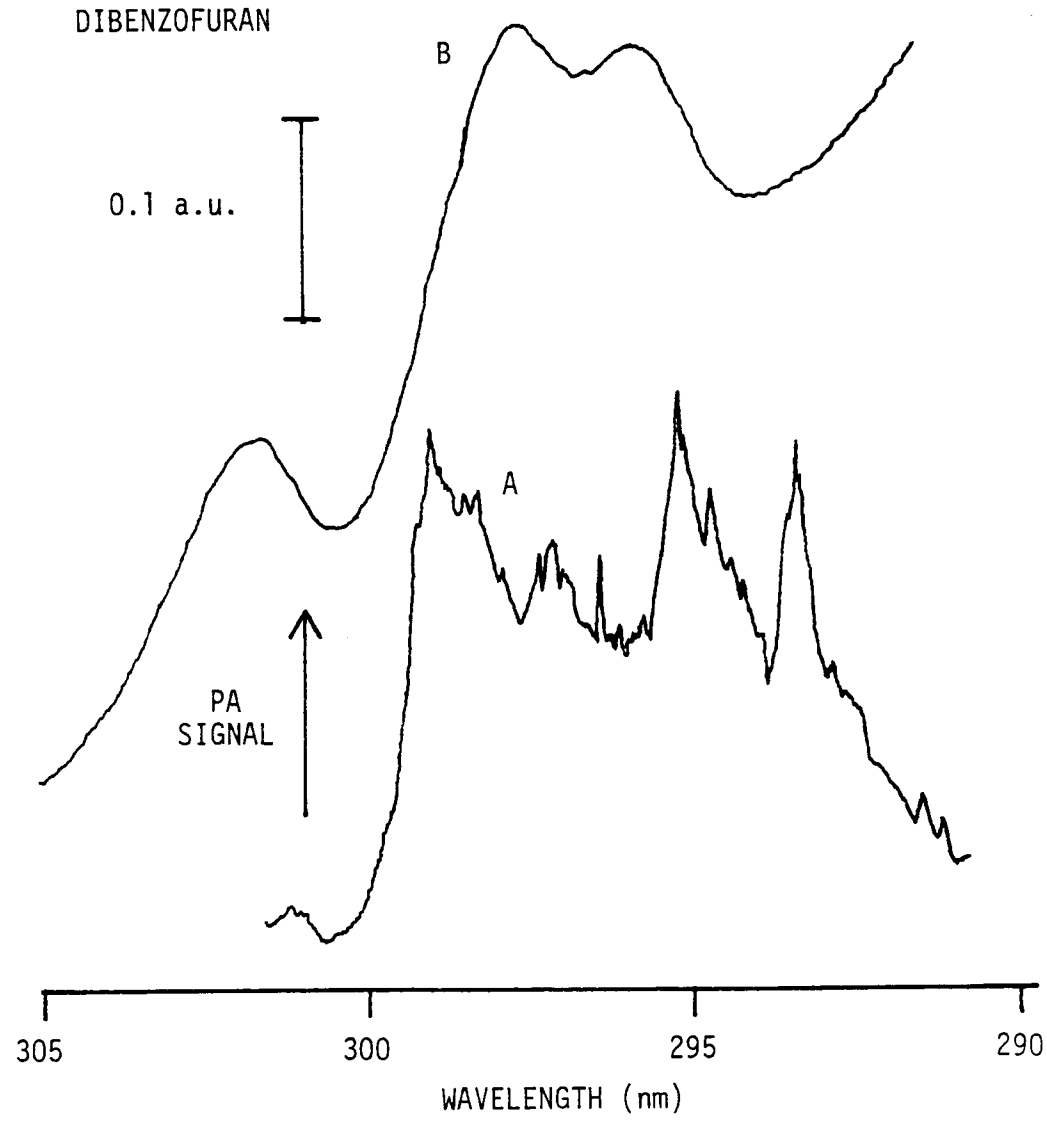


Figure 32. Spectra of dibenzofuran. (A) MI-PA spectrum of 5 μg in Ar at 5 K. (B) Room-temperature solution absorption spectrum, 10^{-4} M in hexane.

TABLE III-1

PACS FOR WHICH MI-PA SPECTRA WERE RECORDED

Compound	Matrix[a]	Quantity, μg	Principal Band Position, cm^{-1}	MI Spectral Bandwidth, cm^{-1}	Bandwidth Reduction MI/298 K	MI Spectral Shift vs. 298 K, cm^{-1}[b]
Quinoline	N_2	5	32,100	185	0.36	350
	Ar	5	32,100	185	0.36	350
	Xe	3	31,950	185	0.36	<25
3-Bromoquinoline	Ar	4	31,150	145	0.38	190
3-Methylisoquinoline	Ar	20	31,100	115	0.30	280
2,6-Dimethylquinoline	Xe	1	31,100	290	0.50	<25
3,4-Benzoquinoline	Ar	2	29,325	120	0.36	170
5,6-Benzoquinoline	Ar	2	29,200	120	0.36	190
	Xe	5	30,395	260	0.80	<25
7,8-Benzoquinoline	Ar	2	29,070	120	0.36	100
Pyrene	Ar	0.5	30,350	185	0.53	545
Naphthalene	Ar	30	32,350	140	0.30	150
	Xe	20	31,200	260	0.56	<25
1-Bromonaphthalene	Ar	3	31,900	140	0.30	180
	Xe	2	31,850	170	0.36	<25
Dibenzothiophene	Ar	5	30,960	285	0.67	285
Dibenzofuran	Ar	5	33,445	250	0.50	285
	Ar	5	33,900	230	0.50	330
	Ar	5	34,100	180	0.50	330

[a] ~5 mg of matrix.

[b] n-alkane solution.

factors can be categorically classified as those which are due to instrumental parameters and those which are a consequence of the various properties of the molecules and matrix materials.

a. Instrumental Parameters. Several important instrumental parameters pertinent to pulsed-laser PAS have been discussed previously (p. 7). They include a high laser pulse energy, a high PE transducer sensitivity, good acoustic coupling between the sample and PE transducer, and a good frequency match between the laser pulse and transducer resonance.

The enhanced sensitivity that has been achieved by pulsed-laser PA measurements compared with conventional absorption measurements is primarily a consequence of the fact that the PA signal magnitude is directly proportional to the laser pulse energy (Eqn. I-2, p. 7). The dye laser used in the present work provided pulse energies of 1-2 mJ in the visible (fundamental) and 0.02-0.2 mJ in the UV (second harmonic). These pulse energies are moderate compared with those which can be obtained from other commercially available high-energy dye lasers, e.g., Nd^{3+}:YAG and excimer-laser pumped dye lasers, which can provide at least 10 times higher pulse energies in the visible and up to 100 times higher pulse energies in the UV. Thus, the overall sensitivity (or limit of detection) in the present work presumably could have been improved had one of these more powerful lasers been available. However, the moderate energy output of the laser used was adequate in order to investigate the general utility of MI-PAS.

Perhaps the primary limitation imposed by the dye laser, which is characteristic of any dye laser, was the limited wavelength tuning

range (~15-25 nm in the UV) that could be obtained for any one particular dye solution. Because of the experimental difficulty involved and time required, it was not practical to switch back and forth between different dye solutions in order to cover large spectral ranges. In fact, there were some spectral ranges for which the dye laser pulse energy was very poor (<285 nm) and other ranges for which no dyes were available (350-400 nm). Also, it was not at all uncommon to find that the main absorption bands of some molecules came near the edge of a dye tuning range or in the weakly overlapping region of two adjacent dye tuning curves. The occurrence of either of these two situations made it difficult, if not impossible, to obtain spectra for those particular compounds. A specific example of this problem was the case of isoquinoline whose principal absorption band was located at 315.5 nm, between the ranges covered by Rhodamine 6G in Ammonyx/H_2O and Kiton Red 620 in methanol/H_2O (see Table II-2, p. 31). Because of this problem, a MI-PA spectrum of isoquinoline was never obtained.

A possible alternate solution to the problems encountered when utilizing a tunable dye laser to scan over large spectral ranges is Fourier transform-photoacoustic spectroscopy (FT-PAS) using a continuum source. This technique is now widely used in the IR region and it has been recently demonstrated for the near-IR and visible regions (360-3,000 nm) with 16 cm^{-1} resolution.[89] FT-PAS is, experimentally, very similar to conventional FT-IR spectroscopy, except that detection is accomplished photoacoustically rather than photoelectrically.

As noted previously, the laser used in the present work produced light pulses having an ~1 μs temporal width at half-height. In

order to determine if the frequency content of the laser pulses was well matched with the resonance of the PE transducers used,[18] power spectra (i.e., responsitivity vs. frequency) were obtained for the laser pulses and transducer output signals subsequent to laser excitation. Figure 33-A shows the output signal obtained from the 3 mm thick (7 mm diameter) PZT disc (Fig. 8, p. 48) when measuring the PA spectrum of quinoline (5 μg) in Ar at 10 K. The laser excitation wavelength corresponded to the quinoline peak at 311 nm. The power spectrum of the PA waveform is shown in Figure 33-B. Notice the sharp resonance at 290 kHz. This agrees with the frequency that is predicted from the transducer waveform in Figure 33-A (i.e., a period of ~3.3 μs). Since the calculated shear mode resonance frequency of this 7 mm diameter disc is 285 kHz at 298 K, it appears that the observed resonance corresponds to a shear mode. The evidence of shear waves for this geometrical arrangement is further supported by the observed acoustic delay times (i.e., the time delay between the laser pulse and the onset of the transducer ringing). An acoustic delay time of 10×10^{-6} s was observed when a 3 mm thick (7 mm diameter) PZT disc was placed 3.5 cm from a thin-film glue sample (p. 64) which was located on a room-temperature fused quartz substrate. This data results in a calculated acoustic velocity of 3.5×10^{5} cm/s. This number more closely corresponds to the shear acoustic velocity (3.75×10^{5} cm/s) in fused quartz than the longitudinal acoustic velocity (5.90×10^{5} cm/s).[80]

Figure 34-A shows the temporal profile of the laser pulse in the UV (second harmonic) at 310 nm. The temporal width at half-height is ~1 μs. The high-frequency signal at the onset of the laser pulse

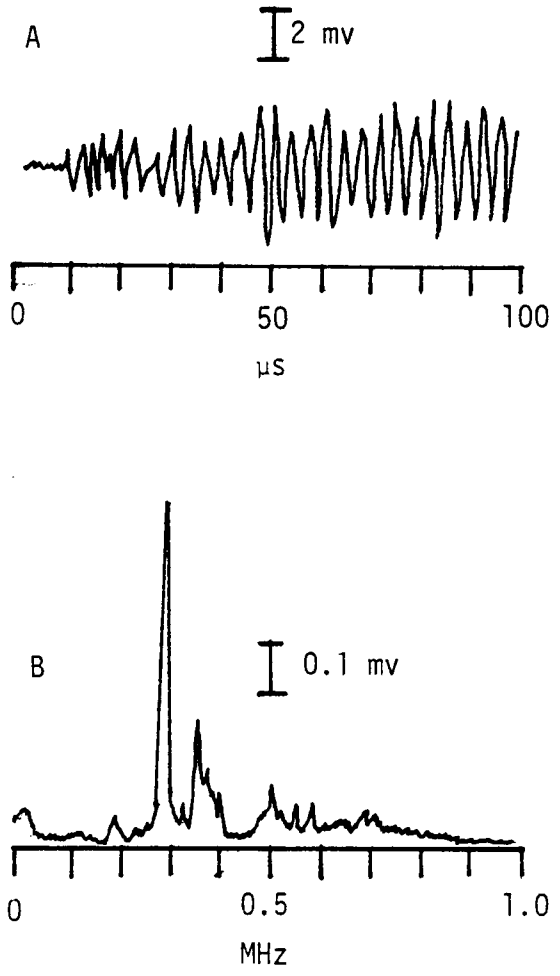


Figure 33. (A) Output signal obtained from the 3 mm thick (7 mm diameter) PZT disc following pulsed laser excitation of the MI sample. (B) Power spectrum of the PA waveform shown in (A).

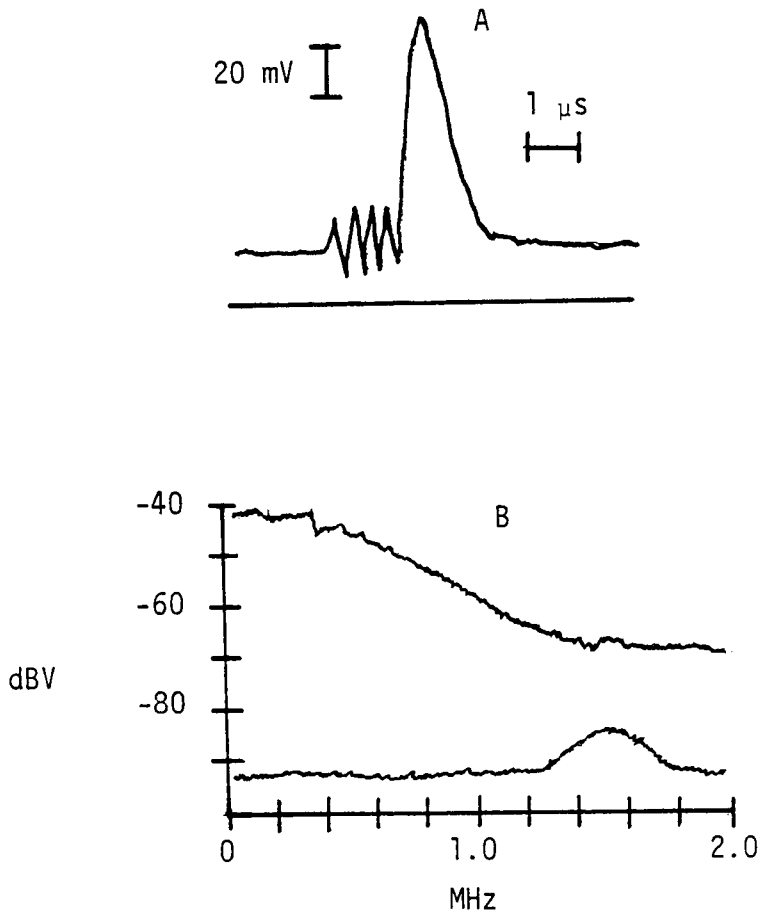


Figure 34. (A) Temporal profile of a UV (second harmonic) laser pulse, 310 nm. (B) Upper trace, power spectrum of the UV laser pulse shown in (A). Lower trace, background noise power spectrum obtained with laser beam blocked.

profile originated from electrical pick-up noise associated with the firing of the laser. The power spectrum of the laser pulse is shown in Figure 34-B. According to the power spectrum, the laser pulse energy is down by ~2 dBV (or 20%) at 290 kHz, the observed resonance frequency of the 3 mm thick (7 mm diameter) PE (PZT) transducer. Thus the power spectrum of the laser pulse had not fallen off significantly at the resonance frequency of the 3 mm thick (7 mm diameter) PZT disc which was used for most of the MI-PA experiments (Fig. 33-B). The energy of the UV laser pulse is down by ~5 dBV (or ~44%) at 500 kHz and ~18 dBV (or 88%) at 1 MHz.

Different results were obtained for a visible wavelength laser pulse. Figures 35-A and 35-B show the temporal profile and resulting power spectrum, respectively, for a laser pulse in the visible (fundamental) region at 620 nm. The temporal width of the pulse at half-height is ~1 μs, the same as observed for the UV pulse (Fig. 34-A). However, the power spectrum of the visible pulse falls off more rapidly than the power spectrum of the UV pulse (Fig. 34-B). For the visible pulse, the power spectrum falls off ~7 dBV (or ~55%) at 300 kHz, ~16 dBV (or ~84%) at 500 kHz, and ~30 dBV (or ~97%) at 1 MHz. The faster rate of fall-off for the visible pulse is due to the fact that the UV pulse was obtained by generating the second harmonic of the visible (fundamental) lasing modes inside the laser cavity. This second harmonic process is quadratically dependent on the power of the fundamental mode. This caused the UV pulse to have sharper leading and trailing edges than the fundamental pulse. This subtle difference can be seen in a careful comparison of the UV and visible pulse temporal

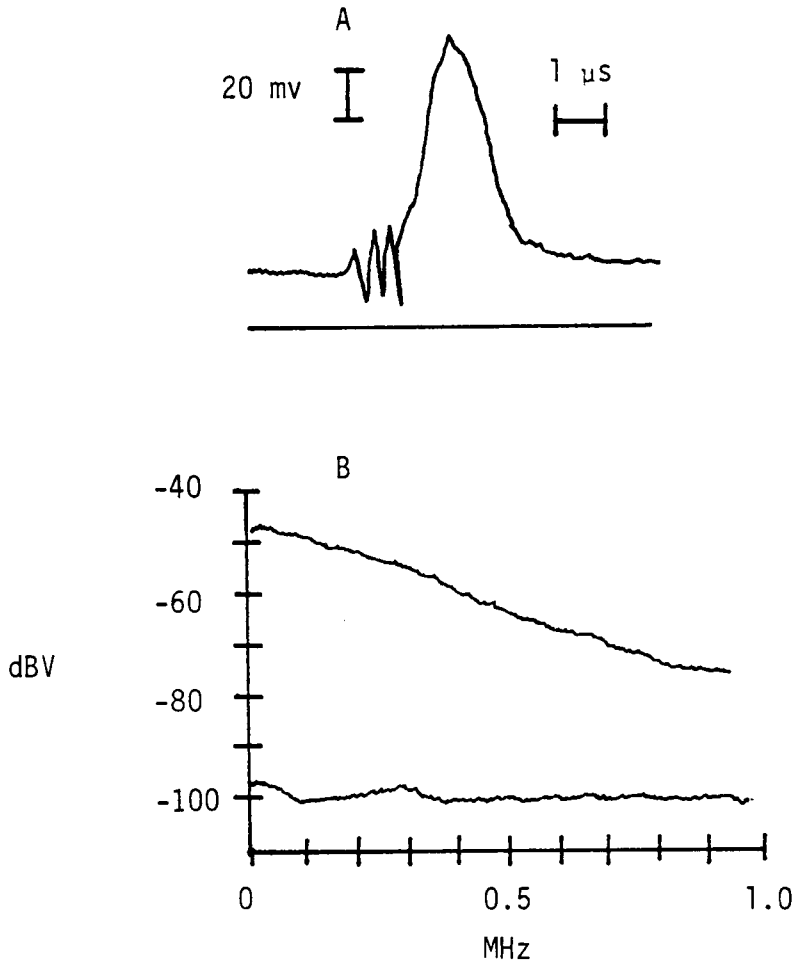


Figure 35. (A) Temporal profile of a visible (fundamental) laser pulse, 620 nm. (B) Upper trace, power spectrum of the visible laser pulse shown in (A). Lower trace, background noise power spectrum obtained with laser beam blocked.

profiles in Figures 34-A and 35-A, respectively. Thus, the power spectrum roll-off of the laser pulses was slightly worse (1.8 times) in the visible region at the transducer resonance (290 kHz).

When comparing the power spectra of the UV laser pulse (Fig. 34-A) with the transducer response (Fig. 33-A), it appears that only a small portion (~1 %) of the laser pulse frequency distribution was used to excite the transducer because of the relatively narrow frequency bandwidth of the transducer resonance. A transducer resonance bandwidth can be broadened by damping the transducer. This is usually done by backing the transducer with a relatively thick piece of material having a matched acoustic impedance (discussed below). However, damping the transducer to reduce the resonance bandwidth usually has the effect of decreasing the transducer sensitivity at its resonance frequency so that the total area (i.e., the integrated sensitivity) under the resonance peak does not change appreciably.[99-101] Therefore, since the UV laser pulse and transducer frequencies were fairly well matched in the present work, increasing the resonance bandwidth of the transducer would have not provided any appreciable enhancement in sensitivity.

The sensitivity obtained in piezoelectrically-detected PAS is also dependent upon the PE transducer sensitivity (Eq. I-1, p. 6). The two PE materials used in the present work, X-cut crystalline quartz and PZT, have high PE sensitivities relative to most commonly used PE materials. The reported value of the PE thickness mode sensitivity of X-cut quartz is 0.057 V m N^{-1} ± 2% from 10-298 K,[77-79] and the manufacturer's specified value for the PE thickness mode sensitivity of

the PZT was 0.025 V m N^{-1} at 298 K and 0.033 V m N^{-1} at 10 K.[16] The reported shear mode sensitivity of X-cut quartz is 0.021 V m N^{-1} from 10-298 K,[77-79] and the specified shear mode sensitivity of the PZT disc was 0.011 V m N^{-1} at 298 K and 0.013 V m N^{-1} at 10 K.[16] Based upon these values, X-cut quartz should have exhibited approximately twice the sensitivity in PA measurements as that of PZT used at room temperature and low temperature. However, it was found experimentally that PZT disc gave a ~10 times higher voltage output than X-cut quartz at room temperature. This determination was made by comparing the relative voltage outputs of each transducer resulting from the UV (320 nm) laser excitation of the same sample, 5,6-benzoquinoline in a thin film of glue (p. 64). The sample was located on one end of a fused quartz substrate (25 x 50 x 3 mm). A 3 mm thick PZT disc and a 3 x 5 mm piece of X-cut quartz were mounted side-by-side on the other end of the fused quartz substrate.

A possible explanation for this finding is that the dielectric constant of X-cut quartz (4.5)[79] is very low compared with the dielectric constant of PZT (1700).[16] The dielectric constant (ε) is important because it determines the capacitance ($C \propto \varepsilon$) and, thus, the voltage output obtained from the transducer. The fundamental quantity produced by the PE transducer is surface charge, Q_s. This charge is measured as voltage, V, determined by the ratio of charge to capacitance, i.e., $V = Q_s/C_T$. C_T is the total capacitance of the entire transducer network, i.e., the transducer capacitance plus cable and stray capacitance (recall that parallel capacitances add linearly).

From the values of the dielectric constants, the capacitance of the 3 x 5 mm piece of X-cut quartz and the 3 mm thick PZT disc (7 mm diameter) used in the experiment described above are calculated to be 0.3 pF and 193 pF, respectively, at 298 K. The extremely low capacitance value calculated for the X-cut quartz piece indicates that only a few pF of stray capacitance are needed to seriously reduce its voltage output. In fact, the input capacitance of the JFET preamplifier was 4 pF; thus, it alone was sufficient to cause a ~90% reduction of the X-cut quartz output voltage. This can account for the lower PA sensitivity obtained with the X-cut quartz transducer.

A similar situation was observed for MI-PA experiments. Although a side-by-side sensitivity comparison of the two transducers was not carried out as it was at room temperature, it was generally observed that the PZT detector in its final form (Fig. 8, p. 48) was much more (~10 times) sensitive than the X-cut quartz detector (p. 47). In the MI-PA experiments the quartz pick-up electrodes were ~4 x 10 mm; thus the capacitance was ~0.8 pF. The dielectric constant of X-cut quartz is temperature-independent.[79] The dielectric constant of PZT is temperature-dependent (1700 at 298 K and 310 at 10 K).[16] The capacitance of the 3 mm thick (7 mm diameter) PZT disc at 10 K is calculated to be 35 pF. Although much lower than the 298 K value, it was still much larger than the capacitance of the X-cut quartz piece (0.8 pF). A stray capacitance of ~100 pF is probably a more realistic estimate for the PA detector network. A stray capacitance of this magnitude would reduce the PZT disc output voltage by a factor of ~4, but the output voltage of the X-cut quartz piece would be reduced by a factor of

~125. Consequently, the voltage output of the PZT disc was probably not as severely attenuated as that of the X-cut quartz substrate by the preamplifier input capacitance or other stray capacitance. Therefore, the PZT disc is thought to have higher overall sensitivity for PA measurements at room temperature and low temperature.

The sensitivity of a PE transducer is also affected by the way that the transducer is mounted. When compressed against a substrate or loaded with a suitable backing material, a transducer usually experiences some degree of damping. This effect is characterized by a reduction in the duration of the bipolar oscillations (compare Fig. 13, p. 62 with Fig. 33, p. 104). This reduction was noticed in the present work when using the PA detector designs in Figure 5 (p. 42), Figure 6 (p. 43), and Figure 10 (p. 53). As discussed above (p. 108), heavy damping will increase the resonance bandwidth at the expense of decreasing the sensitivity at the resonance frequency. This fact was probably not of any serious consequence in the present work, provided that the integrated sensitivity remained constant, because of the broad power spectrum of the laser pulse. However, damping the transducer by compressing it could have severely reduced the shear sensitivity by not allowing the transducer to move in the shear mode. This was one of the reasons for gluing the PZT disc directly to the sapphire window. By mounting the PZT disc in an unclamped fashion, the shear mode was not impeded.

The second reason for gluing the PZT disc to the sapphire window was to reduce the chance of acoustic bond failure resulting from the differential thermal contractions of the various materials in the PA

detector. Of the materials used in the PA detector (pp. 41-49) (sapphire, copper, aluminum, PZT, and nylon), the nylon (used in the screws) is reported to have the largest coefficient of thermal contraction[67,102] (Table II-3, p. 49). The acoustic bond should have become stronger with decreasing temperature due to the larger thermal contraction value of the nylon.

In order to achieve maximum sensitivity in piezoelectrically detected PAS, it is essential to have good acoustic coupling between the sample and PE transducer. Throughout the present work, care was taken to achieve this requirement. In room-temperature PA experiments, Nonaq stopcock grease was used at all acoustic interfaces. This material is widely used in the field of ultrasonics because of its good acoustic coupling properties.[103] Superglue and Five Minute Epoxy were also found to provide equally good coupling. These materials were used when it was desired to make a more permanent bond between the transducers and sample substrates.

In the initial MI-PAS experiments, the Nonaq stopcock grease was used at the interfaces between the PZT disc and sapphire (as in Fig. 7, p. 46). This grease also is reported to have good low-temperature acoustic properties.[103] Evidence that the grease joint functioned well at low temperatures was derived from the fact that some MI-PA spectra were obtained with relatively high sensitivity, viz., 1 μg of 2,6-dimethylquinoline (Fig. 20, p. 80). However, the inability to obtain MI-PA spectra on a regular basis raised the suspicion of intermittent bond failure. Consequently, a more permanent (and presumably more reliable) low-temperature bonding agent was sought. Attempts to

bond the PZT disc to the sapphire window with superglue were unsuccessful. Apparently, temperature cycling fractured the bond. Finally, a glue, Versamid-140 polyamid epoxy (p. 33), formulated for low-temperature use was found. With this glue, the bond between the PZT disc and sapphire substrate remained permanent after repeated temperature cyclings, and the ability to obtain MI-PA spectra on a much more reliable basis became possible.

The acoustic coupling efficiency between two media is determined by the amount of acoustic energy that is transmitted from one medium to another.[15] The pressure amplitude, P_a, of an acoustic wave is related to the magnitude of the particle displacement, U, by the equation $P_a = \rho v_a U$, where ρ is the density and v_a is the sound velocity. The acoustic energy can also be expressed as the acoustic pressure intensity, I_a, where $I_a = 1/2\ \rho v_a U^2$. For the simple case of a longitudinal acoustic wave incident perpendicular to the interface of two media which are in intimate contact, the acoustic transmittance is determined by the relative acoustic impedances of the two media. The acoustic impedance, Z, of a medium is defined as $Z = \rho v_a$. The acoustic amplitude (or pressure) transmittance, T_a, of an acoustic wave passing from medium 1 to medium 2 is independent of frequency and is calculated from[15]

$$T_a = 1 + \frac{\frac{Z_2}{Z_1} - 1}{\frac{Z_2}{Z_1} + 1} \qquad \text{(III-1)}$$

where Z_1 and Z_2 refer to the acoustic impedances of media 1 and 2,

respectively. According to this formula, the acoustic wave amplitude (or pressure) transmittance may be > 1 when $Z_2 > Z_1$. This situation is possible because the acoustic amplitude within a medium is proportional to the acoustic impedance of the medium. Conversely, the acoustic wave amplitude reflectance at an interface, R_a, is calculated from[15]

$$R_a = \frac{Z_2 - Z_1}{Z_2 + Z_1} \qquad \text{(III-2)}$$

Implicit in this relationship is the possibility that the reflected acoustic wave amplitude may be negative, i.e., $R_a < 0$. This occurs when $Z_2 < Z_1$. The physical significance of this fact is that the reflected wave experiences a phase shift relative to the phase of the incident wave. The acoustic intensity transmittance, T_i, between two media is calculated from[15]

$$T_i = 1 - \frac{(\frac{Z_2}{Z_1} - 1)^2}{(\frac{Z_2}{Z_1} + 1)^2} \qquad \text{(III-3)}$$

The acoustic intensity reflectance is expressed as $R_i = 1 - T_i$. Unlike T_a and R_a, $T_i < 1$ and $R_i > 0$ for all cases. Acoustic amplitude transmittance and reflectance are applicable to the MI-PA experiments.

Table III-2 lists the acoustic impedances for various materials.[80,104] Values of acoustic amplitude and acoustic intensity transmittances for interfaces of several media are presented in Table III-3. These values were calculated from the data in Table III-2 using

TABLE III-2

PHYSICAL PROPERTIES OF VARIOUS MATERIALS

Material[a]	Density, ρ ($g\ cm^{-3}$)	Longitudinal Sound Velocity, v_a ($cm\ s^{-1}$) x 10^5	Acoustic Impedance, $Z_5 = \rho v_a$ ($g\ cm^{-2}\ s^{-1}$) x 10^5
Aluminum	2.7	6.42	17
PZT[b]	7.5	3.87	29
Epoxy[c]	~1.2	~2.68	~3.2
X-cut quartz[b]	1.2	5.65	15
Sapphire	4.0	11.2	45
Fused Quartz	2.2	5.90	13
CCl_4	1.6	0.926	1.5
Air (dry)	1.3×10^{-3}	0.331	4.3×10^{-4}
Ar (10 K)[d]	1.8	1.64	2.9

[a]All values at 298 K unless otherwise indicated. "CRC Handbook of Chemistry and Physics", 58th ed., R. C. Weast, Ed., CRC Press, Cleveland, OH, 1977.

[b]P. A. Walthers, Edo Western Corp., Salt Lake City, Utah, personal communication.

[c]Assuming hardened epoxy has same values as Lucite.

[d]O. G. Peterson, D. N. Batchelder, and R. O. Simmons, Phys. Rev., 150, 703 (1966).

TABLE III-3

ACOUSTIC AMPLITUDE AND ACOUSTIC INTENSITY TRANSMITTANCE VALUES FOR VARIOUS MEDIA INTERFACES

Material 1→ Material 2	Z_2/Z_1[a]	Acoustic Amplitude Transmittance	Acoustic Intensity Transmittance
Epoxy→PZT	9.1	1.8	0.36
PZT→Epoxy	0.11	0.20	0.36
Al→Epoxy	0.19	0.32	0.53
Epoxy→Al	5.3	1.7	0.53
Sapphire→Al	0.38	0.55	0.80
Ar(10K)→Sapphire (10K)[a]	16	1.9	0.22
Ar(10K)→X-cut quartz[a]	5.2	1.7	0.54
CCl_4→Fused quartz	8.7	1.8	0.37
Fused quartz→CCl_4	0.12	0.21	
Air→Al	4.0×10^{4}	2.0	1.0×10^{-4}
Al→Air	2.5×10^{-5}	5.0×10^{-5}	1.0×10^{-4}
Any material→Vacuum[b]	0	0	0
Vacuum→any material[b]	undefined	undefined	undefined

[a]Assuming ρv_a for sapphire at 10 K is the same as at 298 K.

[b]Undefined because vacuum does not support sound waves.

Equations III-1 and III-3. It is observed that T_a is highly dependent upon the sequence of the media, whereas T_i is not. For example, T_a = 2.0 for air→aluminum, but $T_a = 5.0 \times 10^{-5}$ for aluminum→air. T_a is greater than 1 whenever $Z_2 > Z_1$. On the other hand, $T_i = 1.0 \times 10^{-4}$ for an air-aluminum interface regardless of the sequence. The difference between the relative values of intensity and amplitude transmission coefficients is due to the fact that the amplitude and acoustic intensity of acoustic waves have different dependencies upon particle displacement and acoustic impedance. As the table shows, the acoustic amplitude transmittance is ~0.8-0.9 between two solids and >1 from a liquid to a solid. The acoustic amplitude transmittance is $\sim 10^{-5}$ for a solid-air interface and 0 for a solid-vacuum interface. These calculations show the need for having a good acoustic coupling in the MI-PA experiments. Cracks in the acoustic bonds between the sapphire window and PZT disc would have been "filled" by vacuum causing a severe reduction in the acoustic transmittance.

In the field of ultrasonic testing, knowledge of an accurate value of the acoustic transmission coefficient between the sample and PE transducer is often necessary for the purpose of quantitative materials evaluation. Therefore, this subject has received considerable attention from both the theoretical and experimental standpoint. Obtaining an accurate value for the acoustic transmission coefficient between the sample and transducer can sometimes be difficult due to the presence of additional layers of materials between them. Such layers are typically the wall of the sample container, acoustic coupling layers (e.g., Nonaq grease), or the wall of the transducer housing. In

the final design of the PA detector used for the MI-PAS experiments in the present work (Fig. 8, p 48), there were four acoustic interfaces between the MI sample and the PZT disc. The sequence of media was Ar matrix-sapphire-aluminum-epoxy-PZT. The acoustic amplitude transmittance for this sequence is 0.60 (from Table III-3). The acoustic amplitude transmittance between Ar (10 K) and X-cut quartz is 1.7.

Hill and El-Dardiry[105] have recently presented a quantitative theory to calculate the acoustic transmission coefficients for multilayered systems. The theory is derived for the one-dimensional case of a longitudinal wave at normal incidence to each interface. The presence of shear waves, two- and three-dimensional effects, and reflections and reverberations within the various layers are not included in the theory. It would be convenient if this theory could be applied to the situation in the present work. Unfortunately, there are several reasons which may cause the theory to be inapplicable. First, the exact nature of the acoustic waves produced in the MI-PA experiments is not known. Acoustic waves produced by optically induced thermal expansion of a highly absorbing surface layer are launched perpendicular to the surface.[15,106] On the other hand, weakly absorbing surface layers, such as the MI samples, are reported to produce a significant amount of shear waves.[106] Shear waves which have different transmission coefficients than longitudinal waves[15] were not treated in the theory.[105] A further complication arises from the fact that acoustic wave mode conversion can take place at any interface,[15] i.e., shear waves can be converted in part to longitudinal waves and vice versa. Second, because of the geometrical

orientation of the transducer with respect to the sample, it would have been necessary for an acoustic wave generated in the MI sample to undergo reflections within the sapphire substrate in order to reach the PZT disc. Thus, an acoustic wave reaching the PZT disc would have probably traversed some of the interfaces at angles other than normal incidence. Acoustic transmission coefficients are also dependent upon incidence angle. Third, there were probably extensive reverberations in the sapphire substrate and detector assembly. Finally, the acoustic impedance of the epoxy was not accurately known.

Suffice it to say that the MI-PA detector was far from being an ideal system. An exact calculation of an acoustic transmission coefficients for an ideal system is difficult; moreover, it would have been nearly impossible to make a realistic calculation for the MI-PA detector. However, since all interfaces were well contacted solid-solid interfaces, it is safe to assume that the acoustic transmission was as efficient as possible.

Table III-4 provides a comparison of how the factors discussed above (i.e., piezoelectric sensitivities, stray capacitance, and the acoustic amplitude transmittance) are predicted to affect the relative sensitivities observed for PZT and X-cut quartz at 10 K. The ~6:1 higher overall sensitivity predicted for PZT is close to the experimentally observed ratio of ~10:1. The main factor is the effect of the stray capacitance which severely reduces the voltage output of the X-cut quartz device.

b. Photophysical Properties of the Samples. The second category of factors upon which the PA signal is dependent is comprised of the

TABLE III-4

COMPARISON OF FACTORS THAT AFFECT THE OBSERVED SENSITIVITIES OF PZT AND X-CUT QUARTZ DETECTORS

Factor (10K)	PZT	X-cut Quartz
g_{xy}	1	2
Stray capacitance	30	1
Acoustic amplitude transmittance	1	2.7
Total Predicted Sensitivity Ratio	~6	1
Observed Sensitivity Ratio	~10	1

optical properties of the sample molecules. These factors govern the processes which determine the acoustic wave amplitude produced via interaction with the incident electromagnetic radiation. The acoustic amplitude dependence upon optical absorbance of the sample is expressed in Equation I-2 (p. 7). This equation states that the acoustic amplitude is proportional to $1-10^{-A}$, where A is the absorbance of the sample, and proportional to A for $A < 0.01$. In terms of relating the quantity of a particular PAC molecule in an ~0.5-1.0 cm diameter matrix sample to an absorbance, the following relationship was found: ~0.02 μmole of a compound with a molar absorptivity of ~3,000 $\underline{M}^{-1}$ cm^{-1} (room-temperature solution value) gave an absorbance of 0.02 a.u. This is only a rough approximation (± 50%), but it was generally found to be reliable. A more precise relationship for any particular compound could only be found by trial and error.

In PAS, the acoustic amplitude of the signal depends upon the absorptivity, but it is also essential that some fractional amount of the absorbed energy be liberated by non-radiative (i.e., thermal) processes. Moreover, in pulsed PAS the time scale of the non-radiative relaxation relative to the transducer rise-time is also critical. Quantitatively, the effective contribution of a non-radiative process to the acoustic pressure amplitude is calculated by multiplying the appropriate non-radiative quantum yield, Φ_{NR}, of the particular process by the factor $1-\exp[-\tau_{PE}/\tau_{NR}]$ where τ_{PE} is transducer response-time (1/resonance frequency x 1/4) and τ_{NR} is the non-radiative decay time.[82] For $\tau_{PE}/\tau_{NR} < 0.1$, $1-\exp[-\tau_{PE}/\tau_{NR}]$ is very small. The value of $1-\exp[-\tau_{PE}/\tau_{NR}]$ is ~0.1 for $\tau_{PE}/\tau_{NR} \approx 0.1$, ~0.5

for $\tau_{PE}/\tau_{NR} \approx 0.7$, and > 0.98 for τ_{PE}/τ_{NR} 2.3. Thus, in order to be at least 10 % effective, the decay time of the non-radiative process must be no more than 10 times longer than the transducer response-time.

In the present work, the PA signal was generated by a ~1 μs laser pulse which induced ~300 kHz (~1/3.3 μs) oscillations in the PE transducer. The transducer response-time was 0.83 μs (3.3 μs/4). Consequently, non-radiative relaxation times of > 8.3 μs did not contribute more than 10 % to the PA signal.

The various photophysical processes of a typical PAC were discussed on pp. 15-20. The primary non-radiative processes occurring for PACs in rigid low-temperature media and their relative contributions to the MI-PA signal are discussed below. ($\sim\!\!\rightarrow$ is used to denote a non-radiative process. A radiative process is denoted by $\rightarrow$. S_n and T_n are used to denote the various levels of singlet and triplet electronic states).

The primary non-radiative processes of a typical PAC in rigid, low-temperature media are $S_n \sim\!\!\rightarrow S_1$, $S_1 \sim\!\!\rightarrow S_o$, $S_1 \sim\!\!\rightarrow T_1$, and $T_1 \sim\!\!\rightarrow S_o$.[31] Since the S_1-S_o energy gaps for most of the PACs studied in the present work were ~90-95 % of the total S_n-S_o energy gaps (i.e., the absorbed photon energy), most of the thermal energy liberated was attributed to the non-radiative depopulation of S_1. This process can proceed by two paths, $S_1 \sim\!\!\rightarrow S_o$ and $S_1 \sim\!\!\rightarrow T_1 \sim\!\!\rightarrow S_o$.

For most PACs, $T_1 \sim\!\!\rightarrow S_o$ occurs on a time scale of $> 10^{-3}$ s.[31] This decay time is much longer than the 3×10^{-6} s response-time of the PE transducer used in the MI-PA experiments. Consequently,

$T_1 \rightsquigarrow S_0$ would be expected to contribute insignificantly to the MI-PA signal. Thus, the two main sources of liberated thermal energy in the MI-PA experiments were attributed to $S_1 \rightsquigarrow S_0$ and $S_1 \rightsquigarrow T_1$.

For most of the PACs studied, the S_1-T_1 energy gap was 30-40 % of the total S_1-S_0 energy gap. Therefore, in order to achieve a maximum PA sensitivity, it was desirable for $S_1 \rightsquigarrow S_0$ to be the primary depopulation mechanism of S_1. Unfortunately, for most classes of PACs, the rate for of $S_1 \rightsquigarrow S_0$ is small compared with that of $S_n \rightsquigarrow T_1$.[31] Thus, in the cases where $S_1 \rightsquigarrow T_1$ was the primary depopulation mechanism of S_1, the total thermal energy contribution to the PA signal corresponded to a maximum of ~30-40 % of the total S_1-S_0 (i.e., absorbed) energy. For those cases in which $S_1 \rightsquigarrow T_1$ rate was comparable to the radiative depopulation rate of S_1 (i.e., fluorescence), less than 30-40 % of the total S_1-S_0 energy was contributed to the PA signal.

Several experiments were conducted to determine what effect, if any, the relative non-radiative rates had upon the magnitude of the PA signal. The specific objective was to explore the possibility of improving the PA sensitivity for a particular molecule by using a heavy-atom matrix (Xe) to enhance the non-radiative $S_n \rightsquigarrow T_1$ process. The heavy-atom effect is generally thought to alter the rates of only those processes which result from spin-orbit coupling, e.g., $S_1 \rightsquigarrow T_1$ and $T_1 \rightsquigarrow S_0$.[31] The relative effect upon $S_n \rightsquigarrow S_1$ and $S_1 \rightsquigarrow S_0$ is considered negligible. Table III-5 lists the reported $S_1 \rightsquigarrow T_1$ quantum yields (Φ_{ST}) for several compounds. The potential PA enhancement, assuming an external heavy-atom matrix produces $\Phi_{ST} \approx 1$, is also given.

TABLE III-5

SINGLET-TRIPLET INTERSYSTEM CROSSING YIELDS
FOR SOME PAHS IN RIGID MEDIA[a]

Compound	Φ_{ST}	Potential PA enhancement due to external heavy atom
Naphthalene	0.5	2
Phenanthrene	0.8	1.2
1,2-Benzanthracene	0.7	1.4
Chrysene	0.7	1.4
1-Bromonaphthalene	1.0	1
1-Nitronaphthalene	1.0[b]	1
1-Naphthaldehyde	1.0[b]	1
Benzophenone	1.0	1

[a]Data for frozen organic solvents at 77 K. J. B. Birks, "Photophysics of Aromatic Molecules," John Wiley & Sons, London, 1970; R. S. Becker, "Theory and Interpretation of Fluorescence and Phosphorescence", John Wiley & Sons, New York, 1969.

[b]Assuming $\Phi_{ST} = 1$ because $\Phi_F \approx 0$.

Naphthalene was chosen for the study because there is a considerable amount of photophysical data available for it; thus, it was possible to compare the present results with previously reported data. Naphthalene was also chosen because it represented a typical case (Table III-5) and its photophysical rates, particularly $S_1 \sim\!\!\!\rightarrow T_1$, are reported to be sensitive to the heavy-atom effect.[31,49]

Figure 36-B shows a MI-absorption spectrum of naphthalene (20 μg) and 1-bromonophthalene (20 μg) in Ar at 5 K. The MI-PA spectrum of the same sample is shown in Figure 36-A. In the MI-absorption spectrum, the compounds have approximately equal absorbance values (~0.05 a.u.). However, in the MI-PA spectrum, the 1-bromonaphthalene peak is dominant. The interpretation from these results is that the internal heavy-atom effect due to the Br significantly enhanced the PA response for the 1-bromonaphthalene relative to that response for naphthalene. However, further studies were needed to more fully understand these results.

Figure 28-A (p. 90) shows a MI-PA spectrum of naphthalene (30 μg) and 1-bromonaphthalene (3 μg) in Ar at 5 K. The corresponding MI-absorption spectrum is shown in Figure 28-B (p. 90). The peak height ratio of naphthalene:1-bromonaphthalene in the absorption spectrum is ~7:1, whereas in the MI-PA spectrum, the peak height ratio is ~3:1. These values were obtained by averaging the peak heights on repetitive scans of the original spectra and may not exactly correspond to the value measured from the tracings in Figures 28-A and 28-B, (p. 90). The results indicate that the presence of the internal Br atom causes an enhancement of a factor of 2.3 in the PA signal derived from

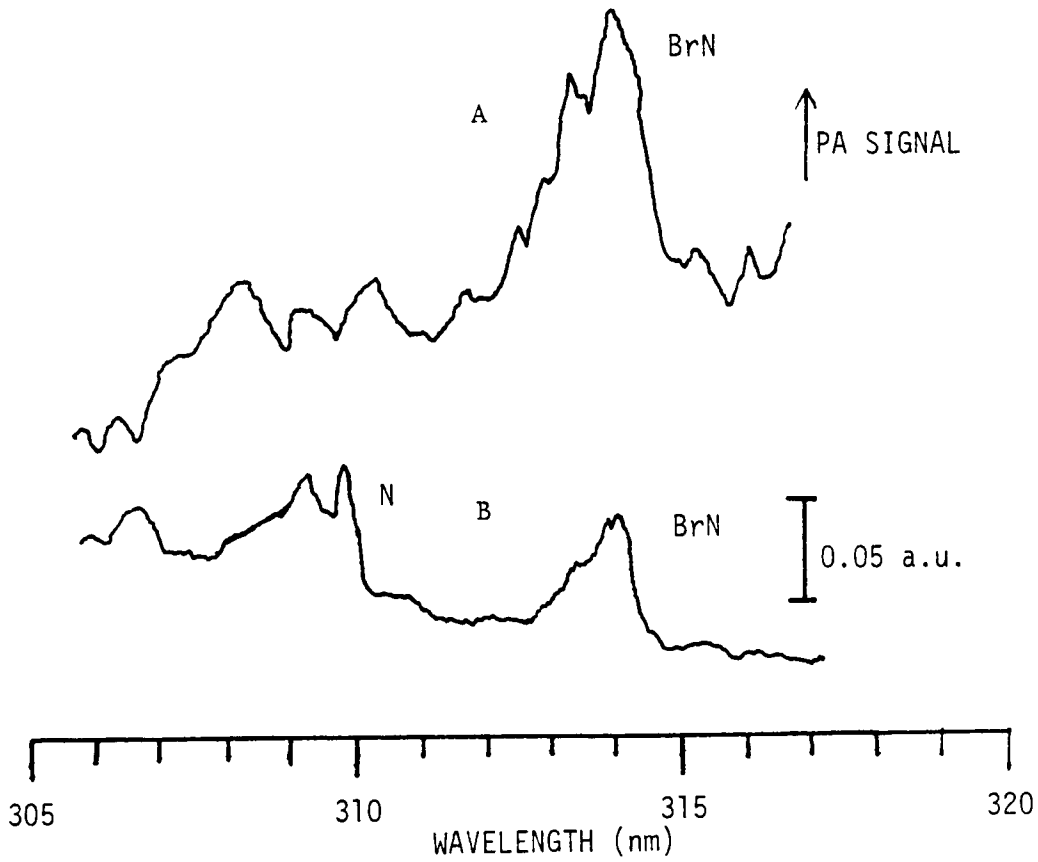


Figure 36. (A) MI-PA spectrum and (B) MI-absorption spectrum of 20 μg of naphthalene (N) and 20 μg of 1-bromonaphthalene (BrN) in Ar at 5 K.

the naphthalene molecule. This corresponds well to the reported 2-fold enhancement of the $S_1 \rightarrow T_n$ quantum yield observed for 1-bromonaphthalene ($\Phi_{ST} = 1$) compared with that for naphthalene ($\Phi_{ST} = 0.5$) in low-temperature organic glasses.[31,49] The 1-bromonaphthalene band at ~314 nm (~31,850 cm^{-1}) and the naphthalene band at ~310 nm (~32,260 cm^{-1}) are ~11,000 cm^{-1} above their respective T_1 energy levels.[49] Thus, the ratio of the signal strenghts in the MI-PA spectrum should not be biased due to different S_1-T_1 energy gaps. The $T_1 \sim\!\!\!\rightarrow S_0$ relaxation time for naphthalene in Ar (i.e., the phosphorescence lifetime) has been measured to be ~1.7 s;[107] therefore, the $T_1 \sim\!\!\!\rightarrow S_0$ decay time is of the same magnitude. Thus, the $T_1 \sim\!\!\!\rightarrow S_0$ process in naphthalene should not have contributed appreciably to the PA signal. The $T_1 \sim\!\!\!\rightarrow S_0$ decay time for 1-bromonaphthalene in Ar is not known either, but it is 0.028 s in a low-temperature organic glass.[49] However, this rate was also too slow to contribute to the PA signal. Thus, the PA signal from 1-bromonaphthalene is attributed to the $S_1 \sim\!\!\!\rightarrow T_1$ process, and the PA signal from naphthalene is also attributed to $S_1 \sim\!\!\!\rightarrow T_1$. Since the overall S_1-T_1 energy gaps are roughly the same, the enhanced sensitivity of the 1-bromonaphthalene is attributed to the larger $S_1 \sim\!\!\!\rightarrow T_1$ quantum yield.

Although the results in the present work correspond well to the data others have reported for naphthalene in low-temperature organic glasses, it must be admitted that Metzger, et al.[107] found that even Ar matrices exhibit a heavy-atom effect upon the photophysics of naphthalene. They found that ratio of fluorescence to phosphorescence for naphthalene was 50 times less in an Ar matrix than in a CH_4

matrix. The significance of this fact cannot be fully interpreted because they did not report any quantum yields and the only rate constant reported was that for the phosphorescence. However, from the fluorescence to phosphorescence intensity ratio decrease 50, it is possible that the Ar matrix may have increased the $S_1 \sim\!\!\!\!\!\!\sim\!\!\!\!\!\!\sim \rightarrow T_1$ yield so that it was greater than that which is observed in CH_4. Thus, while the present results and the data for organic glasses may not be directly comparable, the general trend can still be observed.

Figure 37 shows a MI-PA spectrum obtained for naphthalene (20 μg) and 1-bromonaphthalene (2 μg) in Xe at 5 K. The ~2:1 ratio of the peak heights was not expected. An external heavy-atom effect is known to significantly enhance the $S_1 \sim\!\!\!\!\!\!\sim\!\!\!\!\!\!\sim \rightarrow T_1$ quantum yield in naphthalene so that it becomes close to that in 1-bromonaphthalene.[49] If this were true, a ~10:1 ratio of naphthalene to 1-bromonaphthalene PA signal would have been observed in the MI-PA spectrum, assuming $S_1 \sim\!\!\!\!\!\!\sim\!\!\!\!\!\!\sim \rightarrow T_1$ to be the primary source of liberated thermal energy, and since both of the S_1-T_1 energy gaps were approximately the same (~10,000 cm^{-1}). A possible explanation of this unexpected result is that, in the Xe matrix, the rate of the $T_1 \sim\!\!\!\!\!\!\sim\!\!\!\!\!\!\sim \rightarrow S_0$ process may have been enhanced sufficiently to make a substantial contribution to the PA signal. An external heavy-atom effect is known to increase the spin-orbit coupling effect already present due to an internal heavy-atom effect.[108] That is, the two mechanisms can have an additive effect upon a non-radiative process involving spin-orbit coupling. For the case of 1-bromonaphthalene, the T_1 lifetime is reduced by a factor of ~1.5 in a heavy-atom solvent (n-propyl iodide) compared with the lifetime in a

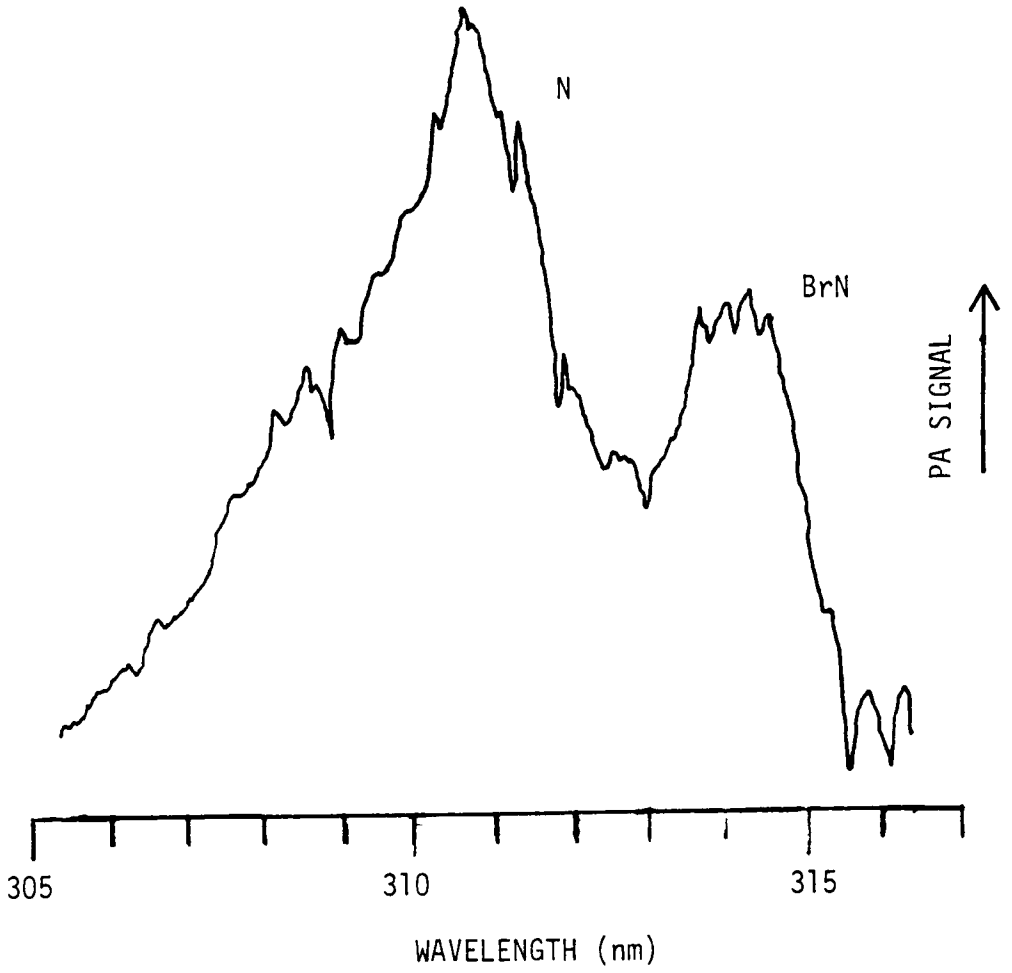


Figure 37. MI-PA spectrum of 20 μg of naphthalene (N) and 2 μg of 1-bromonaphthalene (BrN) in Xe at 5 K.

non-heavy atom solvent (ether:alcohol). The triplet lifetime in the heavy-atom solvent is ~0.014 s.[108] Unfortunately, this value is also far too large to have an appreciable effect on the PA signal. Thus, the reason for the lack of expected enhancement for the naphthalene PA signal in xenon is not readily explained by a simple comparison of the relative rate constants.

The net result obtained for the naphthalene/bromonaphthalene study was that (at least for naphthalene) a dramatic enhancement in the PA sensitivity could not be obtained by using a Xe matrix. Given the additional fact that Xe matrices often give large background signals due to their highly scattering nature, it seems that there is no obvious advantage in using Xe matrices for MI-PAS. Although only the case of naphthalene was studied, it is probably not too dangerous to extrapolate this result to other molecules.

A similar study was made with 1-bromonaphthalene and quinoline (1-azanaphthalene). In non-hydroxylic media, the lowest excited singlet state (i.e., S_1) of quinoline is reported to be an n,π* state.[109,110] Because of this fact, $S_1 \rightsquigarrow T_1$ is supposedly an efficient process due to the spin-orbit coupling induced by the non-bonding electrons in the n,π* state. In low-temperature non-hydroxylic organic glasses, quinoline is observed to have a 0.5 quantum efficiency for triplet formation[109] which implies that 50 % of the molecules reaching the S_1 state eventually decay to T_1. The fluorescence quantum efficiency in non-hydroxylic media is very small ($< 10^{-2}$). This fact implies that the $S_1 \rightsquigarrow S_0$ quantum efficiency is 0.5 (i.e., 50 % of the total absorbed energy is liberated by $S_1 \rightsquigarrow S_0$). The $T_1 \rightsquigarrow S_0$

decay time is > 1s,[109] thus it is not expected to contribute to the PA signal. In Ar, the S_1-T_1 energy gap (21,740 cm^{-1}) in quinoline is ~33 % of the S_1-S_0 energy gap (32,150 cm^{-1}). Thus, for quinoline, ~66 % of the absorbed S_1-S_0 energy is expected to contribute to the PA Signal (i.e., 0.5 of S_1-S_0 due to $S_1 \curvearrowright\!\!\!\rightarrow S_0$ plus 0.5 x 0.33 of S_1-S_0 due to $S_1 \curvearrowright\!\!\!\rightarrow T_1$).

Figure 38-A shows the MI-PA spectrum of quinoline (5 μg) and 1-bromonaphthalene (30 μg) in Ar at 5 K. The corresponding MI-absorption spectrum of the same sample is shown in Figure 38-B. The peak at 311 nm corresponds to quinoline and the peak at 314 nm corresponds to 1-bromonaphthalene. For 1-bromonaphthalene, Φ_{ST} = 1; therefore ~33 % of the absorbed S_1-S_0 energy is expected to contribute to the PA signal (discussed on p. 125). For equal amounts of absorbed energy, the PA signal for quinoline is expected to be 2 times larger than that for 1-bromonaphthalene (i.e., 0.66/0.33 = 2). This prediction is not observed in Figure 38. The respective absorbances, A, of quinoline and 1-bromonaphthalene are 0.25:0.15 (Fig. 38-B). This absorbance ratio corresponds to an absorbed energy ($1-10^{-A}$) ratio of 1.6:1. Based upon the discussion above, the ratio of the PA signal strengths is predicted to be 3.2:1 (i.e., 2 x 1.6:1). However, the observed ratio of the PA signal strengths in Figure 38-A is 1.3:1. This value is 2.5 times less than the predicted value. Thus, the MI-PA data obtained for quinoline in Ar are not consistent with reported photophysical data for quinoline in frozen organic solutions. However, regardless of the photophysical processes of quinoline in Ar matrices, it appears that quinoline liberates ~33 % of its absorbed photon energy non-radiatively.

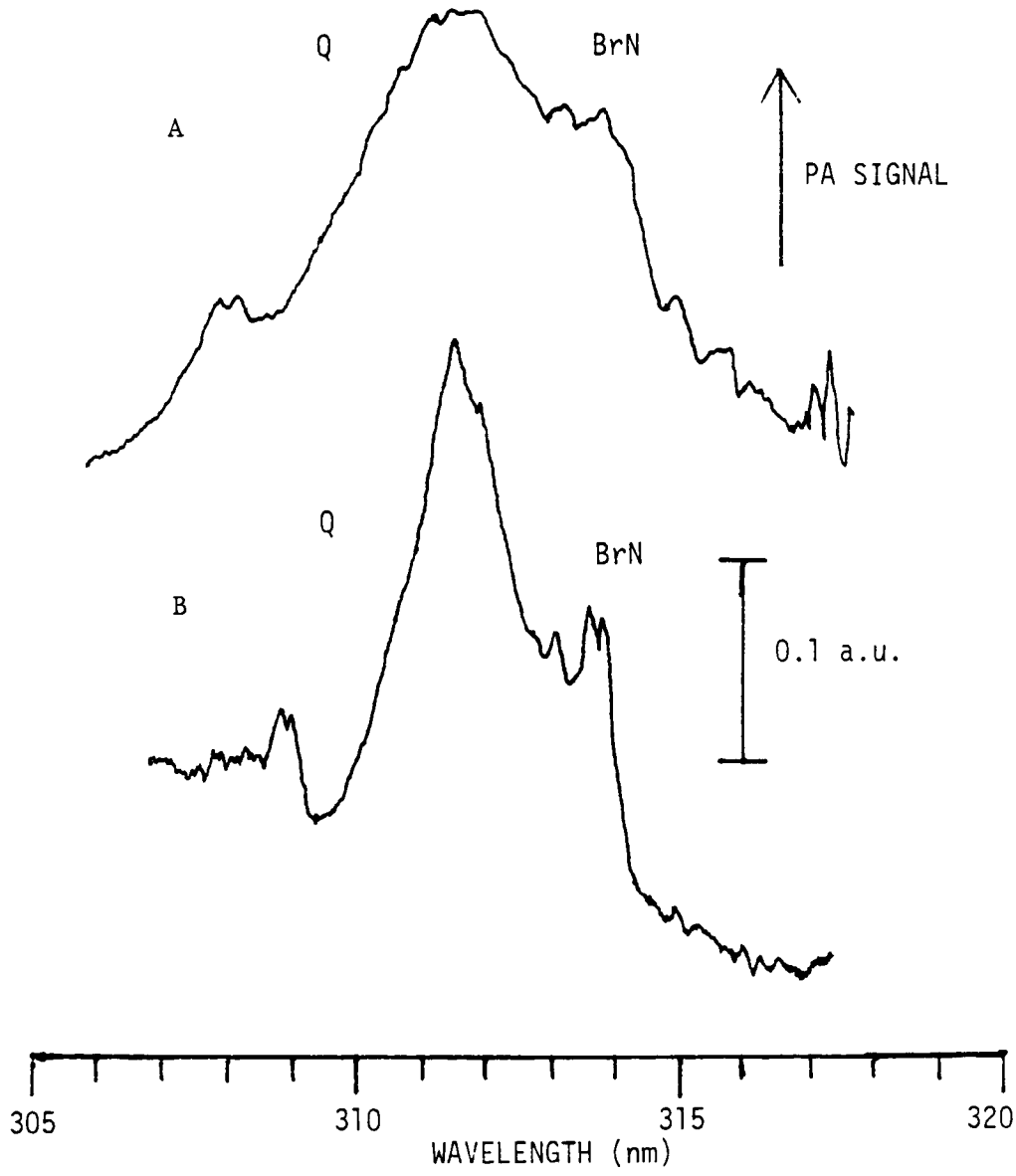


Figure 38. MI-PA spectrum and (B) MI-absorption spectrum of 5 μg of quinoline (Q) and 30 μg of 1-bromonaphthalene (BrN) in Ar at 5 K.

c. Properties of the Matrix Materials. The acoustic pressure amplitude produced in pulsed PAS is also dependent upon the thermal, elastic, and geometrical properties of the sample medium. This relationship is expressed in Equation I-2 (p. 7) which states that the acoustic pressure amplitude produced by deposition of thermal energy is proportional to $\beta v_a/C_p$, where β is the volume coefficient of thermal expansion, v_a is the sound velocity, and C_p is the isobaric heat capacity. In order to determine how these properties of solid Ar and Xe compared with those of other media, their relative values were compared. Some thermal and elastic properties of various materials[104,111-114] are shown in Table III-6. Values of $\beta v_a/C_p$ and the ratios of $\beta v_a/C_p$ for some of the materials are presented in Table III-7. Carbon tetrachloride (CCl_4) is seen to have the highest $\beta v_a/C_p$ value at 298 K for any of the liquids shown. The values for Ar and Xe at 10 K are slightly higher than the value calculated for CCl_4 at 298 K. The relative ratios of $\beta v_a/C_p$ predict that solid Ar at 10 K should produce an acoustic amplitude 2.1 times higher than CCl_4 at 298 K for equivalent thermal energy inputs. The main point of these comparisons is to show that solid Ar and Xe have desirable properties for producing a relatively large acoustic pressure wave, and thus were not an important limitation to the MI-PAS sensitivity.

Unlike conventional optical absorption spectroscopy, the PA signal is critically dependent upon the geometrical properties of the sample. This dependence is a result of the processes involved in the generation and propagation of the acoustic pressure wave.[1] Optically-generated acoustic waves are produced by a local heating which is

TABLE III-6

THERMAL AND ELASTIC PROPERTIES OF SOME MATERIALS

	Temperature T (K)	Thermal Expansion $\beta \times 10^{-4}$ (K^{-1})	Sound Speed v_a (m/s)	Heat Capacity C_p (J/kg•K)
Ar	10	1.38[a]	1640[b]	82.8[c]
	20	5.55[a]	1630[b]	313[c]
Xe	10	1.56[a]	1331[d]	59.1[c]
	20	3.66[a]	1330[d]	131[c]
H_2O[e]	298	1.8	1497	4200
n-C_7H_{16}[e]	298	12.4	1160	2240
CCl_4[e]	298	12.2	926	863
EtOH[e]	298	10.8	1162	2300

[a] "Thermophysical Properties of Matter", Vol. 13, Plenum, New York, 1977.

[b] O. G. Peterson, D. N. Batchelder, and R. O. Simmons, Phys. Rev., 150, 703 (1966).

[c] "Selected Values of the Thermodynamic Properties of the Elements", American Society for Metals, Metals Park, OH, 1973.

[d] N. A. Lurie, G. Shirane, and J. Skalyo, Phys. Rev. B, 9, 2661 (1974).

[e] "Tables of Physical and Chemical Constants", Longman, Inc., New York, 1977.

TABLE III-7

RATIOS OF $\frac{\beta v_a}{C_p}$

$\frac{\text{Ar (10 K)}}{H_2O \text{ (298 K)}} = 43$	$\frac{\text{Ar (10 K)}}{\underline{n}\text{-}C_7H_{16} \text{ (298 K)}} = 4.3$
$\frac{\text{Ar (10 K)}}{CCl_4 \text{ (298 K)}} = 2.1$	
$\frac{\text{Ar (10 K)}}{\text{Ar (20 K)}} = 0.95$	$\frac{\text{Ar (10 K)}}{\text{Xe (10 K)}} = 0.79$
$\frac{\text{Ar (10 K)}}{\text{EtOH (298 K)}} = 5.0$	

$\frac{\beta v_a}{C_p} \times 10^{-4}$ (kg m s^{-1} J^{-1})

Ar (10K) = 27.4	H_2O (298K) = 0.64
Ar (20K) = 28.8	Ethanol (298K) = 5.5
Xe (10K) = 35.1	$\underline{n}\text{-}C_7H_{16}$ (298K) = 6.4
Xe (20K) = 37.2	CCl_4 (298K) = 13.1

dissipated within a very short distance by excitation of vibrational modes (i.e., phonons) to produce bulk acoustic waves in the sample medium. This distance is called the thermal wavelength, λ_t. Thermal waves are very sensitive to discontinuities greater than or equal to λ_t in the locally heated region. Such discontinuities can critically scatter the thermal waves resulting in an effective loss in the bulk acoustic wave amplitude.

The fact that vapor deposited rare gas and N_2 matrices are polycrystalline[67-69] implies the existence of crystal grain boundaries which could have scattered the thermal waves produced in the MI samples. Horl and Suddeth[115] have estimated that the typical size of a microcrystal formed from a condensing gas is on the order of 10 nm.

Rosencwaig[1] has given a formula for calculating the thermal wavelength in a medium due to the absorption of amplitude modulated radiation:

$$\lambda_t = \left\{\frac{2\ k}{\pi \rho C_p f}\right\}^{1/2} \qquad \text{(III-4)}$$

where k is the thermal conductivity, ρ is the density, C_p is the isobaric heat capacity, and f is the modulation frequency. The thermal wavelength of solid Ar at 10 K is calculated to be 3 μm at 500 kHz using this equation and the following values: $\rho = 1.76 \times 10^3$ kg m^{-3} [104], $C_p = 82.5$ J kg^{-1} K^{-1} [112], and $k = 1.3$ W m^{-1} K^{-1}.[68] The value of 3 μm calculated for the thermal wavelength is ~300 times greater than the estimated size (10 nm) of a typical Ar microcrystal.

If this estimate is realistic, then thermal wave interference should not have been a problem in the MI-PAS experiments.

The amplitude of an acoustic wave launched into a solid as a result of optically induced transient surface heating is strongly dependent upon the boundary conditions of the surface.[1] This subject has been studied by several investigators.[116-119] Most studies have dealt with optically dense thin (< 100 nm) films of solids or liquids which absorb optical energy to produce acoustic waves in the substrates to which they are contacted. It has been observed by those investigators that, if the thin absorbing layer is backed by a relatively thick piece of non-absorbing material (i.e., sandwiched between the backing and substrate), the amplitude of the acoustic wave launched into the substrate can be enhanced 100-1,000 times compared with the amplitude obtained when the sample has no backing material. This enhancement is believed to result from the minimization of the destructive interference derived from acoustic reflection at an unbound interface.[116-119] These two conditions are referred to as constrained and non-constrained samples, respectively.

The vapor-deposited matrices in the present work resembled a non-constrained sample. However, there are several differences between the MI samples and the thin-film sample discussed above. First, most of the MI samples studied were weakly absorbing ($A < 0.1$), unlike the strongly absorbing thin films studied by others. The importance of this fact is that the nature of the acoustic waves produced in the MI samples was probably different from those produced by the strongly absorbing thin films. Strong sample absorption is reported to produce

longitudinal waves perpendicular to the surface,[15,106] whereas weak sample absorption reportedly produces mostly shear waves.[106] Second, the MI samples were considerably thicker than the 10 nm thin films studied by others. Based upon the density of Ar (1.76 g cm^{-3}),[104] the thickness of a 100 μmole Ar matrix of a 1 cm diameter is calculated to be ~0.3 mm. Thus, it was not clear whether the results reported for non-constrained vs. constrained samples by other workers can be applied to the MI deposits.

An experiment was performed in order to determine what effect a constrained sample surface had upon the PA signal produced from a weakly absorbing thin film. A sample of 5,6-benzoquinoline was dispersed in a thin film (< 0.1 mm) of rubber cement (see p. 64). The sample was located at one end of a 3 mm thick fused quartz substrate and a PZT disc was attached to the other end of the substrate. The sample absorbance was 0.3 at 330 nm, primarily (~80 %) from the absorption of the 5,6-benzoquinoline. The sample was irradiated at 330 nm by the laser and the PA signal was observed directly with the oscilloscope. With a 1.8 mm thick fused quartz backing plate (i.e., constrained), a PA signal of ~5 mV peak to peak (similar to the one in Figure 13, p. 62) was obtained. When the backing plate was removed (i.e., non-constrained), the PA signal was not detectable above the 0.02 mV noise level. Thus, the 1.8 mm thick backing plate produced an enhancement effect of > 250. When a 0.18 mm thick backing plate was used, the PA signal was ~2 mV peak to peak. This represented a > 100 fold enhancement compared with the non-constrained case. These results indicated that a significant amount of sensitivity could be

achieved when the backing plate was relatively thin. These findings were encouraging because they implied that, in the MI samples, a partial backing effect could probably be obtained by depositing a layer of pure matrix over the layer of matrix that contained the PAC sample.

In order to test this hypothesis, several experiments were performed in which a given amount of a compound was deposited in a matrix by the usual procedure. The PA signal was then periodically monitored as additional pure matrix was deposited in order to determine if an enhancement effect could be observed. In one particular experiment, 15 μg of 3-bromoquinoline in Ar was deposited in an ~1 cm diameter matrix sample onto the X-cut quartz PE transducer. After all of the 3-bromoquinoline had been deposited, the sample was probed with a tightly focused laser beam (< 1 mm diameter). The signal was found to be ~0.2 mV peak to peak at 320.5 nm and it was fairly constant as the beam was moved around, implying a uniform concentration. Then, the laser beam was defocused to an ~0.8 cm diameter in order to ensure that any concentration inhomogeneity would be cancelled. The laser wavelength was scanned and a spectrum similar to the one in Figure 17 (p. 75) was obtained. The PA signal at 320.5 nm was measured to be ~0.1 mV peak to peak. The beam diameter and position were left at these values for subsequent measurements.

The deposition of the extra matrix was started and PA spectra and signal magnitudes were recorded after extra matrix had deposited for 30, 90, and 180 min. Surprisingly, the signal magnitude was found to decrease rather than increase with time. After 30 minutes of extra matrix deposition, the signal decreased by ~40 %. After 90 min.,

the signal had decreased by a total of ~60 %, and after 180 min. the decrease in the signal was still ~60 %. At the end of the 180 min. period, the sample was again probed with the tightly focused laser beam. Very strong signals, as large as ~5 mV peak to peak, could be found in certain spots. The laser wavelength was scanned while the beam was focused on intense spots and the spectrum of 3-bromoquinoline was obtained. Thus, these "hot-spots" were not caused by scattered light hitting some part of the PA detector. Recall that probing the initial sample produced a fairly uniform PA signal of ~0.2 mV peak to peak. The most intense spot in the final sample gave a PA signal of ~5 mV peak to peak. The signal from the final sample varied as much as 50 % within 1-2 laser beam diameters (~1 mm). Since the original sample was found to be relatively homogeneous, these results seemed to indicate that the deposition of extra matrix over an extended period of time severely deteriorated the "acoustical" homogeneity of the MI sample. This postulate is supported by the fact that, from visual inspection, the initial sample was observed to be uniform with a few small cracks. However, as the deposition of the additional matrix proceeded, the number and size of the cracks increased greatly. Recall from the discussion above (p. 117) that cracks are very deleterious to the propagation of acoustic waves.

The most intense "hot-spot" in the final sample produced a PA signal of ~5 mV peak to peak which corresponded to a ~25 fold increase over that obtained from the original sample (~0.2 mV peak to peak). Thus, it appeared that a large enhancement in the PA signal could be obtained for selected sites at the expense of degrading the overall

acoustical quality of the matrix by depositing additional matrix. This experiment was repeated and the same general results were obtained.

The experiment described above does not conclusively prove that the "hot-spots" in the matrices were not caused by concentration inhomogeneity. An extensive study of this problem was not conducted. Results from an experiment with the three benzoquinoline isomers (500 ng each in Ar) indicated that "hot spots" were not caused by a concentration effect. The laser was focused at three different spots, which were at least 2 mm apart, on the MI sample. The PA signal magnitude varied as much as 200 %, but the ratio of the peak heights in the PA spectra corresponding to the three isomers remained constant. Also, defocusing the beam to cover most of the sample produced the same peak height ratio. Thus, "hot spots" did not seem to be caused by concentration inhomogeneities. For most samples, the laser beam diameter was maintained at ~3 mm in order to partially compensate for "hot spots."

Two attempts to make a constrained vapor-deposited matrix (Ar) were unsuccessful. The end of the sublimation cell capillary tube (Fig. 4, p. 39) was placed at the opening of two parallel sapphire plates which were separated by ~2 mm by an indium gasket. When argon was passed into the cell, it began to condense upon the cold sapphire plates, but instead of filling the area between the plates, it formed a plug that extended outside of the plates and the capillary tube. Another attempt to perform this experiment with slight modifications in the position of the capillary tube was also unsuccessful. Therefore, the experiments were not pursued further.

d. Limit of Detection. There are several ways to express the limit of detection in MI-PAS studies. Perhaps defining a minimum detectable quantity is the best way of determining the analytical utility of the technique. This method allows it to be compared with other analytical methods used for PAC determinations. The minimum detectable quantity is commonly defined as the smallest amount of a substance for which the signal-to-noise ratio (S/N) for the particular measurement technique is 2. In the present work, the minimum detectable quantity of quinoline (in Ar) was determined to be ~500 ng (25 μJ pulse energy). For this determination, the predominant sources of noise were attributed to random electrical and acoustical noise picked up by the PA detector. The minimum detectable quantities of pyrene and 3,4-benzoquinoline were estimated to be 50 ng and 200 ng (100 μJ pulse energy), respectively. All of the determinations were made with the 3 mm thick PZT disc glued to the sapphire window.

Another way to express the limit of detection for PA measurements is in terms of the minimum detectable absorbance. This method defines the minimum fraction of the excitation radiation that must be absorbed by a particular compound in order to produce a measurement with S/N = 2. Consequently, when this method is employed, factors such as the molar absorptivity and the laser pulse energy must be considered in order to compare the minimum detectable quantities for different compounds. Simply specifying a minimum detectable absorbance does not directly indicate the relative efficiency of the PA detector or the amount of the particular compound and the laser pulse energy that were necessary to achieve S/N = 2. For example, Figure 38 (p. 132) shows

that 5 μg of quinoline produced a PA signal larger by a factor of 1.3 than 30 μg of 1-bromonaphthalene. The reason for this occurrence is that the molar absorptivity of quinoline is ~3,000 $\underline{M}^{-1}$ cm^{-1}, whereas the molar absorptivity of 1-bromonaphthalene is ~300 $\underline{M}^{-1}$ cm^{-1}. Similarly, this situation is one of the reasons that the minimum detectable quantity of pyrene was ~50 ng. At the 330 nm absorption peak, pyrene has a molar absorptivity of ~55,000 $\underline{M}^{-1}$ cm^{-1}, as compared with a molar absorptivity of ~3,000 $\underline{M}^{-1}$ cm^{-1} for the quinoline peak at 311 nm. In terms of minimum detectable absorbance, the MI-PA detection limit was 0.01 a.u., corresponding to 500 ng of quinoline in Ar. This value may seem rather poor when compared with the minimum detectable absorbance of 10^{-5}-10^{-6} reported by others.[17-21] However, this comparison does not account for the difference in the laser pulse energies or other factors which are discussed below.

Voigtman, et al.[21] have proposed that expressing PA detection limits in terms of the limiting amount of energy absorbed is the best figure of merit for comparing the efficiencies of various PA transducers. This method normalizes the detection efficiency for the laser pulse energy and the relative absorbance of the sample. This method assumes that all of the absorbed energy is divested non-radiatively on a time scale much less than the detector response-time. It also does not account for different acoustic pressure amplitudes produced by different samples (i.e., Table III-7, p. 135). For the specific case of the 500 ng quinoline sample (Ar), the absorbance detection limit of 0.01 was obtained with a laser pulse energy of ~25 μJ. This corresponded to a limiting amount of energy absorbed ($E_o(1-10^{-A})$) of

~570 nJ. Accounting for the fact that only ~30 % of the absorbed energy contributed to the PA signal (i.e., the S_1-T_1 energy gap), the limiting detectable energy liberated was ~170 nJ. This value is only about 20 times higher than the values reported by Voigtman, et al.[21] and Patel and Tam[18] for liquid solutions. This difference is not unreasonable considering the fact that, for the MI-PA experiments, the PA detector was rigidly attached to a cryostat cold finger which had rapidly expanding helium gas flowing through it. Having the PA detector attached to the cold finger also prevented the PA detector from being acoustically isolated from room vibrations and airborne noise or electrically isolated to minimize electrical pick-up.

A significantly lower minimum detectable energy absorbed was obtained for room-temperature PA measurements of liquid solutions using the liquid cell detector shown in Figure 10 (p. 51). The minimum detectable absorbance for 3-bromoquinoline in CCl_4 was 0.001 a.u. with a laser pulse energy of ~20 μJ. In this particular case, all of the absorbed energy was assumed to undergo rapid ($< 10^{-6}$ s) non-radiative decay. This corresponds to a limiting detectable liberated energy of ~45 nJ which compares well with the values of ~10 nJ reported by Voigtman, et al.[21] and Patel and Tam.[18]

C. Photoacoustic Spectroscopy of Polycyclic Aromatic Compounds and Neodymium Hydroxide in Frozen Solutions at 77 K

Several attempts were made to obtain PA spectra of PACs in frozen n-alkane solutions at 77 K using the PA detector shown in Figure 9 (p. 51). Single component samples of quinoline, 5,6-benzoquinoline, and

pyrene, 10^{-4} M each in n-heptane, were investigated. Immediately before freezing the solutions in liquid nitrogen, room-temperature PA spectra were obtained for each sample that corresponded to the respective absorption spectra shown in Figure 18 (p. 76), Figure 25 (p. 88), and Figure 27 (p. 92).

After the room-temperature PA spectra were recorded, the samples were quench frozen in liquid nitrogen contained in a spectroscopic Dewar. However, attempts to obtain PA spectra of the PACs in the frozen n-alkane solutions were unsuccessful. A rather large background signal (~1 mV peak to peak) was observed for each sample. This background signal was probably produced by scattered light from the sample which "light-piped" up the quartz tube and impinged upon some part of the PA detector. Since attempts to obtain PA spectra at these rather high concentrations (10^{-4} M) were unsuccessful, the investigation was terminated. No further attempts were made to obtain PA spectra of PACs in frozen n-alkane solutions.

Although attempts to obtain PA spectra of PACs in frozen n-alkane solutions were unsuccessful, it was possible to obtain PA spectra of $Nd(OH)_3$ powder dispersed in a frozen solutions at 77 K. These results demonstrated that the PA detector was useful for obtaining PA spectra of species in frozen solutions at 77 K. PA spectra of $Nd(OH)_3$ powder dispersed in isopropanol or glycerine:H_2O (1:1, v:v) at 77 K compared well with those in Figures 14 (p. 67) and 15 (p. 68). The PA spectrum of $Nd(OH)_3$ powder dispersed in isopropanol at 77 K is shown in Figure 39.

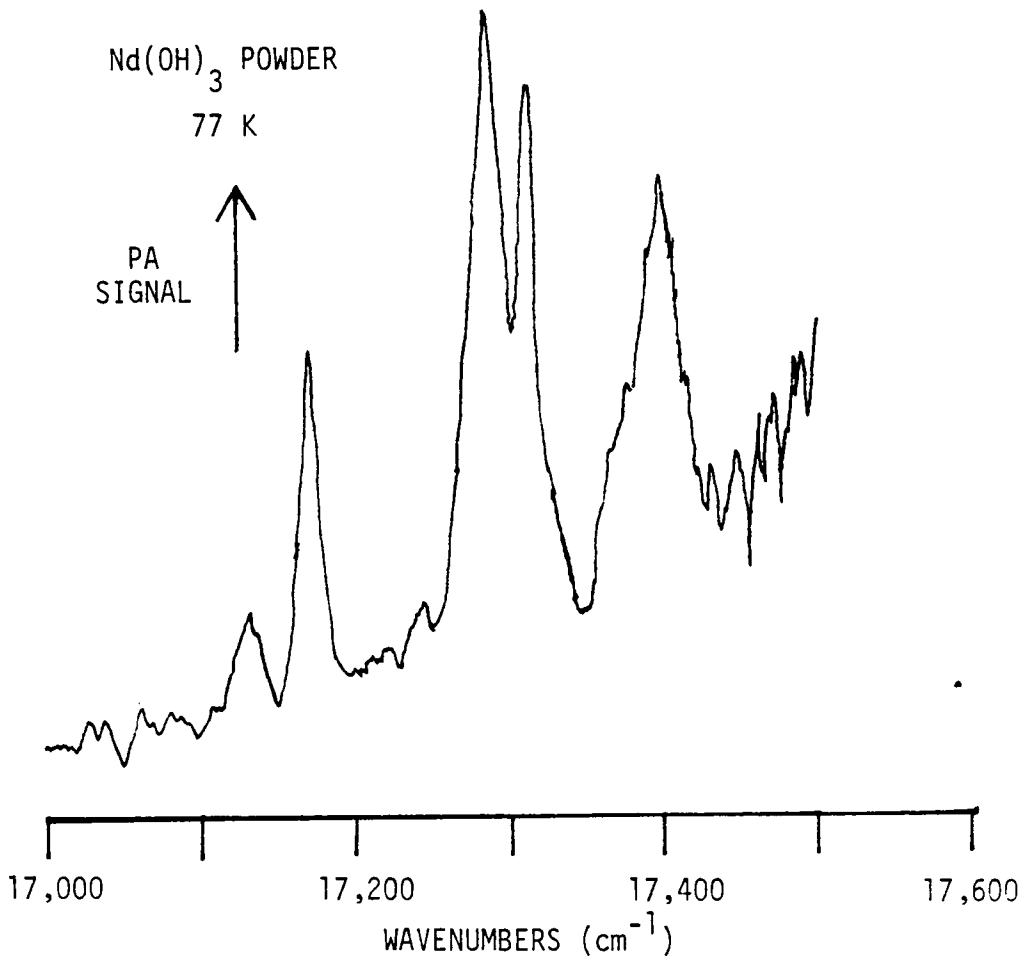


Figure 39. PA spectrum of $Nd(OH)_3$ powder at 77 K from 17,000-17,500 cm^{-1}.

Since the liquid nitrogen-temperature PA detector functioned well for $Nd(OH)_3$, it was concluded that the inability to obtain PA spectra of the PACs in frozen n-alkane solutions was due to a short path length or the high level of background signal due to the highly scattering nature of the samples, or undesirable PA properties of the samples.

CHAPTER IV

CONCLUSION

The technique of piezoelectrically-detected photoacoustic (PA) spectroscopy at cryogenic temperatures has been demonstrated. High resolution, laser-excited PA spectra were obtained for $Nd(OH)_3$ powder at 6-8 K. X-cut crystalline quartz and lead zirconate titanate (PZT) piezoelectric (PE) transducers were found to function well as PA detectors at 5-20 K. At room temperature and low temperature, PZT exhibited higher sensitivity primarily because the low dielectric constant of X-cut quartz caused its response to be seriously attenuated due to stray capacitance. A simple liquid nitrogen-temperature PA detector was also developed. PA spectra of $Nd(OH)_3$ powder dispersed in glycerine/H_2O and isopropanol glasses (i.e., transparent solids) at 77 K were taken to demonstrate the usefulness of this PA detector. However, PA spectra of samples in highly scattering media (e.g., frozen alkane solutions) could not be obtained.

The analytical utility of PA spectroscopy of matrix-isolated (MI) polycyclic aromatic compounds (PACs) was investigated. Laser-excited PA spectra were obtained for a number of PACs isolated in low-temperature matrices (N_2, Ar, and Xe). Singlet-triplet intersystem crossing (i.e., $S_1 \sim\!\!\!\rightarrow T_1$) was determined to be the primary source of liberated thermal energy which generated the PA signal. The S_1-T_1 energy gap is ~30-40 % of the total S_n-S_o energy gap (i.e., the absorbed photon energy) for most PACs; therefore, a maximum of ~30-40 % of the absorbed energy was effective in producing the PA signal when the

quantum efficiency of $S_1 \sim\!\!\!\!\!\!\rightarrow T_1$ was unity. Attempts to significantly enhance the PA signal by employing a heavy-atom matrix (Xe) to increase the $S_1 \sim\!\!\!\!\!\!\rightarrow T_1$ process were not successful.

The detection limit for most of the PACs studied was ca. 50-500 ng, depending upon the molar absorptivity and photophysical properties of the particular compound. This mass detection limit corresponded to a limiting detectable liberated thermal energy of ~175 nJ. This figure of merit was approximately a factor of 20 higher than the lowest detectable energies that have been reported in the literature for room-temperature liquid solutions. Calculations involving the relative physical properties of the MI samples and transducer materials that determine the PA signal magnitude and the PE transducer sensitivities, respectively, predicted a two-fold gain in overall sensitivity for MI samples in Ar compared with the sensitivity for room-temperature liquid solutions. The somewhat higher minimum detectable energy obtained in the present work was attributed to the fact that the MI samples were found to be acoustically poor. Undesirable acoustical properties of the MI samples, such as cracks and their thin, unconstrained nature, were believed to have been a major cause for the lower than expected sensitivity.

The primary limitation to the analytical utility of PA spectroscopy of matrix-isolated PACs is that most of the weakly fluorescing and non-fluorescing PACs studied did not yield highly resolved MI-PA (or MI-absorption) spectra. This fact adversely affected the ability to resolve spectra of multi-component samples, particularly isomers. Typical bandwidths in the MI-PA spectra were 120-200 cm^{-1}, only a

factor of 2 or 3 less than in room-temperature liquid solutions. Although the mass detection limits for matrix-isolated PACs by PA spectroscopy and Fourier Transform Infrared (FTIR) spectroscopy are comparable, the resolution capabilities in the infrared region are far superior. Without an internal standard, the relative precision in the MI-PA measurements was ±50 %. Thus, for the detection of most PACs, FTIR spectroscopy seems more analytically useful than PA spectroscopy at the present time.

The analytical utility of PA spectroscopy of matrix-isolated PACs appears limited. Although the technique of low-temperature PA spectroscopy was not determined to be particularly advantageous for this specific analytical problem, it is possible that other chemical and physical applications of this technique may eventually be identified.

REFERENCES

1. A. Rosencwaig, "Photoacoustics and Photoacoustic Spectroscopy", John Wiley & Sons, New York, 1980.

2. Y.-H. Pao, Ed., "Optoacoustic Spectroscopy and Detection", Academic Press, New York, 1977.

3. A. G. Bell, Am. J. Sci., 20, 305 (1880).

4. M. E. Mercadier, C. R. Hebd. Seances Acad. Sci., 92, 409 (1881).

5. W. H. Preece, Proc. R. Soc. Lond., 31, 506 (1881).

6. J. Tyndall, Proc. R. Soc. Lond., 31, 307 (1881).

7. W. C. Roentgen, Phil. Mag., 11, (5)308 (1881).

8. M. L. Viengerov, Dokl. Akad. Nauk SSSR, 19, 687 (1938).

9. M. L. Viengerov, Dokl. Akad. Nauk SSSR, 46, 182 (1945).

10. A. Rosencwaig, Opt. Commun., 7, 305 (1973).

11. J. E. Michaels, Planetary Space Sci., 7, 427 (1961).

12. R. M. White, J. Appl. Phys., 34, 2123 (1963).

13. J. Curie and P. Curie, C. R. Hebd. Seances Acad. Sci., 91, 294 (1881).

14. M. O'Donnell, L. J. Busse, and J. G. Miller, in "Methods in Experimental Physics: Ultrasonics", Vol. 19, P. D. Edmonds, Ed., Academic Press, New York, 1981, Chapter 1.

15. J. Szilard, "Ultrasonic Testing", John Wiley & Sons, New York, 1982.

16. P. A. Walthers, Edo Western Corp., Salt Lake City, Utah, personal communication.

17. A. Hordvik and H. Schlossberg, Appl. Opt., 16, 101 (1977).

18. C. K. N. Patel and A. C. Tam, Rev. Mod. Phys., 53, 517 (1981).

19. M. M. Farrow, R. K. Burnham, M. Auzanneau, S. L. Olsen, N. Purdie, and E. M. Eyring, Appl. Opt., 17, 1093 (1978).

20. A. Rosencwaig and T. W. Hindley, Appl. Opt., 20, 606 (1981).

21. E. Voigtman, A. Jurgensen, and J. D. Winefordner, Anal. Chem., 53, 1442 (1981).

22. A. C. Tam and C. K. N. Patel, Appl. Phys. Lett., 35, 843 (1979).

23. J. B. Smith and G. A. Laguna, Phys. Lett., A 56, 223 (1976).

24. M. B. Robin and N. A. Kuebler, J. Chem. Phys., 66, 169 (1977).

25. H. Parker, K. W. Hipps, and A. H. Francis, Chem. Phys., 23, 117 (1977).

26. J. C. Murphy and L. C. Aamodt, J. Appl. Phys., 48, 3502 (1977).

27. P. S. Bechthold, M. Campagna, and J. Chatzipetros, Opt. Commun., 36, 369 (1981).

28. P. S. Bechtold and M. Campagna, Opt. Commun., 36, 373 (1981).

29. E. T. Nelson and C. K. N. Patel, Proc. Natl. Acad. Sci. U.S.A., 78, 702 (1981).

30. C. N. Ironside and R. G. Denning, J. Phys. (E), 15, 142 (1981).

31. N. J. Turro, "Modern Molecular Photochemistry", Benjamin/ Cummings, Menlo Park, Calif., 1978.

32. E. L. Wehry and G. Mamantov, in "Modern Fluorescence Spectroscopy", Vol. 4, E. L. Wehry, Ed., Plenum Press, New York, 1981, Chapter 6.

33. M. L. Lee, M. V. Novotny, and K. D. Bartle, "Analytical Chemistry of Polycyclic Aromatic Compounds", Academic Press, New York, 1981.

34. M. R. Guerin, in "Polycyclic Hydrocarbons and Cancer", H. V. Gelboin and P. O. P. Ts'O, Eds., Academic Press, New York, 1978, p. 3.

35. A. Dipple, in "Chemical Carcinogens" (ACS Monograph 173), C. E. Searle, Ed., American Chemical Society, Washington, D.C., 1976, p. 248.

36. R. I. Freudenthal and P. W. Jones, Eds., "Carcinogenesis - A Comprehensive Survey", Raven Press, New York, 1978.

37. A. W. Pucknat, "Health Impact of Polynuclear Aromatic Hydrocarbons", Noyes Data Corp., Park Ridge, N.J., 1981.

38. M. Cooke and A. J. Dennis, Eds., "Polynuclear Aromatic Hydrocarbons", Battelle Press, Columbia, Ohio, 1981.

39. P. W. Jones and P. Leber, Eds., "Polynuclear Aromatic Hydrocarbons", Ann Arbor Science, Ann Arbor, Mich., 1979.

40. M. R. Guerin, J. L. Epler, W. H. Griest, B. R. Clark, and T. K. Rao, in "Carcinogenesis - A Comprehensive Survey", Vol. 3, R. I. Freudenthal and P. W. Jones, Eds., Raven Press, New York, 1978, p. 30.

41. A. Lacassagne, N. P. Buu-Hoi, F. Zajdela, F. Perrin, and P. Jacquignon, Nature, 191, 1005 (1961).

42. D. J. Futoma, S. R. Smith, J. Tanaka, and T. E. Smith, CRC Crit. Rev. Anal. Chem., 12, 69 (1981).

43. J. E. Schiller, Anal. Chem., 49, 2292 (1977).

44. H. S. Hertz, J. M. Brown, S. N. Chesler, F. R. Guenther, L. R. Hilpert, W. E. May, R. M. Parris, and S. A. Wise, Anal. Chem., 52, 1650 (1980).

45. M. Novotny, R. Kump, F. Merli, and L. J. Todd, Anal. Chem., 52, 401 (1980).

46. M. Dong, I. Schmeltz, E. LaVoie, and D. Hoffman, in "Carcinogenesis - A Comprehensive Survey", Vol. 4, R. I. Freudenthal and P. W. Jones, Eds., Raven Press, New York, 1978,

47. S. R. Smith, J. Tanaka, D. J. Futoma, and T. E. Smith, CRC Crit. Rev. Anal. Chem., 11, 375 (1981).

48. D. J. Futoma, S. R. Smith, and J. Tanaka, CRC Crit. Rev. Anal. Chem., 13, 117 (1982).

49. J. B. Birks, "Photophysics of Aromatic Molecules", John Wiley & Sons, London, 1970.

50. S. G. Schulman, "Fluorescence and Phosphorescence Spectroscopy", Pergamon Press, New York, 1976.

51. H. O. Brotherton, Jr., M. S. Thesis, University of Tennessee, 1976.

52. E. L. Wehry and G. Mamantov, Anal. Chem., 51, 643A (1979).

53. Reference 31, Chapter 6.

54. E. L. Wehry, in "Fluorescence", G. G. Guilbault, Ed., Marcel Dekker, Inc., New York, 1967, Chapter 2.

55. N. J. Turro, "Molecular Photochemistry", W. A. Benjamin, Inc., New York, 1967, Chapter 4.

56. Reference 49, Chapter 6.

57. M. D. Lumb, Ed., "Luminescence Spectroscopy", Academic Press, London, 1978.

58. T. Vo-Dinh, in "Modern Fluorescence Spectroscopy", Vol. 4, E. L. Wehry, Ed., Plenum Press, New York, 1981, Chapter 5.

59. T. C. O'Haver, in "Modern Fluorescence Spectroscopy", Vol. 1, E. L. Wehry, Ed., Plenum Press, New York, 1976, Chapter 3.

60. A. W. Hawthorne, J. H. Thorngate, R. B. Gammage, and T. Vo-Dinh, in "Polynuclear Aromatic Hydrocarbons", P. W. Jones and P. Leber, Eds., Ann Arbor Science, Ann Arbor, Mich., 1979.

61. E. L. Wehry, R. R. Gore, and R. B. Dickinson, Jr., in "Lasers in Chemical Analysis", G. M. Hieftje, J. C. Travis and F. E. Lytle, Eds., The Humana Press, Clifton, N.J., Chapter 10.

62. E. V. Shpol'skii, A. A. Il'ina, and L. A. Klimova, Dokl. Akad. Nauk SSSR, 87, 935 (1952).

63. G. F. Kirkbright and C. G. DeLima, Analyst, 99, 338 (1974).

64. B. S. Causey, G. F. Kirkbright, and C. G. DeLima, Analyst, 101, 367 (1976).

65. R. Farooq and G. F. Kirkbright, Analyst, 101, 566 (1976).

66. E. Whittle, D. A. Dows, and G. C. Pimentel, J. Chem. Phys., 22, 1943 (1954).

67. B. Meyer, "Low Temperature Spectroscopy", American Elsevier Pub. Co., New York, 1971.

68. H. E. Hallam, Ed., "Vibrational Spectroscopy of Trapped Species", John Wiley & Sons, London, 1973.

69. S. Cradock and A. J. Hinchcliffe, "Matrix Isolation", Cambridge University Press, Cambridge, 1975.

70. G. Mamantov, A. A. Garrison, and E. L. Wehry, Appl. Spectrosc., 36, 339 (1982).

71. J. C. Brown, J. M. Hayes, J. A. Warren, and G. J. Small, in "Lasers in Chemical Analysis", G. M. Hieftje, J. C. Travis, and F. E. Lytle, Eds., The Humana Press, Clifton, N.J., 1981, Chapter 12.

72. E. Voigtman, A. Jurgensen, and J. D. Winefordner, Analyst, 107, 408 (1982).

73. E. P. Lai, A. Jurgensen, E. Voigtman, and J. D. Winefordner, Appl. Spectrosc., 36, 589 (1982).

74. R. C. Stroupe, Ph.D. Dissertation, University of Tennessee, 1977.

75. R. R. Gore, Ph.D. Dissertation, University of Tennessee, 1981.

76. A. A. Garrison, Ph.D. Dissertation, University of Tennessee, 1981.

77. W. P. Mason, "Piezoelectric Crystals and Their Application to Ultrasonics", D. Van Nostrand, New York, 1950.

78. "International Critical Tables of Numerical Data, Physics, Chemistry, and Technology", E. W. Washburn, Ed., McGraw-Hill, New York, 1929, Volume VI, p. 211.

79. A. Paulovic and R. Pepinsky, J. Appl. Phys., 25, 1344 (1954).

80. "CRC Handbook of Chemistry and Physics", 58th ed., R. C. Weast, Ed., CRC Press, Cleveland, OH, 1977.

81. T. Boublik, V. Fried, and E. Hala, "The Vapor Pressures of Pure Substances", Elsevier Scientific, New York, 1973.

82. M. R. Fisher, D. M. Fasano, and N. S. Nogar, Appl. Spectrosc., 36, 125 (1982).

83. R. W. Shaw, Appl. Phys. Lett., 35, 253 (1979).

84. D. M. Munroe and H. S. Reichard, Am. Lab., 9, 119 (1977).

85. M. J. Adams, B. C. Beadle, and G. F. Kirkbright, Analyst, 102, 569 (1977).

86. H. E. Eaton and J. O. Stuart, Anal. Chem., 50, 587 (1978).

87. R. E. Blank and T. Wakefield, Anal. Chem., 51, 50 (1979).

88. A. Rosencwaig, in "Advances in Electronics and Electron Physics", L. Marton, Ed., Academic Press, New York, 1978, p. 107.

89. D. Débarre, A. C. Boccara, and D. Fournier, Appl. Opt., 20, 4281 (1981).

90. G. H. Dieke, "Spectra and Energy Levels of Rare Earth Ions in Crystals", John Wiley & Sons, New York, 1968.

91. B. G. Wybourne, "Spectroscopic Properties of Rare Earths", John Wiley & Sons, New York, 1965.

92. P. Caro and J. Derouet, Bull. Soc. Chim. Fr., 1972, 46 (1972).

93. R. W. Shaw and H. E. Howell, Appl. Opt., 21, 100 (1982).

94. "The Sadtler Handbook of Ultraviolet Spectra", W. W. Simons, Ed., Sadtler, Philadelphia, 1979.

95. "Absorption Spectra in the Ultraviolet and Visible Region", L. Lang, Ed., Academic Press, New York, 1963.

96. E. L. Wehry, University of Tennessee, personal communication.

97. J. R. Maple and E. L. Wehry, Anal. Chem., 53, 266 (1981).

98. P. V. Bilotta, M.S. Thesis, University of Tennessee, 1978.

99. B. Carlin, "Ultrasonics", McGraw-Hill, New York, 1960.

100. J. Krautkramer and H. Krautkramer, "Ultrasonic Testing of Materials", Springer-Verlag, New York, 1969.

101. L. Filipczynski, Z. Pawlowski, and J. Wehr, "Ultrasonic Methods of Testing Materials", K. R. Schlachter, Trans., Butterworth & Co., London, 1966.

102. G. K. White, "Experimental Techniques in Low-Temperature Physics", 2nd ed., Oxford Press, London, 1968.

103. R. T. Beger and S. V. Letcher, "Physical Ultrasonics", Academic Press, New York, 1969.

104. O. G. Peterson, D. N. Batchelder, and R. O. Simmons, Phys. Rev., 150, 703 (1966).

105. R. Hill and S. El-Dardiry in, "Advances in Acoustic Emission", H. L. Dunegan and W. F. Hartman, Eds., Dunhart Publishers, Knoxville, TN, 1981.

106. W. Jackson and N. M. Amer, J. Appl. Phys., 51, 3343 (1980).

107. J. L. Metzger, R. E. Smith, and B. Meyer, Spectrochim. Acta A, 25A, 1177 (1969).

108. S. P. McGlynn, T. Azumi, and M. Kinoshita, "Molecular Spectroscopy of the Triplet State", Prentice-Hall, Englewood Cliffs, N.J., 1969.

109. F. Wilkinson, in "Organic Molecular Photophysics", Vol. 2, J. B. Birks, Ed., John Wiley & Sons, London, 1975.

110. S. G. Hadley, J. Phys. Chem., 75, 2083 (1971).

111. "Thermophysical Properties of Matter", Vol. 13, Plenum, New York, 1977.

112. "Selected Values of the Thermodynamic Properties of the Elements", American Society for Metals, Metals Park, OH, 1973.

113. N. A. Lurie, G. Shirane, and J. Skalyo, Phys. Rev. B., 9, 2661 (1974).

114. "Tables of Physical and Chemical Constants", Longman, Inc., New York, 1977.

115. E. M. Horl and J. A. Suddeth, J. Appl. Phys., 32, 2521 (1961).

116. R. J. von Gutfeld and R. L. Melcher, Appl. Phys. Lett., 30, 257 (1977).

117. M. P. Felix, Rev. Sci. Instrum., 45, 1106 (1974).

118. G. C. Wetsel, IEEE Ultrasonics Symp., 645 (1980).

119. G. C. Wetsel, IEEE Ultrasonics Symp., 810 (1981).

VITA

Huston Edward Howell, Jr. was born on Feburary 13, 1955, and raised in Cherokee County, Alabama. He graduated from Cherokee County High School in 1973. In 1977, he received his B.S. degree in Chemistry from the University of Alabama in Birmingham and began graduate studies at Texas A&M University. Upon the completion of the work for his M.S. degree in Chemistry from Texas A&M University in 1979, he enrolled at the University of Tennessee-Knoxville in pursuit of his Ph.D. degree. He completed his Ph.D. degree in Chemistry in 1983 and entered employment with the Procter & Gamble Company in Cincinnati, Ohio. He is a member of the American Chemical Society.

In 1978, he married Susan Appleton, of Centre, Alabama. He and Susan currently reside in Cincinnati, Ohio.